Investigating the Capability of a New Surface-based EM Instrument, the Sea Ice Sensor (SIS), to Measure Sea Ice Thickness

Mojtaba Daneshvar Nilu

A THESIS SUBMITTED TO THE FACULTY OF GRADUATE STUDIES IN PARTIAL FULFILLMENT OF THE REQUIREMENTS FOR THE DEGREE OF MASTER OF SCIENCE

EARTH AND SPACE SCIENCE

YORK UNIVERSITY

TORONTO, ONTARIO

April 2019

Abstract

Sea ice thickness measurement is an important parameter in climate system models, safety and efficiency of offshore operations and maritime navigation. Electromagnetic (EM) induction instruments are commonly used to measure this parameter. Sea Ice Sensor (SIS) is a new surface-based EM instrument that utilizes single frequency and multiple transmitter-receiver coil configurations to measure sea ice thickness.

This thesis investigates SIS capability to measure sea ice thickness over a variety of sea ice types. Signal sensitivity, the accuracy of the inversion algorithm used and the pitch and roll effect on the inversion results were investigated.

Overall SIS proved to provide accurate sea ice thickness estimates over a variety of sea ice types. Utilization of 2 m coil spacing and a single EM data component appeared to be effective and sufficient for most sea ice types. Utilization of Pitch and roll measurements improved results accuracy.

Acknowledgments

I gratefully acknowledge the support and guidance of my supervisor Dr. Christian Haas. I am also thankful for the extraordinary Arctic field opportunity he provided me.

I would like to express my appreciation to Dr. Alec Casey and Dr. Anne Irvin for providing me feedbacks and exposing me to a variety of topics related to sea ice.

I would like to thank Justin Beckers who was responsible for the collection of Polarstern EM data used in this research.

I would like to thank Marosz-Wantuch for sharing her field photos and for her contribution in collecting sea ice drill-hole measurements for Qikiqtarjuaq survey. I was fully responsible for the EM data collection in Qikiqtarjuaq.

Lastly, I would like to acknowledge the Natural Sciences and Engineering Research Council (NSERC) for partial funding of the transportation costs to Qikiqtarjuaq. No other financial support was received for this research from any institution.

Table of Contents

List of Tables

List of Figures

Fig. 4.1: Schematic diagram of SIS coil configurations. 21

Fig. 4.2: Relative (a) and cumulative (b) in-phase response of HCOP and PRP for 1.1 m, 2.1 m, and 4.1 m coil spacing as a function of normalized depth 24

Fig. 4.3: Relative (a) and cumulative (b) quadrature response of HCOP and PRP orientation for 1 m, 2 m, and 4 m coil spacing as a function of normalized depth. 26

1 Introduction

1.1 Motivation

Measurements of sea ice thickness in the Arctic and Antarctic Oceans is essential for a variety of scientific studies and operational applications. From a scientific perspective, sea ice thickness is a key parameter in global climate change. Its variability is considered as an indicator and amplifier of climate change. Sea ice thickness has an essential influence on climate by controlling the exchange of energy, mass and momentum between the atmosphere and ocean in the polar regions (Haas et al. 1997; Strass 1998). Furthermore, sea ice thermodynamics is an important driving force of global thermohaline ocean circulation (Strass 1998).

The interaction between the atmosphere and ocean in the Polar Regions is greatly affected by the dynamics and thermodynamics of sea ice. Therefore, in the context of climate change, accurate measurements of sea ice thickness are vital to improve our understanding of sea ice dynamic and thermodynamic processes and to correctly quantify its influence as an input in general circulation models.

From an operational perspective, knowledge of sea ice thickness is essential for supporting safe and efficient marine operations (e.g. navigation routes for ships and over-ice vehicles) and for designing offshore structures (e.g. oil well drilling platforms, bridges) in polar regions (Rossiter and Holladay 1994).

1.2 Thesis objective

The objective of this thesis is to investigate the capability of a new surface-based electromagnetic (EM) induction instrument, the Sea Ice Sensor (SIS), to determine sea ice thickness of different sea ice types. Of particular interest is the capability of the SIS to measure the thickness of ridged sea ice type and flooded sea ice type where existing EM instruments have been shown to provide inaccurate estimates of sea ice thickness. The results presented in this

thesis will indicate whether or not the SIS is a superior EM system for collecting accurate measurements of sea ice thicknesses.

To achieve this research objective, the following three questions are answered:

1. What is the spatial sensitivity of the various SIS coil configurations and what is the most suitable coil configuration for the accurate estimation of sea ice thicknesses?
2. Does SIS inversion software provide reliable estimates of sea ice thickness?
3. How does SIS respond to changes in instrument pitch and roll?

1.3 Thesis outline

This thesis is presented in seven chapters. Chapters 2 and 3 present the motivation and background knowledge required for this research. Chapters 4 through 7 answer the questions posed in the previous section.

- In Chapter 2, an overview of sea ice formation and the sea ice thickness distribution is presented. Dynamic and thermodynamic processes that affect the sea ice thickness distribution are briefly explained through mathematical means.
- In Chapter 3, the need to measure sea ice thickness is explained. The techniques commonly used to measure sea ice thickness are explained, including a detailed description of the use of electromagnetic (EM) induction sounding of sea ice. The new ground-based EM instrument (SIS), which is the focus of this thesis research, is also introduced.
- In Chapter 4, SIS's spatial sensitivity is discussed through theoretical models.
- In Chapter 5, field observations are discussed. The quality of acquired SIS data is assessed through a series of graphical and statistical analysis.
- In chapter 6, SIS performance over a variety of sea ice conditions is investigated. The most effective coil configuration and suitable layered earth inversion models that generate accurate sea ice estimates are determined. The accuracy of the inversion results is evaluated based on in situ drill-hole measurements.

- In Chapter 7, an investigation is conducted on the reliability of the inverted data for various instrument pitch and roll measurements. The aim is to see if the inversion algorithm effectively utilizes the recorded instrument pitch and roll in estimating sea ice thicknesses.

2 Sea ice formation and distribution

2.1 Sea ice formation and thickness distribution

The formation of sea ice and its thickness distribution are governed by dynamic and thermodynamic mechanisms. Sea ice formation and growth are initiated by thermodynamic processes. Ice crystals form and grow at sea surface when cold air brings sea water temperature to -1.8 degrees Celsius (Wadhams 2000). Under calm sea states, thin ice sheets (i.e. nilas) continue to grow through congelation ice growth (thermodynamics). As thin ice sheets develop, thermodynamics are coupled with dynamic processes, through which wind and ocean current fracture and break the newly formed thin ice sheets into fragments. Ice fragments may raft over or under each other forming thicker ice sheets (floes) and areas of open water (leads). When thick ice floes collide, pressure ridges form. The thickness of pressure ridges is much greater than the thickness of the thermodynamically grown level sea ice from which ridges form. Pressure ridges can form 30-80% of the total ice volume of an ice floe (Haas 2010).

The continuous combined effect of dynamic and thermodynamic mechanisms involved in sea ice formation and decay generates substantial spatial and temporal variability in the sea ice thickness distribution, leading to a complex system of various sea ice formations intersected with a complex network of open water leads and polynyas (Wadhams 2000). Leads and Polynyas are open water areas where sea ice cover is expected. Leads form by the divergent motion of the sea ice while Polynyas form from either upwelling warm ocean water or persistent winds pushing sea ice away from a fixed point such as coastlines.

Based on sea ice age and thickness, sea ice is generally classified into four major categories: first-year ice (ice that has not yet survived a summer melt season), second-year sea ice (ice that has survived one summer melt season), multi-year sea ice (ice that has survived at least two summer melt cycles) and open water (Wadhams 2000).

2.2 Statistical characterization of the sea ice thickness distribution

The sea ice thickness distribution can be expressed by a probability density function (PDF) *g(h).* Consider a finite region R within an ice pack, centred on a point x. Let $dA(h, h + dh)$ be an area

in region R aggregated with ice thickness between h and $h + dh$. Then the probability density function $g(h; x, t, R)$ at time t is defined by (Thorndike et al. 1975):

$$g(h; x, t, R)d(h) = dA(h, h + dh)/R \qquad (2.1)$$

Since the sea ice thickness distribution is commonly acquired along linear tracks, dA and R are modified to *dL* and *L* to represent a linear track. The dimension unit along a linear track is m^{-1}. In any given region *R*, the thickness distribution is dominated by level sea ice. Therefore, modal thickness(es) in the sea ice thickness distributions represent the thickness of thermodynamically grown level sea ice. The tail of the thickness distribution represents the ice thickness of the multi-year ice and deformed ridged ice (Wadhams 2000).

A set of examples of the sea ice thickness distribution from three different regions prepared by Haas (2010) is presented in Figure 2.1 to visually and statistically demonstrate the spatial and temporal variability of the sea ice thickness distribution. Figure 2.1 shows oblique aerial photos of three different ice covers and their associated ice thickness distributions. Figure 2.1a shows first-year ice in the Weddell Sea, an area dominated by uniformly level first-year ice. Its log-normal distribution shows a sharp modal thickness of about 2 m, which represents the thickness of the prominent level first-year ice cover, while the decaying tail represents deformed ice. Figure 2.1b shows deformed multi-year ice in the Lincoln Sea, an area that consists of a mixture of different ice formations that have accumulated over the years. The corresponding distribution shows more than a few less distinct modes. The first three modes in the distribution (0.4 m, 1 m, and 2 m) reflect the thickness of the newly formed ice and first-year ice in leads and polynyas while thicker modes represent the thickness of multi-year ice and ridged ice. Figure 2.1c shows summer second-year ice in the North Pole, where second-year ice is intersected with a complex network of open water leads. The presence of open water (zero thickness) introduces a sharp mode in the thickness distribution.

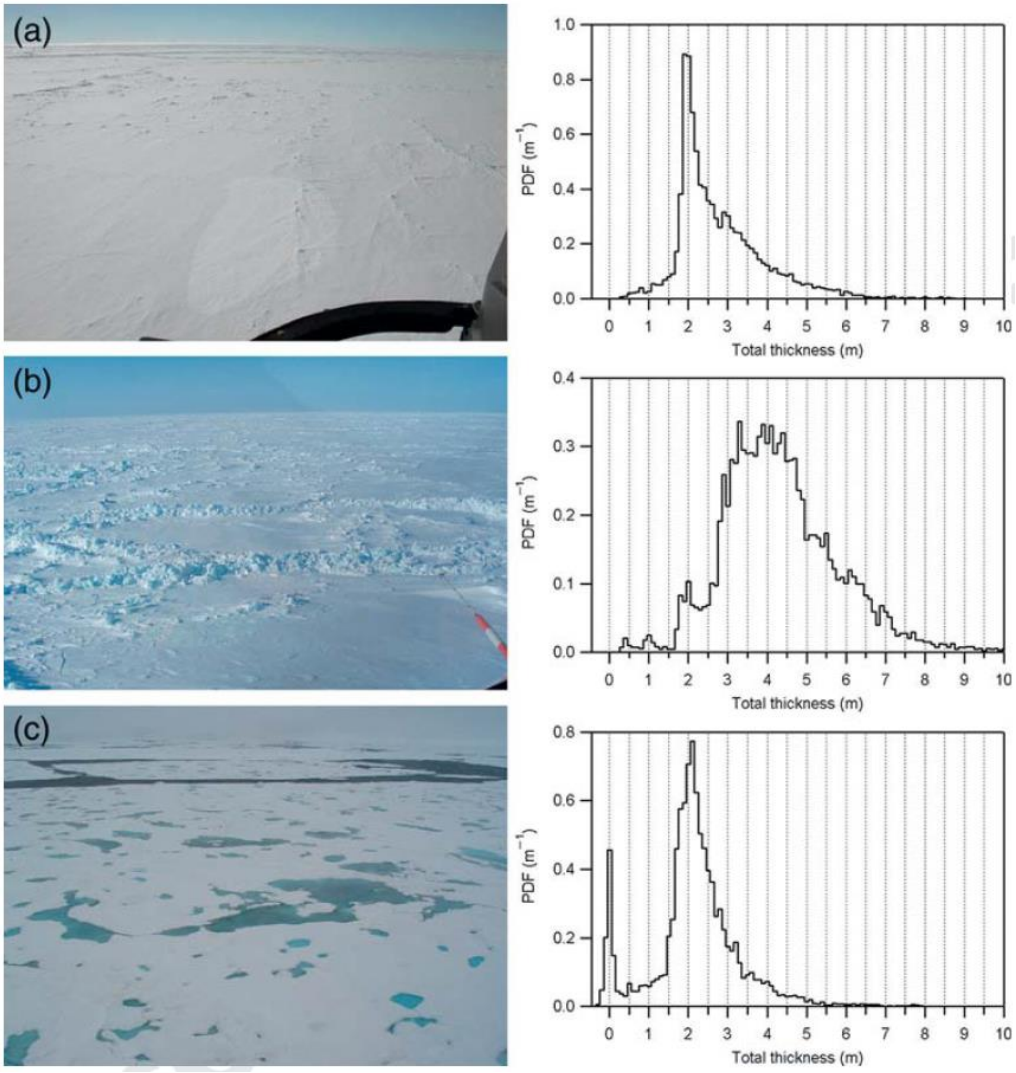

Fig. 2.1: Oblique aerial photographs of a variety of ice covers (left) and their corresponding ice thickness distributions (right). (a): first-year ice in the Weddell Sea, (b): deformed multi-year ice in the Lincoln Sea, and (c): second-year ice and open water leads near the North Pole in summer (Haas 2010).

2.3 Theoretical evolution of the sea ice thickness distribution

The sea ice thickness distribution *g(h)* is controlled by thermodynamic and dynamic mechanisms. The evolution of *g(h)* in response to these mechanisms is determined by a continuous deterministic partial differential equation given by (Thorndike et al. 1975):

$$\frac{\partial g}{\partial t} = -\nabla . (vg) - \frac{\partial}{\partial h} (fg) + \varphi \qquad (2.2)$$

where v is the drift velocity of the ice pack, which is a function of wind and ocean currents, g is the ice-thickness distribution function, f is the growth or melt rate that is dependent on time t and position x of the ice thickness h and can be written as $f(h,x,t) = dh/dt$. In other words, f is the thermodynamic rate of change of the ice thickness. The final term (φ) is the redistribution function which determines how ice ridges under strain. Equation 2.2 is the backbone of many sea ice models.

The first term of Equation 2.2 accounts for the ice motion caused by ice-divergence and advection creating open water areas (i.e. leads and polynyas). External forces caused by wind and ocean currents cause the ice to drift. The direction and velocity of the drift of ice floes mainly depend on the counterbalance force (geostrophic wind) resulting from the Coriolis effect and atmospheric pressure gradients (Haas 2010, Wadhams 2000). In the Arctic, drift is 1% of the mean wind speed at 18° to the right of the wind direction (Colony & Thorndike, 1984). In contrast, sea ice drift in the Weddell Sea (Antarctic) is 1.6% of the mean wind speed and 10-15 degrees to the left of the geostrophic wind (Kottmeier et al. 1992).

The second term of Equation 2.2 represents the thermodynamic processes, which govern the ice thickness from the lower and upper boundaries of the ice through the freezing and melting of the ice pack (Fig. 2.2). Generally, thin ice grows faster compared to thick ice due to greater temperature gradients (Haas 2010). As illustrated in Fig. 2.2, the ice growth rate significantly decreases once the ice thickness reaches 1 m. When the ice reaches thermodynamic equilibrium thickness the ocean heat flux equals the conductive heat flux through the ice. As a result, no more ice forms. If the ice thickness overtakes the thermodynamic equilibrium thickness (e.g. as is the case for ridged ice) then the ocean heat flux may melt the bottom of the sea ice, even in winter (Haas 2010).

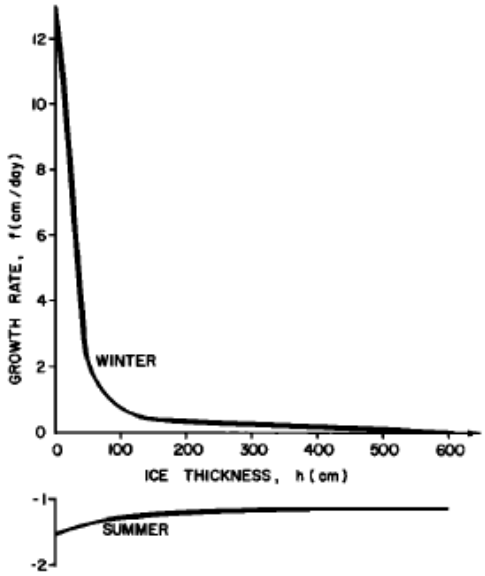

Fig. 2.2: Sea ice growth rate in the central Arctic. The sea ice growth rate is strongly dependent on ice thickness (Thorndike et al., 1975).

Aside from the ice thickness, snow depth is also critical in ice growth and melt. Snow acts as an insulator, slowing the heat flow from the ocean through the ice to the atmosphere. Therefore, snow slows the bottom ice growth rate during the winter ice formation season (Haas 2010). Studies have shown that snow depth has an immense effect on ice melt during the spring-summer melt season as greater snow depths lead to more melt ponds (Kwok and Untersteiner 2011). According to Fig 2.3, snow depth of 45 cm can double the resulting areal coverage of melt ponds during summer and increase the ice melt rate by a factor of 2.5 times, relative to a snow-free ice cover (Kwok and Untersteiner 2011).

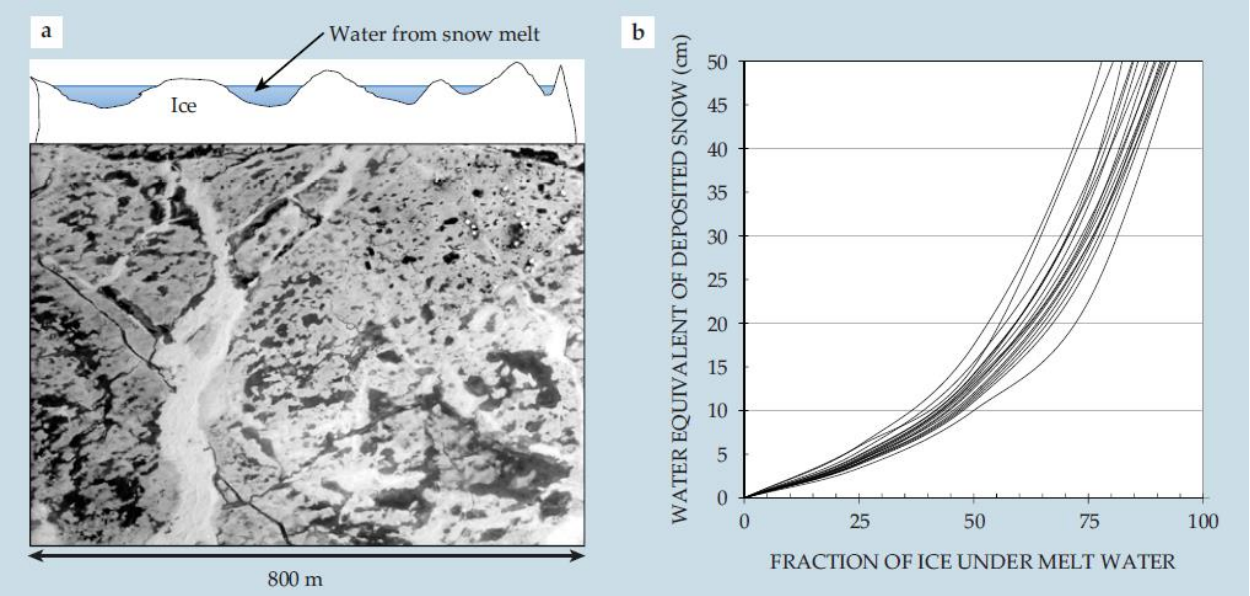

Fig. 2.3: (a) July 1972 photograph of Arctic ice covered with melt ponds during summer. The natural depressions on the ice surface are filled with water derived from snowmelt. (b) Shows the strong relationship between the water equivalent of snow (3 cm snow is equivalent to ~1 cm water) to the pond coverage (Kwok and Untersteiner 2011).

The last term in Equation 2.2 is the redistribution function, which describes the transformation of thin ice into thicker ice through convergence and deformation such that it conserves ice volume within area *R*. The redistribution function is considered to be the most important and difficult term in this equation to estimate. A more accurate estimate of the redistribution function relies on a more adequate understanding of the mechanics and physics of the ridge formation process (Wadhams 2000). The effect of the three terms in Equation 2.2 on the evolution of ice thickness distribution is shown schematically in Fig. 2.4.

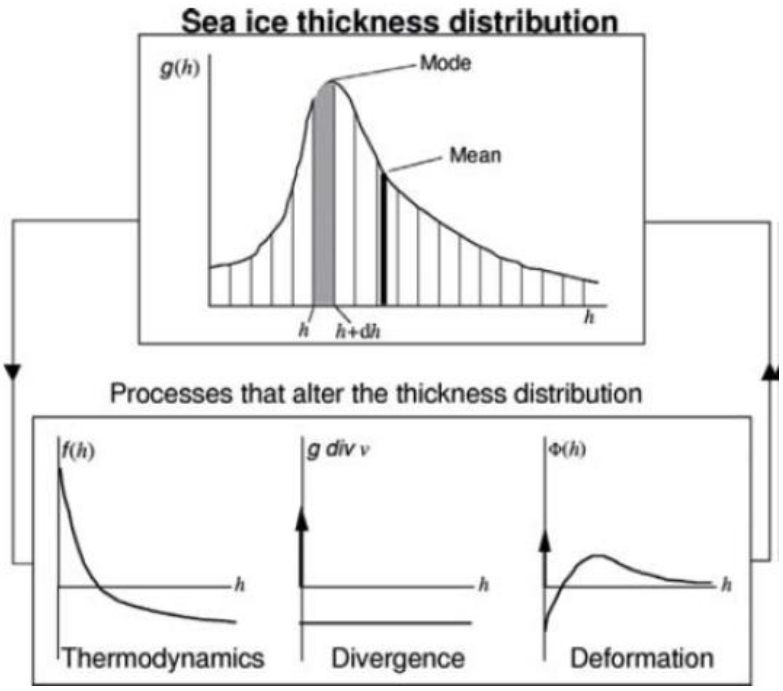

Fig. 2.4: Evolution of sea ice thickness distribution due to the three terms in equation 2.2 (Haas 2010).

The thermodynamic term causes the thinner ice to grow thicker and the thick ice to melt. The divergence term introduces a delta signal at h = 0 in the thickness distribution as a result of the formation of leads. The deformation term simultaneously creates open water and compresses ice to form pressure ridges. It is constantly producing thicker ice from thinner ice and creating regions of open water.

3 Electromagnetic (EM) induction sounding of sea ice thickness

3.1 Sea ice thickness measurement

The need to measure sea ice thickness for scientific and engineering studies has motivated researchers to investigate and develop a variety of techniques and instruments to accurately measure sea ice thickness. The most precise method to measure sea ice thickness is the traditional direct method of drill-hole measurement (Haas 2010). To this date, most of ice thickness data from Antarctica is from drilling technique (Eicken 2009). The accuracy of the drilling method decrease for sea ice over 10 m deep, but this is not of a concern as sea ice in the polar regions are typically below 10 m thick (Eicken 2009). Ridged sea ice thickness can reach as high as 10m while flat ice can barely make it to 3m thickness. Drilling technique is tedious, slow and not suitable for wide-scale surveys of the Polar Regions where the climate conditions are extreme. The hostile climate conditions of the Polar Regions and its remoteness requires remote sensing techniques to measure sea ice thickness, especially for wide-scale surveys.

Submarine and moored upward-looking sonar (ULS) (Strass 1998; Rothrock et al. 1999; Haas 2010), satellite altimetry, ground penetrating radar (GPR) (Kovacs and Morey 1986; Rossiter et al. 1977) and electromagnetic (EM) induction (Haas 2010; Haas et al. 1997; Haykin 1994; Rossiter and Holladay 1994) are effective indirect techniques commonly used in sea ice thickness measurement. The precision, accuracy, and feasibility of most of the mentioned techniques are compromised by different factors.

Upward looking sonar (ULS) has increasingly been used since the mid-1980s (Strass 1998). Factors like uncertainties in sound velocity profiles generated by temperature and pressure and changes in air pressure and tides that affect the ULS depth undermines the accuracy of ULS technique (Strass 1998; Haas 2010). Furthermore operational difficulties of using submarine mounted ULS and moored ULS is an obstacle to conveniently use this technique (Rossiter and Holladay 1994).

Satellite laser and radar altimetry is the most effective method to monitor sea ice seasonal and spatial coverage and concentration, however, sea ice thickness measurements driven from this method show significant uncertainty. This uncertainty can originate from the ambiguity in the actual density values of snow and ice used in the equations, the penetration depth of signals which varies depending on snow and ice conditions or by assumptions that rely on the presence of open water regions within ice pack and being able to frequently detect them (Haas 2010). Open water elevation in ice packed areas is used as a reference for sea ice thickness retrieval calculations. Furthermore, the presence of inhomogeneous sea ice leads to large sea ice thickness errors (Liu and Becker 1990).

Ground penetrating radar (GPR) for sea ice thickness profiling has been practiced since the mid-1970s. This technique has been very successful in accurately measuring freshwater sea ice thickness, but only partly successful for sea ice thickness. Presence of brine volume in the sea ice cause scattering and absorption of GPR signal and consequently decreases penetration depth of GPR transmitted signal to accurately detect the sea ice-water interface. This results in underestimated ice thickness measurements (Rossiter and Holladay 1994).

To this day, electromagnetic (EM) induction is the most effective, contact-free method widely used for measuring precise and accurate sea ice thickness in the Polar Regions (Haas 2010). EM is non-invasive, provides high accuracy with rapid sea ice thickness estimation.

3.2 Electromagnetic induction (EMI) sounding background

Electromagnetic induction (EMI) is one of the most popular geophysical methods widely used for a variety of near-surface applications. Historically, EMI methods were developed for mapping conductive mineral deposits and geological structures (Rossiter and Holladay 1994). Initial test studies conducted in the late 70s and in the '80s proved very low frequency (VLF) EMI to be an effective method in remote sensing of sea ice thickness (Kovacs and Morey 1986; Sinha 1976). Since then numerous airborne, ship-borne and ground-based EMI surveys have been conducted in many Arctic regions (Kovacs and Holladay 1990; Haas et al. 1997; Liu and Becker 1990; Rossiter and Holladay 1994; Haas 1998; Pfaffling 2006; Haas et al. 1997).

Airborne EMI (Kovacs et al. 1987; Haas et al. 2009; Kovacs and Holladay 1990) is considered to be most powerful when deployed from helicopters. An example of such airborne EMI systems is the Alfred Wegener Institute (AWI) helicopter-towed EM-birds (Haas et al. 2009). The accuracy of sea ice thickness measurements over flat sea ice is within ∓ 0.1 m of drill-hole ice thickness (Pfaffling 2006). However, EM thickness measurements over deformed and ridged sea ice are significantly underestimated by up to 50 to 60% (Pfaffling 2006).

Ship-borne EMI surveys (Haas 1998) are most adequate when quick sea ice thickness assessments are needed for icebreakers and ships navigating in ice-covered waters. This type of survey is restricted by ice thickness itself as ships and icebreakers navigate only through thin ice and avoid thicker ice zones (Rossiter and Holladay 1994). Hence ship-borne results are more likely a biased presentation of the regional ice thickness distribution.

Surface-based EMI surveys (Kovacs and Morey 1991; Haas et al. 1997) utilize lightweight, man-portable instruments which can also be easily towed by snow vehicles. It can produce quick and accurate results. A variety of commercially available surface-based EMI instruments are modified and calibrated to measure sea ice thickness (e.g. EM31, EMP and GEM). The most widely used surface-based EM sensor is Geonics-EM31 (Kovacs and Morey 1991).

Regardless of the platform used in EMI sounding of sea ice thickness, the typical operating frequency of VLF EMI systems range between 10 Hz and 100 kHz (Rossiter and Holladay 1994) and are designed to operate under low induction number conditions (McNeill, 1980). In general EMI systems can operate using a single or multiple frequencies and are mainly comprised of one or multiple sets of transmitter and receiver coils that may be arranged in different configurations. The theoretical principle of EMI sounding is explained in later sections. The focus of this thesis is on evaluating the capabilities of a new surface-based EMI sensor called Sea Ice Sensor (SIS).

3.3 Sea Ice Sensor (SIS) instrument specifications

The Sea Ice Sensor (SIS) (Geosensors Inc., Canada) is an advanced ground-based geophysical system that is exclusively designed to measure sea ice thickness. The SIS is a modified version of the DualEM-421 sensor (Dualem Inc., Canada) that is commonly used for agricultural and soil studies (Figure 3.1).

Fig. 3.1: The SIS mounted on a wooden sled before a survey, Qikiqtarjuaq, Nunavut. The photo was taken by Marzena Wantuch.

The magnitude of EM response sensed by the instrument over the sea ice is composed of a real (in-phase) and an imaginary (quadrature) signal component. SIS is able to simultaneously record both in-phase and quadrature responses of two coil orientations for three different coil separations.

Additionally, a pitch and roll sensor, a GPS receiver and a real-time processor unit (RTP) that provides real-time estimates of sea ice thickness and bulk conductivity are integrated into the system.

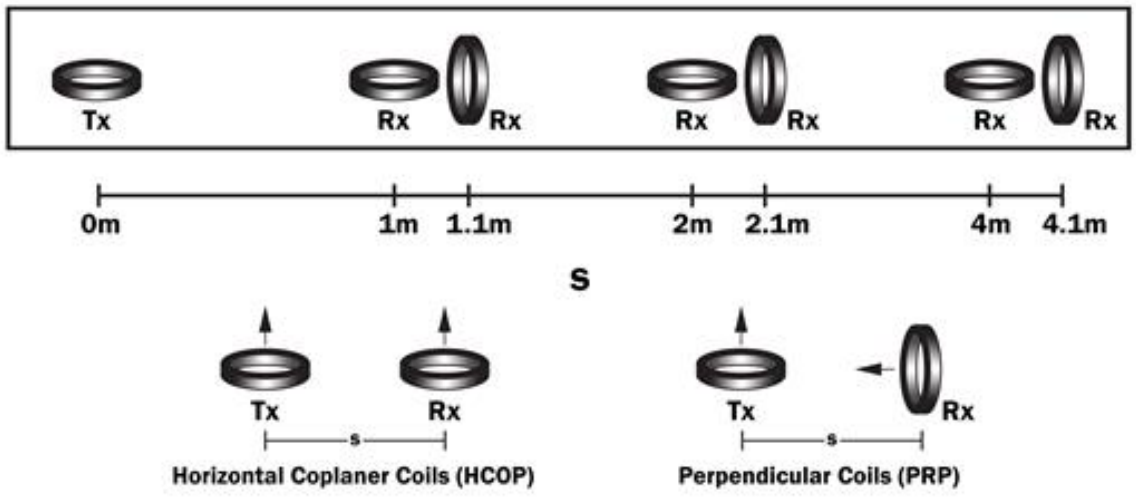

Fig. 3.2: Schematic of the SIS coil configurations.

The SIS can measure level ice thickness with accuracy better than 5 cm or 1% under conditions of 0.2 m level sea ice to 5 m level sea ice over normal seawater (~2.5 S/m) (Holladay, 2016). Over level thick sea ice (5-10 m) estimated accuracy is between 1 - 5% (Holladay, 2016).

What makes this instrument unique among other alternative surface-based EM ice thickness sensors is:

1. Its capability to simultaneously record the response of two coil orientations at three different transmitter-receiver coil separations. This multi-configuration capability enhances the spatial sensitivity of the SIS compared to other EM sensors.
2. Its capability to measure the sensor pitch and roll, which is utilized in the inversion calculations. Most surface-based instruments are assumed to be held in a level position during operation. Therefore, the effect of any change in the sensor's orientation is not considered in the results for sensors other than the SIS.
3. Its capability to simultaneously estimate sea ice thickness and bulk conductivity.

3.4 Theoretical principles of electromagnetic (EM) induction

The propagation of an electromagnetic field in any medium is governed by Maxwell's equations. The differential form of Maxwell's equations in the time domain are four vector functions described as (Telford et al. 1990):

$$\nabla \times \vec{E} = -\frac{\overrightarrow{\partial B}}{\partial t} \qquad 3.1$$

$$\nabla \times \vec{H} = \vec{J} + \frac{\overrightarrow{\partial D}}{\partial t} \qquad 3.2$$

$$\nabla . \vec{D} = \rho \qquad 3.3$$

$$\nabla . \vec{B} = 0 \qquad 3.4$$

where $\vec{E}$ is the electric field intensity (V/m), $\vec{H}$ is the magnetic field intensity (A/m) , $\vec{J}$ is the electrical current density (A/m^2), $\vec{D}$ is the electric flux density (C/m^2), $\vec{B}$ is the magnetic flux density (T), ρ is the electric charge density (C/m^3).

In a homogenous isotropic medium the constitutive relations describe how an electromagnetic field interacts with the medium through which it is propagating (Telford et al. 1990):

$$\vec{B} = \mu \vec{H} \qquad \vec{D} = \epsilon \vec{E} \qquad \vec{J} = \sigma \vec{E} \qquad 3.5$$

where μ is the relative magnetic permeability of the medium (H/m), ϵ is the relative dielectric permittivity of the medium (F/m) and σ is the conductivity of the medium (S/m). Relative dielectric permittivity is the ratio of the medium's absolute dielectric permittivity to free space (vacuum) dielectric permittivity. In other words, the constitutive relations relate Maxwell's equations to the electromagnetic properties of the EM wave as it propagates through a medium. In the above equations, the electrical properties are assumed to be independent of time, temperature or pressure and the magnetic permeability is the same as that of free space.

By utilizing Maxwell's equations together with constitutive relations and through a series of mathematical manipulations, Maxwell's equations are simplified to the following frequency domain wave equations referred to as the Helmholtz wave equation (Haykin 1994; Rossiter and Holladay 1994):

$$\nabla^2 \vec{E} + (\omega^2 \mu\epsilon - j\omega\mu\sigma)\vec{E} = 0 \qquad 3.6$$

$$\nabla^2 \vec{H} + (\omega^2 \mu\epsilon - j\omega\mu\sigma)\vec{H} = 0 \qquad 3.7$$

where ω is the angular velocity and $j = \sqrt{-1}$. The terms $\omega^2\mu\epsilon$ and $\omega\mu\sigma$ are associated with conduction and displacement currents respectively.

Given the relative magnetic permeability μ, the relative dielectric permittivity ϵ and the relative conductivity of a homogenous isotropic medium σ, Equations 3.6 and 3.7 can be used to determine the propagation of the EM field vectors through that medium.

According to the quasistatic approximation assumption, the displacement currents ($\omega^2\mu\epsilon$) are much smaller than conduction currents ($\omega\mu\sigma$) for frequencies less than 500 kHz (Rossiter and Holladay 1994). Hence, the Helmholtz wave equations are simplified to diffusion equations, which are a special case of the Helmholtz equations (Rossiter and Holladay 1994).

$$\nabla^2 \vec{E} \approx j\omega\mu\sigma\vec{E} \qquad 3.8$$

$$\nabla^2 \vec{H} \approx j\omega\mu\sigma\vec{H} \qquad 3.9$$

Half-space models are used to simulate the response of EM induction sensors in propagating media. Layered half-space models consist of a series of horizontally stratified homogenous and isotropic layers with known thicknesses and conductivities.

In sea ice EM sounding, sea ice is characterized as a horizontal resistive layer over very conductive sea water. Typical electrical conductivities of sea ice are 0 to 0.05 S/m and 2.4 to 2.7 S/m for seawater (Haas 2010). The alternating current in the transmitter coil generates a very low frequency quasistatic primary magnetic field which penetrates the sea ice. The primary magnetic field induces eddy currents in the conductive media, which is the seawater below the sea ice. The eddy currents, in turn, generate a secondary magnetic field that propagates towards the sea ice surface. The magnitude of the secondary magnetic field is several orders smaller than the primary magnetic field. The receiver coil detects both the primary and secondary magnetic fields at the surface. The magnitude of the secondary field is a complex number composed of two orthogonal components, the in-phase (real) component, and the quadrature (imaginary) component. EM instruments commonly measure the relative secondary magnetic field (in parts per million), which is the ratio of the secondary magnetic field strength to the primary magnetic field strength.

This measured coupling ratio is strongly related to the distance between the EM instrument and the seawater, or subsequently to the sea ice thickness plus instrument height above the sea ice.

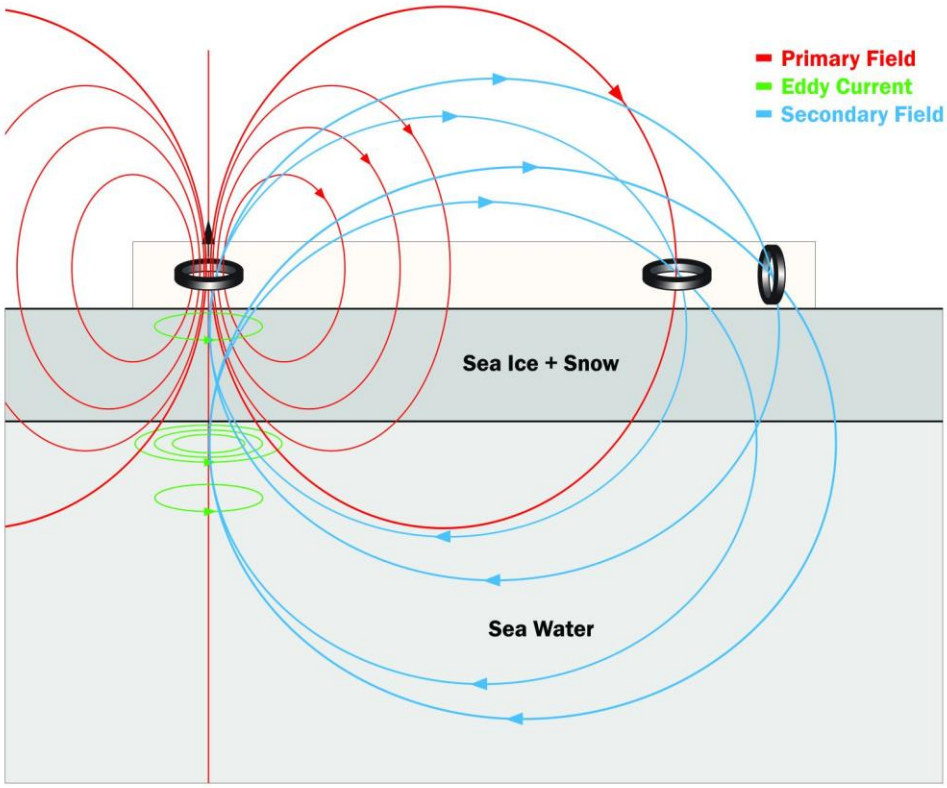

Fig. 3.3: Sketch of basic EM induction sounding of sea ice showing an EM instrument on the sea ice surface. The primary magnetic field (red) is created by the transmitter coil. The eddy currents (green) induced by the primary magnetic field induce a secondary magnetic field (blue) more dominantly at the sea ice boundary which is then sensed by the receiver coils.

For a layered half-space model in cylindrical coordinates and under the quasistatic assumption (Larsson 2007), the coupling ratios for a horizontal coplanar (HCOP) and perpendicular (PRP) coil orientations can be expressed by Hankel transforms (Haykin 1994; Telford et al. 1990; Anderson 1979; Rossiter and Holladay 1994):

$$\left(\frac{Z}{z_0}\right)_{HCP} = l^3 \int_0^\infty R_0(\boldsymbol{p}, f, \lambda) e^{-\lambda(h_1+h_2)} J_0(\lambda l) \lambda^2 d\lambda \qquad 3.10$$

$$\left(\frac{Z}{z_0}\right)_{PRP} = l^3 \int_0^\infty R_0(\boldsymbol{p}, f, \lambda) e^{-\lambda(h_1+h_2)} J_1(\lambda l) \lambda^2 d\lambda \qquad 3.11$$

where l is the transmitter-receiver coil separation, $\boldsymbol{p}$ is a vector of the model parameters such as layer conductivities and thickness, f is the transmitted frequency, R_0 is the complex reflection

coefficient that is determined recursively for an n-layer model, J_0 and J_1 are the zero and first-order Bessel functions, $h_1$and h_2 are the distance of the transmitter and receiver coils above the sea ice surface and λ is the wavenumber (integration constant or Hankel transformation number).

The oscillating nature of the Bessel function and the infinite limit of the integrals make the numerical evaluation of the Hankel transforms difficult. However, linear digital filters are utilized to overcome this issue. Anderson's linear digital filter is used to solve 3.10 and 3.11 Hankel transform integrals (Anderson 1979).

3.5 Electromagnetic properties of sea ice and seawater

Sea ice is a highly dynamic and extremely complex material composed of ice, brine, and air. The electrical conductivity of sea ice depends on its salinity, porosity, temperature, and age (Morey et al. 1984). The complex dynamic and thermodynamic processes involved in sea ice formation lead to non-uniform variations in electrical conductivity distribution both in sea ice and the underlying seawater (Rossiter and Holladay 1994).

For level sea ice, both first-year and multi-year sea ice show a strong vertical gradient in electrical conductivity, which generally increases with depth (Liu and Becker 1990). Sea ice brine volume is very low above sea level but rapidly increases with depth below sea level (Liu and Becker 1990). This rapid increase of brine volume combined with increasing temperature creates the vertical electrical conductivity gradient(Liu and Becker 1990). The vertical profile of electrical conductivity becomes highly erratic under ridged sea ice and flooded sea ice conditions.

In general, younger, first-year ice is more conductive than older, multi-year ice. First-year sea ice contains a higher volume of brine inclusions left from the ice formation process which leads to higher electrical conductivity. In multi-year sea ice, brine is drained by gravity drainage or replaced with freshwater flushed by surface melting processes in summer, hence leading to lower electrical conductivities compared to first-year sea ice. During the melt season, saline sea water may penetrate the complex network of drainage channels and mix with freshwater, thus increasing the conductivity of sea ice matrix.

Seawater electrical conductivity is a function of salinity and temperature (Liu and Becker 1990). The electrical conductivity of seawater is typically two orders of magnitude greater than that of sea ice.

4 Spatial Sensitivity Analysis

4.1 SIS coil configurations

At constant leveled instrument height, SIS's spatial sensitivity, or more specifically, the effective depth of measurement, depends on transmitter-receiver coil separations and their respective orientations.

A horizontally oriented transmitter coil generates a vertical primary magnetic field that couples well with horizontal layers (conductors) (Kovacs et al. 1987). Receiver coils are only sensitive to EM fields that cross their plane perpendicularly (Kovacs et al. 1987). Receiver coils that have the same orientation as the transmitter coil are more sensitive to horizontal layers (Nabighian 1991). Receiver coils that are oriented perpendicular to the transmitter coil are more sensitive to vertical layers (conductors) (Nabighian 1991). Increasing transmitter-receiver coil separation increases the effective penetration depth. The secondary field near transmitter is oriented horizontally. With distance this secondary field becomes vertical. Therefore, a receiver plane at a greater transmitter-receiver separation records stronger signals.

A detailed theoretical analysis of EM response for different coil orientations is explored by (Keller and Frischknecht 1966). There is an infinite number of possible coil orientations and separations that can be utilized for EM profiling. SIS incorporates only two coil orientations (HCOP and PRP) with three different coil separations, Figure 4.1.

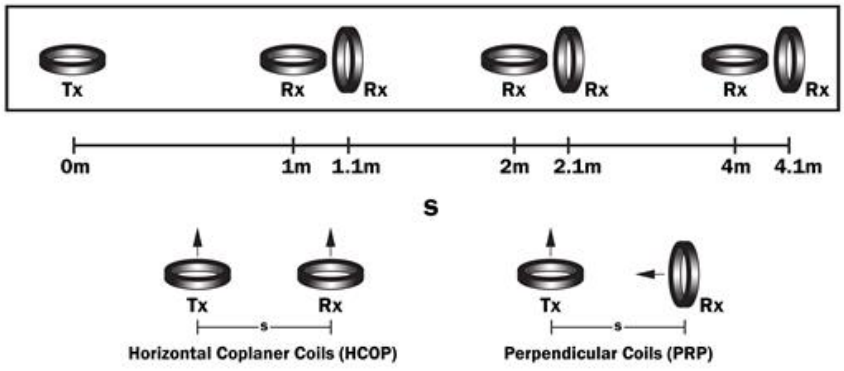

Fig. 4.1: Schematic diagram of SIS coil configurations.

Most EMI instruments only use quadrature components to estimate depth values. However, SIS considers both quadrature and in-phase measurements to estimate sea ice thickness. By varying coil orientations and separations, the sensitivity of the in-phase and quadrature components to depth also changes. The response behavior of each of these components is different from each other for different coil configurations. Therefore, it is also important to understand the behaviour of each component to changes in the coil configurations.

On theoretical bases, utilization of both quadrature and in-phase components for two coil orientations and three coil separations yields twelve different depth response sensitivities. The additional data provided is very valuable to carry out a comprehensive depth analysis and to reduce uncertainty and improve the quality of sea ice thickness inversion results.

The objective of this chapter is to investigate the spatial sensitivity of SIS coil configurations through theoretical models.

4.2 Response theoretical models

The depth sensitivity of EM response for different coil configuration can be analyzed based on mathematical functions proposed by McNeill (1980) and Wait (1962). These analytical functions determine the relative and cumulative contribution of the material at any given depth z to EM response (secondary magnetic field) measured at the receiver. They are based on the assumption that the instrument is placed leveled on the surface and induction numbers are small.

In the presence of a single infinitesimal thin horizontal homogenous layer, the relative quadrature component response function of that layer for HCOP and PRP coil orientations at any given depth z is given by the following expressions (McNeill 1980, Wait 1962):

$$R(HCOP, z, s)_{QD} = \frac{4(z/s)}{(4(z/s)^2 + 1)^{3/2}} \quad 4.1$$

$$R(PRP, z, s)_{QD} = \frac{2}{(4(z/s)^2 + 1)^{3/2}} \quad 4.2$$

where R is relative response, z is depth and s is transmitter-receiver coil spacing.

The quadrature component's relative response of HCOP and PRP coil orientations for three different coil spacing (1 m, 2 m and 4 m for HCOP and 1.1 m, 2.1 m and 4.1 m for PRP) as a function of normalized depth (z/s) is shown in Figure 4.2a. As illustrated in Figure 4.2a, the relative response of HCOP and PRP orientation follow two different patterns. PRP coil orientation is relatively sensitive to near-surface layer depths. Depending on the coil spacing, the sensitivity decreases exponentially with layer depth. In contrast, HCOP coil orientation is insensitive to near-surface layer depths but it slowly peaks to a maximum relative sensitivity where response begins to rapidly decrease with decreasing layer depth. The maximum relative sensitivity depth reached for HCOP orientation varies for each coil spacing (0.4 for 1 m, 0.7 for 2 m and 1.4 for 4 m coil spacing).

In case of a multi-layer earth model where the relative response is influenced by multiple layers, the cumulative sum of all relative contributions for all layers' depths below a given depth z, is expressed as the integration of all of the relative response functions between the surface to a given depth z. These so-called cumulative response functions for the quadrature phase of HCOP and PRP orientations are expressed as (McNeill 1980, Wait 1962):

$$C(HCOP, z, s)_{QD} = 1 - \frac{1}{(4(z/s)^2 + 1)^{1/2}} \quad 4.3$$

$$C(PRP, z, s)_{QD} = \frac{2(z/s)}{(4(z/s)^2 + 1)^{1/2}} \quad 4.4$$

where C is cumulative response.

Fig. 4.2 shows cumulative response as a function of normalized depth of HCOP and PRP coil configurations. The cumulative response curves can be used to determine the depth of exploration (DOE) of EM response. Depth of exploration is conventionally defined as the depth at which 70% of cumulative response is attributed to. This is the depth EM response is most sensitive to.

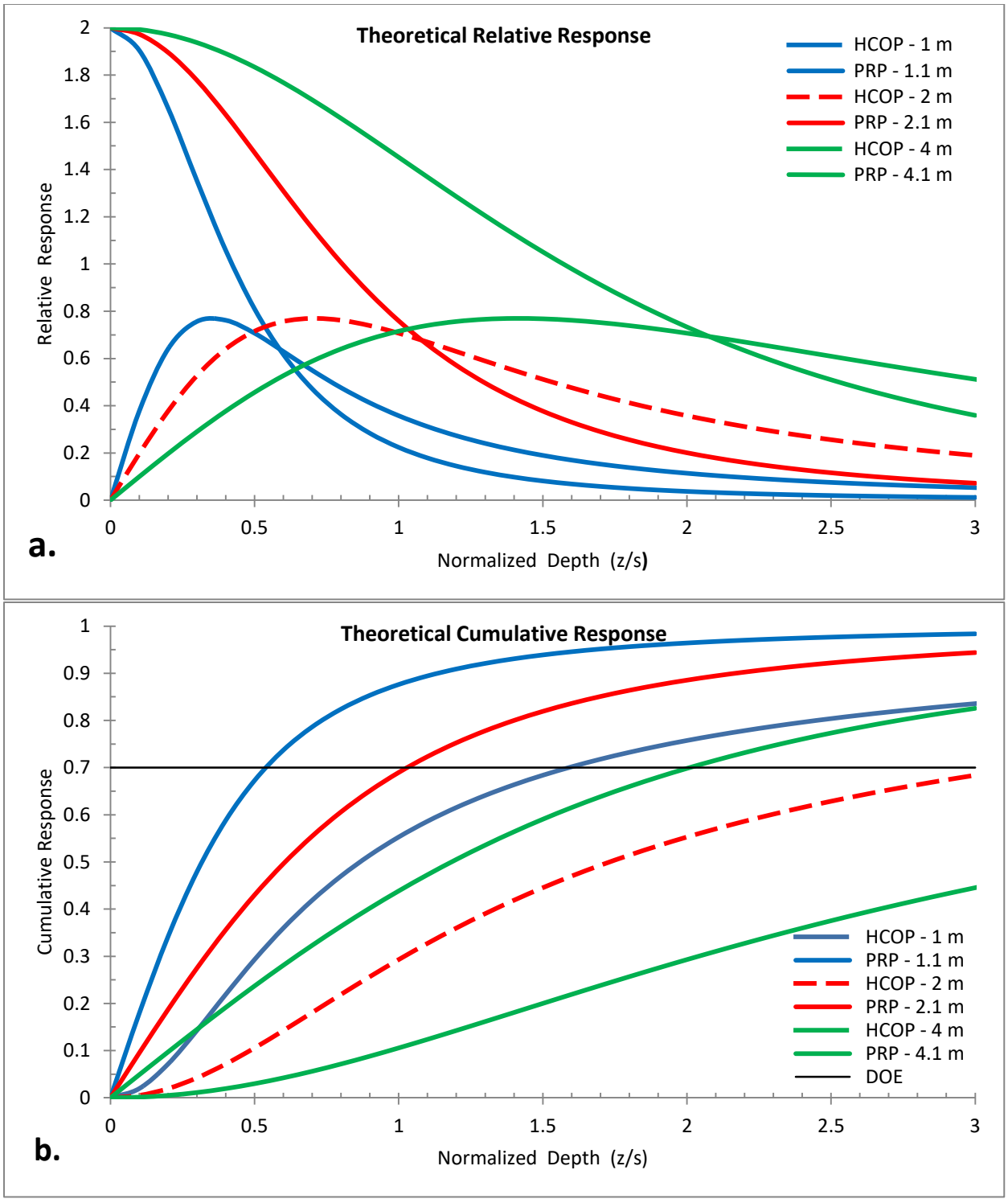

Fig. 4.2: Theoretical relative (a) and cumulative (b) in-phase response of HCOP and PRP for 1.1 m, 2.1 m, and 4.1 m coil spacing as a function of normalized depth.

The relative in-phase response functions of HCOP and PRP coil orientations were approximated by Keller & Frischknecht (1966):

$$R(HCOP, z, s)_{IP} = \frac{1}{(4(z/s)^2 + 1)^{3/2}} \quad 4.5$$

$$R(PRP, z, s)_{IP} = \frac{6(z/s)}{(4(z/s)^2 + 1)^{5/2}} \quad 4.6$$

Fig. 4.2 illustrates the relative and cumulative in-phase response curves of HCOP and PRP coil orientations for all three SIS coil spacings. A basic visual comparison of Fig. 4.3a to Fig. 4.3b reveals that despite the fact that relative in-phase and quadrature responses of HCOP coil orientation have a similar appearance in the pattern; the relative in-phase responses are more sensitive to shallower layer depths. On the other hand, relative PRP in-phase response curves perform very differently compared to relative HCOP response curves. PRP in-phase response sensitivity increases with depth till it reaches a maximum and then slowly decreases with layer depth.

The cumulative in-phase response of HCOP and PRP coil orientations are (Keller & Frischknecht, 1966):

$$C(HCOP, z, s)_{IP} == \frac{12(z/s)}{s(4(z/s)^2 + 1)^{5/2}} \quad 4.7$$

$$C(PRP, z, s)_{IP} == \frac{96(z/s)^2 - 6}{s(4(z/s)^2 + 1)^{7/2}} \quad 4.8$$

The in-phase cumulative response curves of HCOP and PRP (Fig. 4.2) behave differently compared to quadrature cumulative response curves (Fig. 4.3). The DOEs of HCOP configurations are significantly smaller when compared to DOEs of respective quadrature cumulative responses (Fig. 4.2). Furthermore, the cumulative responses of PRP configuration (Fig. 4.3) do not present definite DOEs, but rather a range of DOEs at which the EM response is most sensitive to. Overall, assessment of HCOP and PRP cumulative theoretical models reveals that the quadrature configuration is significantly more sensitive to deeper depths compared to in-phase configuration cumulative responses.

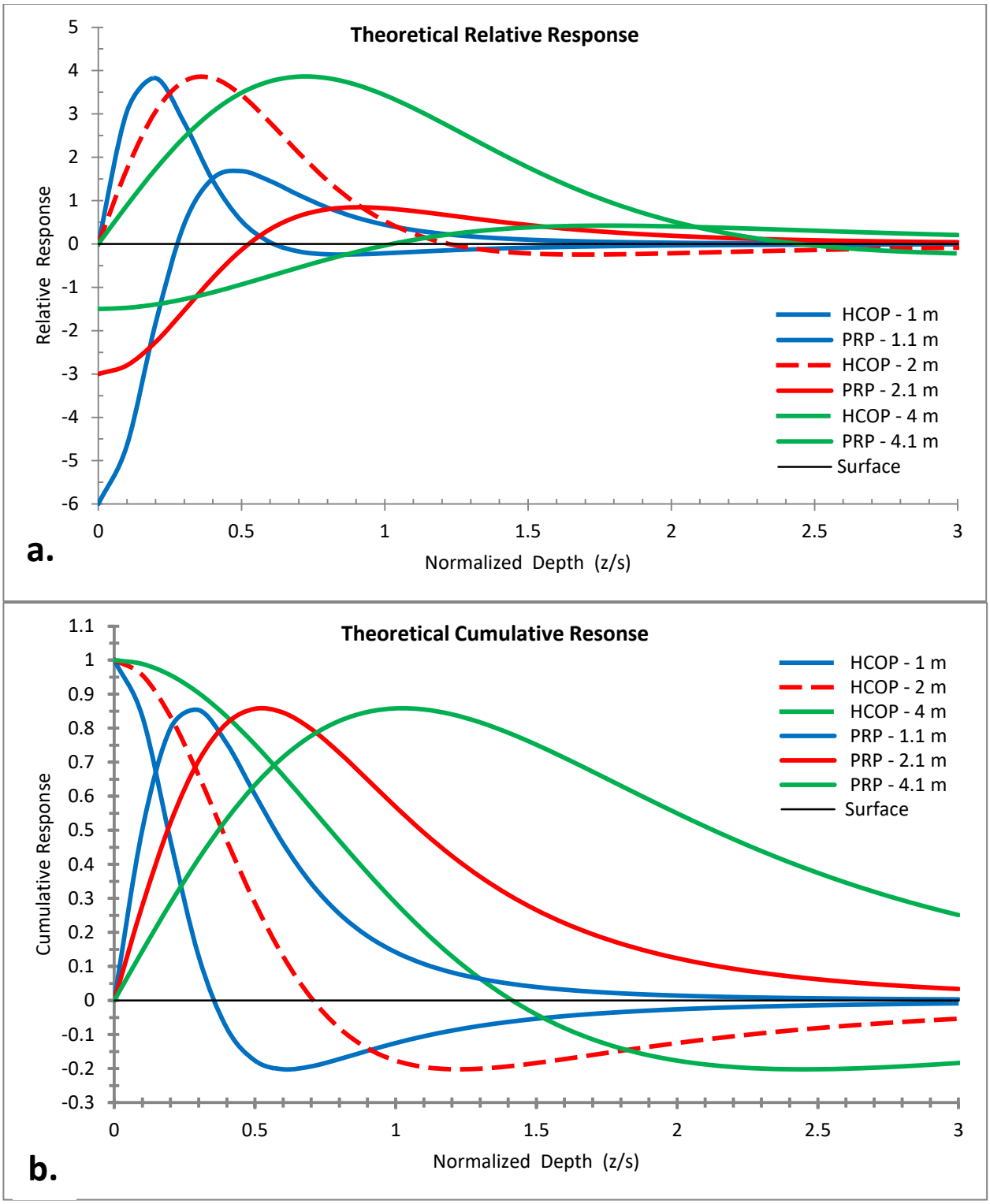

Fig. 4.3: Theoretical relative (a) and cumulative (b) quadrature response of HCOP and PRP orientation for 1 m, 2 m, and 4 m coil spacing as a function of normalized depth.

5 SIS Field Data Analysis

The objective of this chapter is to investigate the spatial sensitivity of SIS coil configurations through evaluation of actual field measurements. The specific research questions to be answered in this chapter are:

1. Do theoretical models correlate with experimental field results?
2. How does SIS measured EM responses behave in different sea ice types?
3. What EM signal component and coil configuration yields the highest quality EM responses for sea ice thickness inversions?

In this research, sea ice is categorized into five different sea ice types based on the physical properties of the sea ice surveyed. Level sea ice, slush-covered sea ice, melt pond covered sea ice, rafted sea ice and ridged sea ice are the five sea ice types studied in this research.

Table 5.1: A short description of each sea ice types studied in this research.

Sea ice type	**Description**
Level sea ice	Relatively flat sea ice that has not gone through deformation.
Slush covered sea ice	Sea ice that is covered with water-saturated snow cover. The saturation level varies from low to high from site to site depending on the source of water (snowmelt or seeping ocean water).
Melt pond	Are formed by the accumulation of snow meltwater in the sea ice surface depressions during sea ice melt season.
Rafted sea ice	Sea ice structures that are formed by overriding sea ice floes. In this study, rafted sea ice is found by the shorelines. Ocean and wind currents push ice floes against the shoreline causing ice floes to override one another.
Ridged sea ice	Ridge structures that are formed by colliding ice floes. Wind and ocean driven currents cause ice floes to collide with each other and the compression of the colliding ice floes create ridged sea ice.

5.1 Observations and data description

SIS EM Data used for this study was acquired in two separate field surveys from two distinct regions of first-year sea ice cover. The first was collected from a series of EM surveys conducted during Polarstern (icebreaker) cruises in September of 2015 over the Arctic Ocean, North Pole (above 88° latitude North), Fig. 5.1. The second was collected in the Canadian Arctic Archipelago, in the vicinity of Qikiqtarjuaq Island (approximately 67° latitude North), Nunavut on April 2016, Fig. 5.1. A summary of the surveys conducted is presented in Table 5.1.

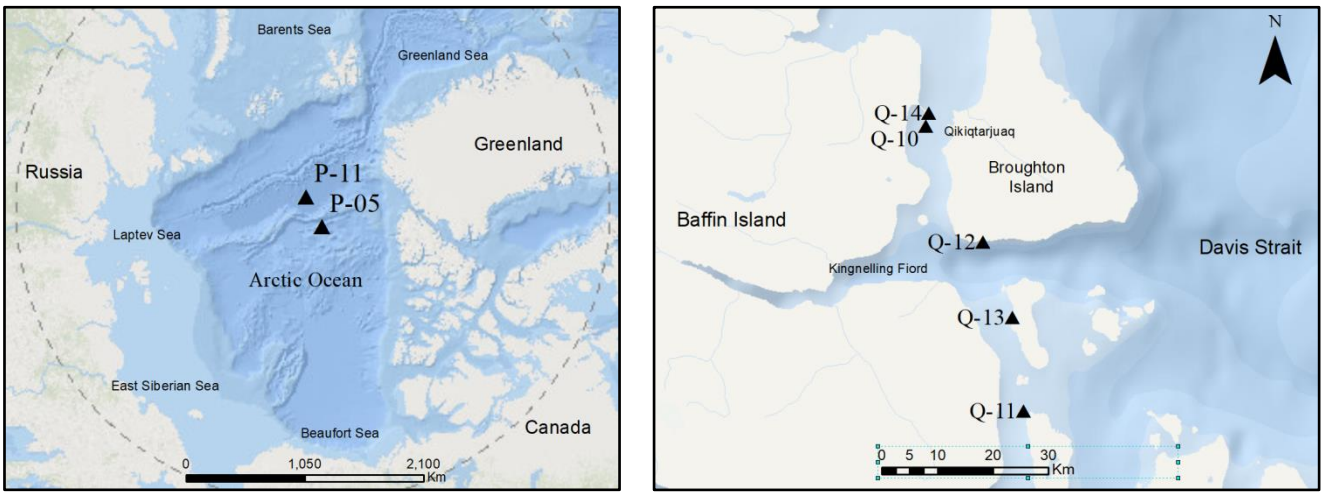

Fig. 5.1: Left: Qikiqtarjuaq survey location map. Right: Polarstern survey location map. The black triangles show the location of the EM survey transects.

Polarstern SIS EM surveys were conducted on first-year sea ice floes in the Arctic Ocean. The data set consists of 50 m long survey transects. Each transect was established to cover all sea ice types present on the ice floe the survey was conducted on. A common sea ice condition shared between Polarstern transects is sea-ice pressure ridges with relatively level sea ice on both sides of the ridge. Transect P-05 contains melt-pond zones that are only particular to this transect. To ensure all sea ice types within each ice floe are effectively surveyed, SIS EM measurements were taken at 1 m spaced intervals. To validate the EM measurements, a detailed drill-hole survey was also conducted at 1 m spaced intervals.

The Qikiqtarjuaq data set consists of multiple survey profiles with varying lengths, acquired at different locations within the proximity of Qikiqtarjuaq Island. Qikiqtarjuaq sea ice is classified as land-fast sea ice. An attempt was made to survey all sea ice types present in the

study region. Sea ice thickness drill measurements (Eicken 2009) were also taken at each transect but were less comprehensive compared to Polarstern drill surveys.

A general comparison based on visual observations and drill measurements reveal the following main differences between Polarstern and Qikiqtarjuaq sea ice formations:

- Qikiqtarjuaq transects were performed on a relatively level sea ice surface; whereas Polarstern transects included ridged sea ice structures in the middle of the profiles, (Fig. 5.2).
- Polarstern sites consisted of significantly thicker sea ice and no, or significantly thinner, snow cover. In contrast, Qikiqtarjuaq contained thinner sea ice but significantly thicker snow cover. Fig. 5.2 is a graphical illustration of the differences between the two study regions sea ice formations.
- Qikiqtarjuaq was dominantly covered with significantly saturated snow cover (slush) however; the degree of the snow saturation and its source differed region to region.

Table 5.2: General information of SIS EM surveys conducted.

Surveys	Transect	Date Acquired	Length & Sampling Interval	Drill	Description
Polarstern	P-5	05.09.2015	50 m, 1 m	Complete at every station	Ridged ice structure in the middle of the profile, Melt-ponds either side of ridged ice, no snow cover
	P-11	11.09.2015			Ridged ice structure in the middle of the profile
Qikiqtarjuaq	Q-10	10.04.2016	100, 2 m	Partial at 2 m interval	Level sea ice surface, Snow cover moderately saturated
	Q-11	11.04.2016	100, 2 m	Partial	Slush sites
	Q-12	12.04.2016	100, 2 m	Partial	Rafted sea ice type, near shoreline
	Q-13	13.04.2016	100, 5 m	Partial	Site flooded with sea water
	Q-14	14.04.2016	160, 10 m	Partial	Contain slush, flat sea ice and rafted sea ice

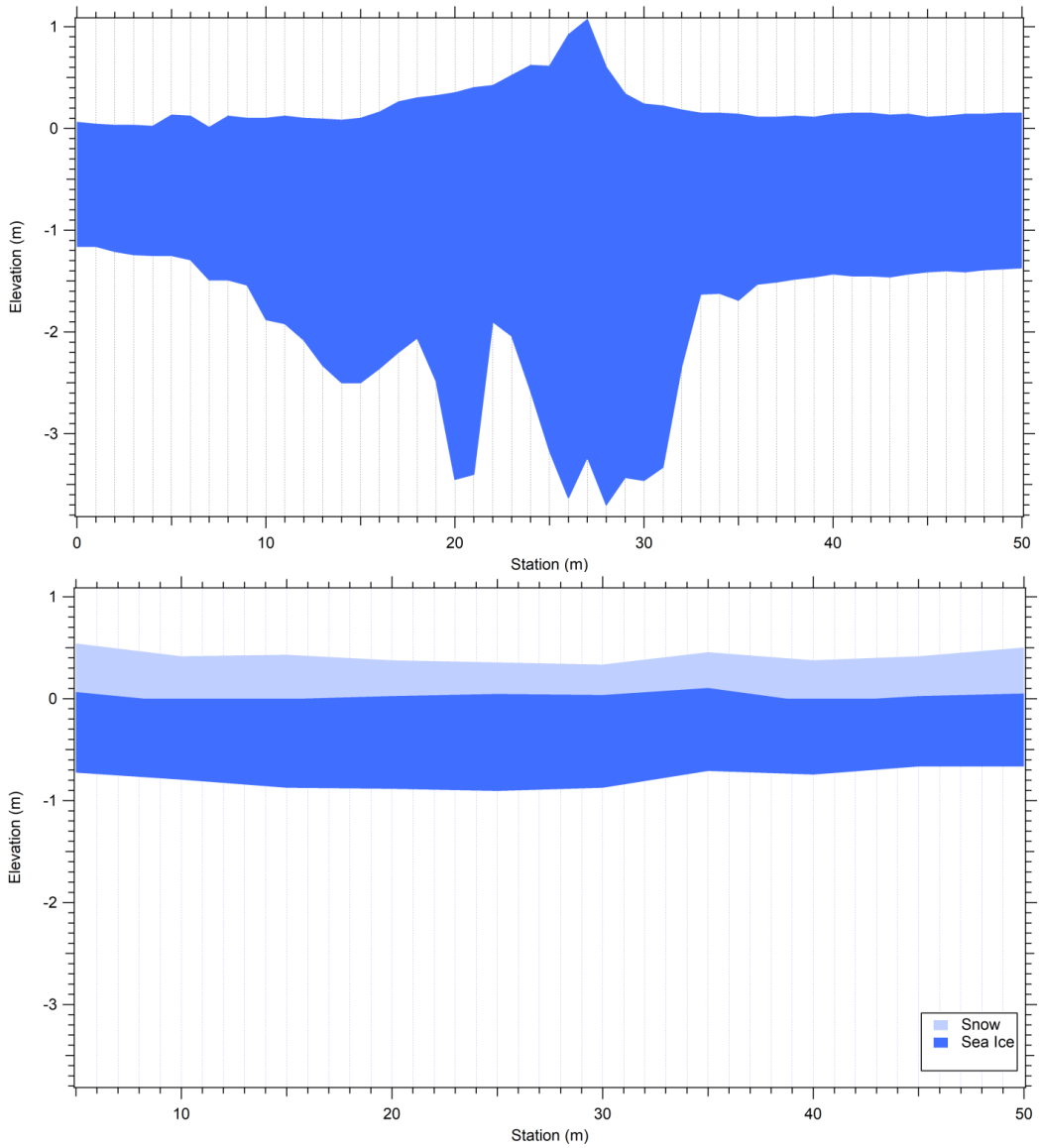

Fig. 5.2: Graphical presentation of sea ice thickness and its structure along two surveyed profiles. Top: Transect P-2 (Polarstern) with no snow cover. Bottom: Transect Q-10 (Qikiqtarjuaq) with relatively even and thinner sea ice. Note, for better comparison and to keep the figures in scale, only 50m of Q-10 transect is presented in the figure.

5.2 Methodology

Signal strength, depth sensitivity and signal quality of SIS coil configurations are primarily evaluated based on statistical and graphical analysis of experimental field data. In this analysis, field data are depicted in a series of plots to clearly illustrate signals behaviour in terms of different coil spacings (1 m, 2 m and 4 m coil spacing), coil orientation (HCOP and PRP orientation) and EM signal component (in-phase and quadrature component). The correlation between EM signal components and their dependency on sea ice thickness is investigated through graphical observations and by statistical means. Statistical tools and indices used for this investigation are mean, standard deviation and coefficient of determination (R^2).

Coil configurations that display stronger quadrature to in-phase signal correlations (high R^2 values) and stronger signal to drill-hole sea ice thickness measurements are considered to be more reliable for sea ice thickness inversions.

Since field data were collected from two entirely distinct regions in the Arctic Ocean, the results are analyzed and discussed in two separate sections followed by an overall assessment of the entire EM data collected. Unreliable data readings (negative values and outliers) were removed from all data sets prior to analysis.

5.3 Polarstern data

5.3.1 General signal observations

Visual observation along with drill-hole measurement results indicate that Polarstern transects contain a ridge sea ice structure in the middle of transects and young level sea ice on either side of the ridge sea ice zone. According to drill measurements, transect P-05 has a mean sea ice thickness of 1.76 m with a standard deviation (SD) of 0.63. Mean sea ice thickness and standard deviation of transect P-11 are 2.21 m and 0.94 respectively. These values indicate that transect P-11 has thicker sea ice and larger variability in sea ice thickness. Fig. 5.3 gives a visual representation of general differences in sea ice thickness variability between transect P-05 and P-11. The ridged sea ice type makes a significant contribution to the mean sea ice thickness of both transects. Transect P-11 contains shallow frozen melt pond zones that are unique to this transect.

These melt ponds have a mean depth of 0.24 m and are covered with a thin layer of ice with a mean thickness of 0.13 m.

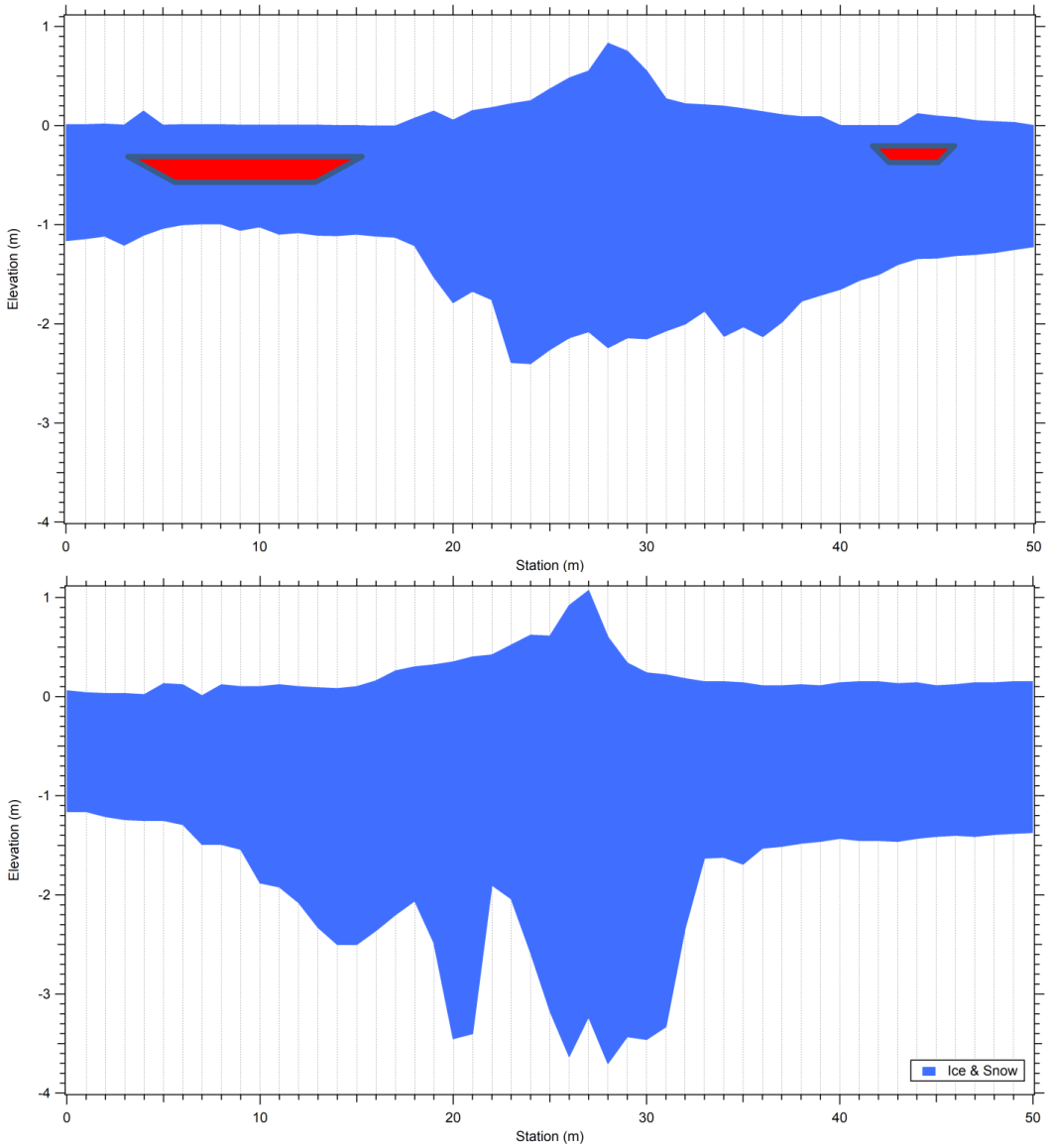

Fig. 5.3: Schematic presentation of sea ice thickness along transects P-05 and P-11. Sea ice thickness measurements are from drill-hole surveys performed at 1 m spaced intervals. Mid-sections of the profiles are ridged sea ice structure on the surface and keel at the bottom. The red coloured areas are refreezing melt-pond zones. The size and shape are approximate and not to scale.

Fig. 5.4 shows SIS signal readings for all possible coil configurations along transects P-05 and P-11. A common trend observed in Fig. 5.4 is decreasing signal strength (lower ppm values)

for all coil configurations as SIS moves towards the center of transects. This decreasing trend in signals is related to the sea ice thickness and sea ice structure along transects. Both P-05 and P-11 contain pressure ridge sea ice structure in the middle sections and relatively level sea ice on either side of the ridges. Ridged sea ice structure is characterized by lower EM signal strength. As SIS moves away from the ridged sea ice structures towards either end of the line transects, the ice thickness decreases, leading to stronger EM signal readings. All coil configurations follow the same signal strength pattern for both transects.

Transect P-05 shows an interesting signal anomaly from station 4 to 19 (Fig. 5.4). All coil configurations show a spike in the signal strength that begins at station 5 and ends at station 18. Quadrature signals component appear to be more influenced than IP signals component. The reason for this spike in signal readings may be explained by the presence of the melt-pond that extends from station 7 to 16.

The salinity of the melt pond should not differ from the surrounding sea ice cover. However, the ridging process in the middle of the transect may have contaminated the melt pond with brine contents. An increase in the salinity of the melt pond increases the bulk sea ice conductivity of the sea ice covered by melt pond and hence causing elevated EM signals relative to surrounding sea ice cover.

Interestingly, a second but smaller melt-pond extends from station 40 to 43. However, the signals over this smaller pond are not influenced with the same intensity as the larger pond. In fact, the only configurations that appear to be influenced by the smaller melt pond are quadrature responses of 1 m and 2 m PRR coil configuration. None of the 4 m coil spacing configurations show any apparent influence from the smaller melt pond. This can be explained due to the small length of the melt-pond and large footprint size of the 4 m coil spacing. Although, it appears that even with smaller footprints of 1 m coil spacing and 2 m coil spacing, only the quadrature signal of PRP orientation is influenced and all other configurations are unaffected. Another reason that may have contributed to smaller signal anomalies of the smaller melt pond may be explained by possible lower salinity of the smaller melt-pond compared to the larger melt-pond.

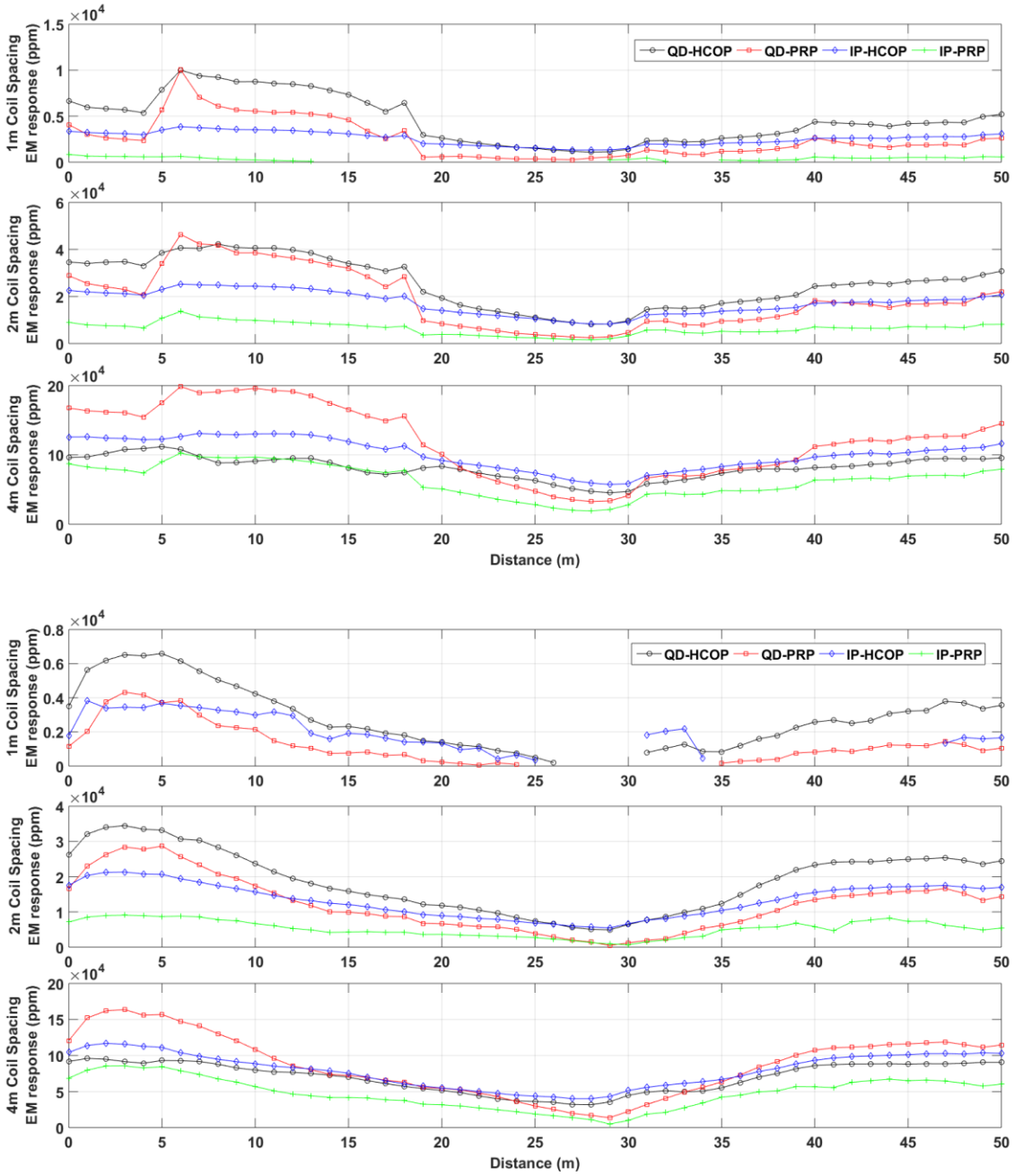

Fig. 5.4: Field SIS EM Signals plotted along transect P-05 (top) and P-11 (bottom) as a function of coil spacing. Signals are strongest (higher ppm) on either side of transects where sea ice is thinner and lowest in middle sections where ridged sea ice structure exists. The missing signal points were noisy unreliable data that were removed in the pre-processing stage.

5.3.2 Signal sensitivity of Polarstern data

Performing a general analysis on transects P-05 and P-11 field data reveals that regardless of what EM signal component (in-phase or quadrature) or coil orientation (HCOP or PRP) is utilized, 4m coil spacing configuration is the most sensitive coil spacing configuration towards the variability in sea ice thickness, followed by 2 m and 1 m coil spacing configurations (Fig. 5.5) at the observed sea ice thickness range. This is indicated by stronger in-phase and quadrature signal readings on both P-05 and P-11 transects (Fig. 5.5).

Within 4 m coil spacing configurations, quadrature PRP configuration records the strongest EM responses followed by in-phase HCOP, quadrature HCOP, and in-phase PRP coil configuration. However, the quadrature PRP response is no longer the dominant signal recorded once sea ice thickness exceeds a 1.8 m limit (Fig. 5.4). The in-phase HCOP signal gradually overlaps and bypasses quadrature PRP signal strength, reaching its maximum divergence over the peak of the ridged sea ice zone. This transition in signal components can be observed on stations 21 to 39 in transect P-05 and on stations 12 to 35 in transect P-11.

For 2 m and 1 m coil configurations, quadrature HCOP response readings dominate for the most part of the transect. However, this changes when in-phase HCOP readings overlap or even exceed, quadrature HCOP signal readings as soon as sea ice thickness exceeds certain limits near the peak of the ridged zone. The limit of the ice thickness at which this change occurs is roughly around 3 m. This is due to the change in sensitivity of different coil orientations as shown in chapter 4.

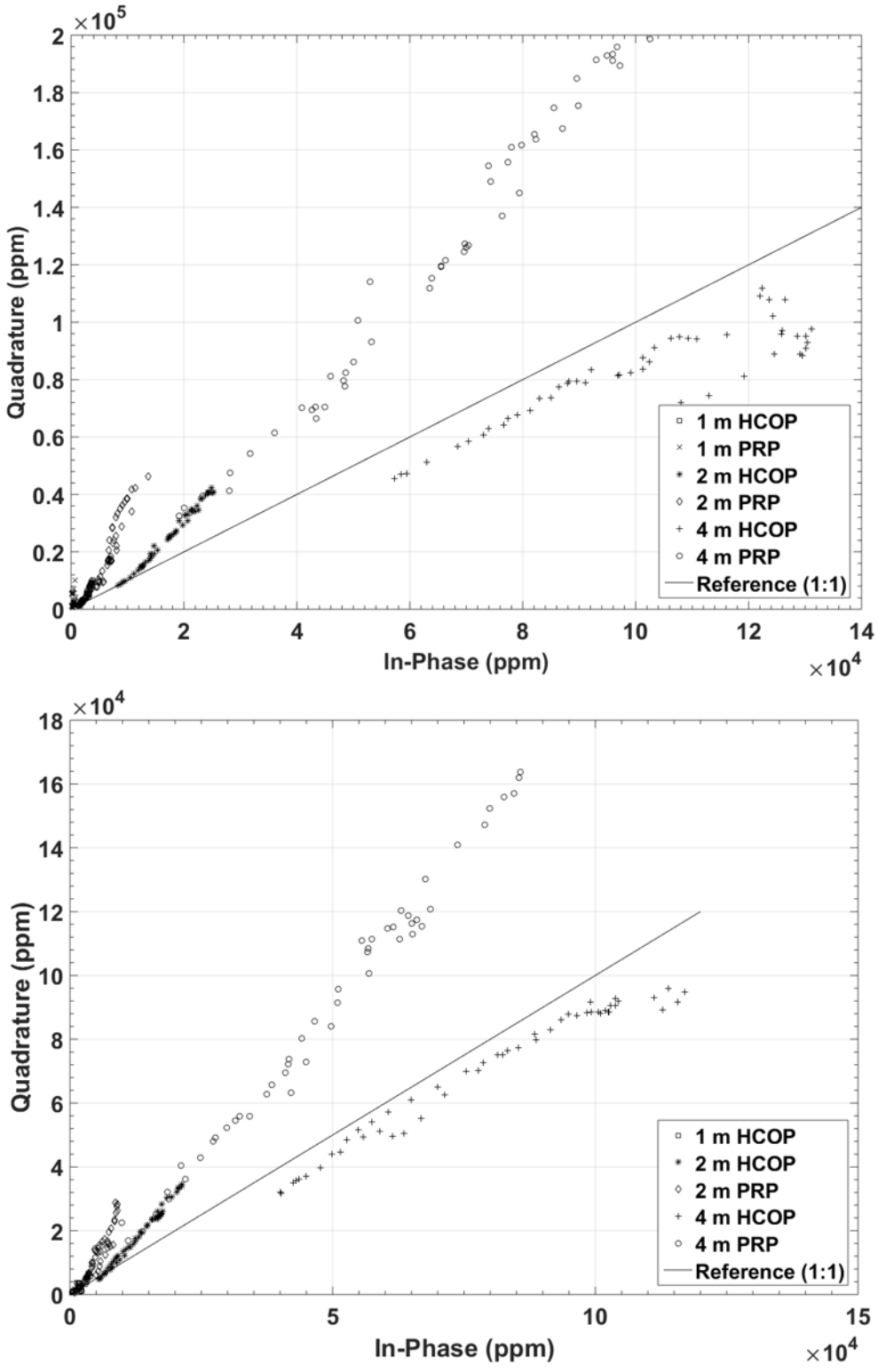

Fig. 5.5: Quadrature versus in-phase signal for all three coil spacing for P-05 and P-11 transects. For transect P-11 the 1 m PRP data were unreliable to be used in this analysis.

To determine which coil configuration yields the highest signal quality, the correlation between in-phase and quadrature response readings and their distribution on plots are examined. Theoretically in-phase and quadrature data components should generally have a good linear correlation. A statistical analysis was used to investigate the correlation between in-phase and quadrature components of measured EM response for both transects. The in-phase response values were plotted against quadrature response values in Fig. 5.6 and 5.7. A visual inspection of transect P-05's correlation plots shows a lens like data distribution. This lens like coil distribution is more obvious in 1 m HCOP and PRP coil configuration, 2 m PRP configuration and 4m HCOP configuration. An in-depth examination of the data indicates that one side of the lens pattern is associated with the signals acquired over the melt-pond. These data points are circled in red in Fig. 5.6.

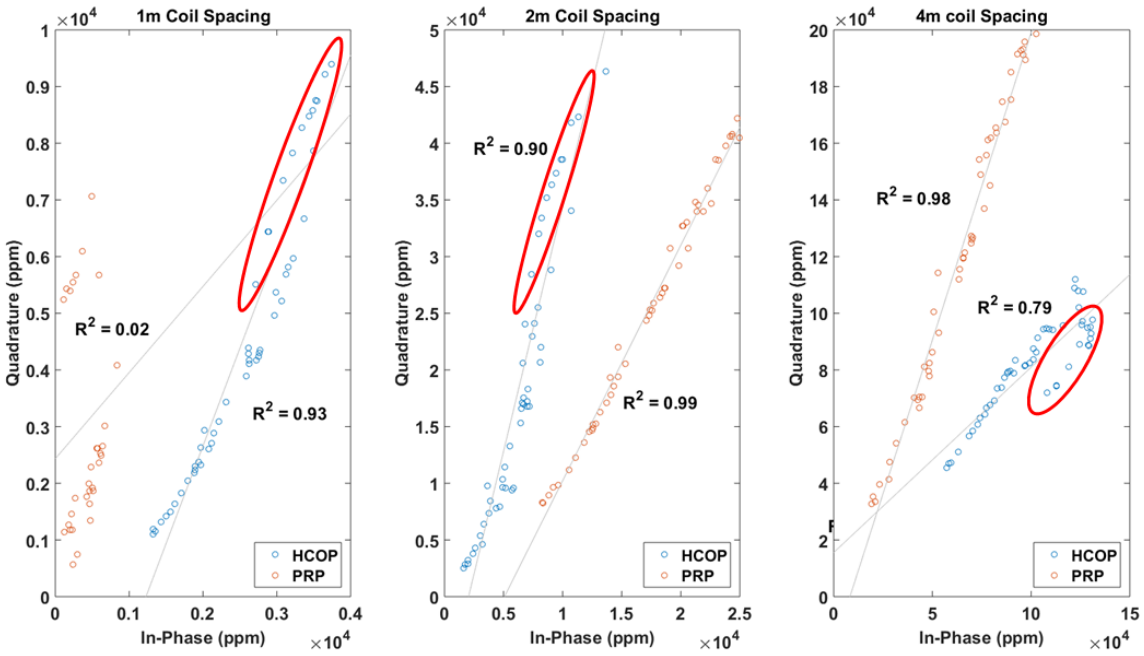

Fig. 5.6: HCOP and PRP, quadrature vs. in-phase signals for 1 m coil spacing (left), 2 m coil spacing (middle) and 4 m coil spacing (right) for transect P-05.

Visual inspection of transect P-11 correlations (Fig. 5.7) shows particularly noisy data points for 1 m coil spacing configurations and 2 m PRP coil configuration. Surprisingly these noisy data points do not correspond to any specific sea ice type along the transect as it was the case for transect P-05. These data points belong to level sea ice zones on either side of the ridged sea ice

type where even the subsurface sea ice zone appears to be relatively uniform. There is not enough information available to explain what might have caused the noisy data points.

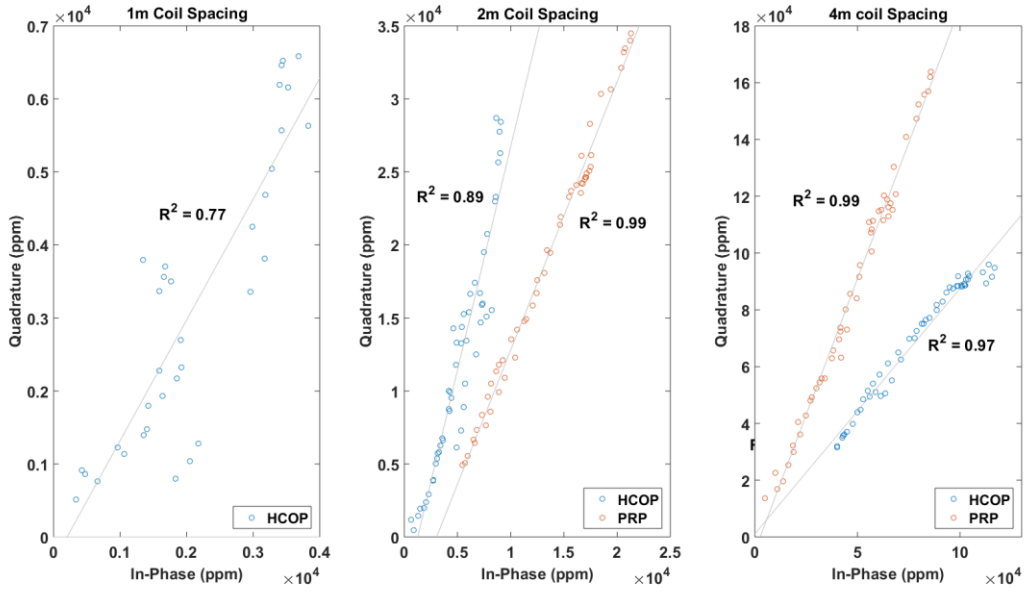

Fig. 5.7: HCOP and PRP, quadrature vs. in-phase signals for 1 m coil spacing (left), 2 m coil spacing (middle) and 4 m coil spacing (right) for transect P-11. 1 m coil spacing PRP data were noisy and unreliable to be used in this analysis.

Linear regression was applied to the data and coefficient of determination values (R^2) for both transects were calculated (Table 5.2). According to table 2, the R^2 values indicate that the majority of the coil configurations show a strong correlation between the in-phase and quadrature responses. However, the objective is to determine what configurations common to both transects, yields the highest data quality that can be used for sea ice thickness inversions.

Table 5.3: Calculated R-squared values for the regression of in-phase and quadrature EM responses in Fig. 5.6 and Fig. 5.7.

Profile	P-05		P-11	
Configuration	HCOP	PRP	HCOP	PRP
1 m spacing	0.93	0.02	0.77	-
2 m spacing	0.99	0.90	0.99	0.89
4 m spacing	0.78	0.98	0.97	0.98

According to the R^2 values, in 4 m coil spacing category, PRP orientation yields the highest quality data for both transects. HCOP orientation of transect P-11 also yield high R^2 value but in transect P-11, R^2 coefficient is not equally strong. With the 2 m coil spacing, the HCOP coil

configuration shows the highest data quality with respect to R^2 values. PRP configurations also show a reasonably high R^2 value, but compared to the HCOP configuration, HCOP performs better by 10%. Due to the presence of noisy data in 1 m spacing configurations, no reliable conclusion can be made as to which configuration offers the highest quality data common to both transects.

EM responses collected on transects P-05 and P-11 were plotted collectively as a function of drill-hole sea ice thickness for all coil configurations (Fig. 5.8). Transect P-05 shows a good correlation between signal readings and sea ice thickness measurements for all coil configurations except for 2 m and 1 m in-phase PRP configurations. In 4 m coil spacing category, it is evident that PRP configuration yields the highest quality data featuring both strong signals and great signal to sea ice thickness correlations. In this category 4 m, PRP quadrature signal is outstanding. This component records both the strongest and widest signal range, making it the most reliable signal reading within this coil space category.

In the 2 m coil spacing category, HCOP configuration shows very good signal to sea ice thickness correlations. The HCOP quadrature response component appears to be the strongest signal in this category. Arguably PRP quadrature response may also be considered a good candidate in this category as it also possesses the same signal strength and a wider signal range than HCOP quadrature response. However, the signal to sea ice thickness correlation of PRP quadrature response is not equally as strong.

For 1 m coil spacing category, HCOP coil configuration yields reasonably good signal to sea ice thickness correlation. HCOP quadrature response is the winner in this category as it captures the strongest responses and has a wide signal range relative to other configurations.

For transect P-11, correlations between signal responses and the ice thickness measurements are weaker compared to transect P-05. Transect P-11 display a noisier data set compared to transect P-05. This is especially more evident in smaller coil spacing configurations. The source of this noise may be explained by the more complex keel sea ice structure of this transect. Transect P-11 has a considerably larger ridged sea ice zone with significant fluctuation in sea ice thickness and sharp keel boundaries (stations 18 to 25 and stations 31 to 34) (Fig. 5.2). Such extreme fluctuation in sea ice thickness may also be indicative of a significantly more complex internal sea ice structure.

Smaller coil spacing configurations are more responsive to this extreme sea ice thickness fluctuation. This is attributed to the footprint size of different coil spacings. The larger the coil

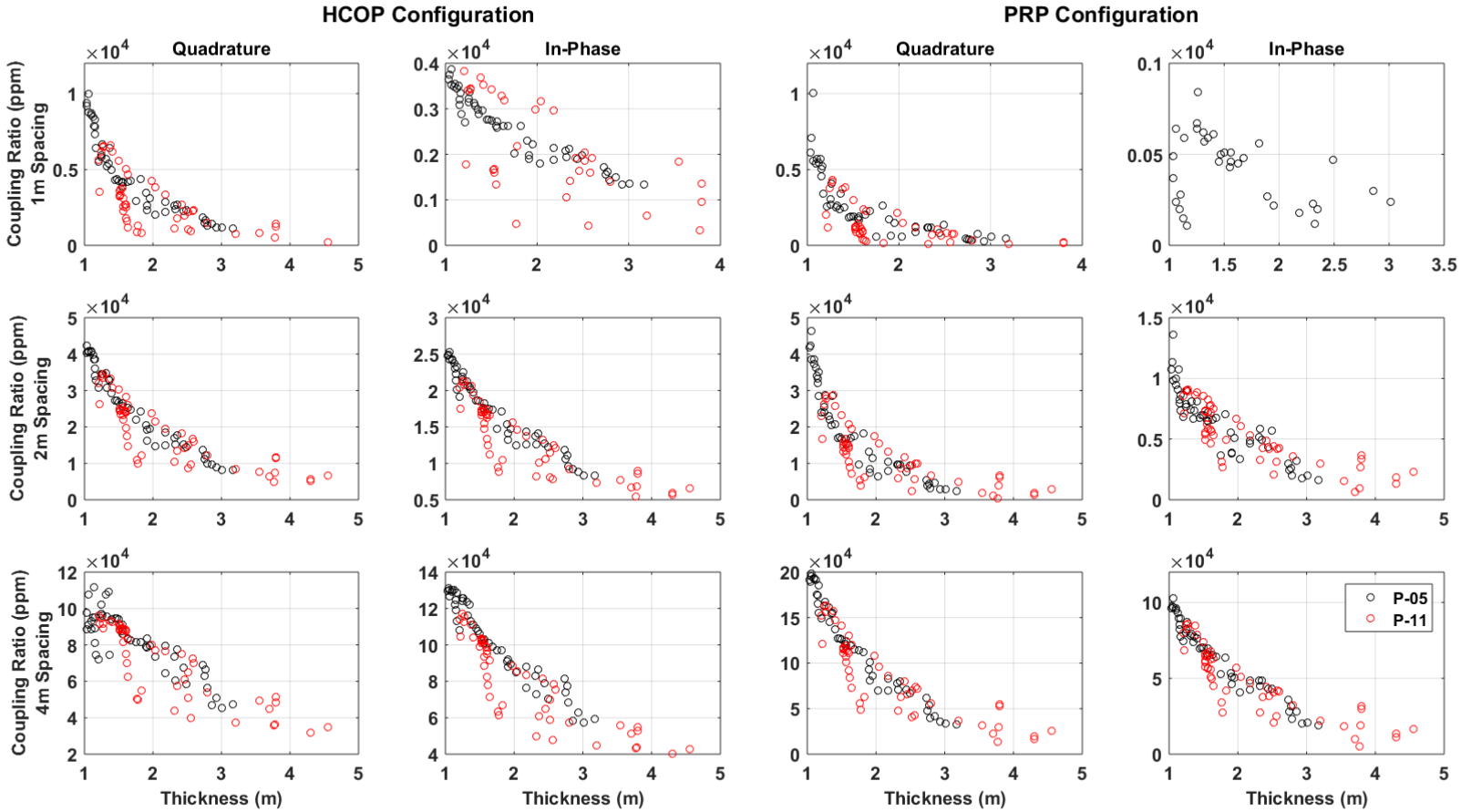

Fig. 5.8: Signal (In-phase and quadrature response) vs. sea ice thickness from drill-hole data for entire Polarstern EM data.

spacing is, the larger the footprint size. Larger footprint size implies that the signal recorded is the average of sea ice thicknesses of a larger area under the instrument; this causes smoothing of the data. With the smaller coil spacing, smoothing is less significant to smaller footprint size. 4 m PRP and 2 m HCOP coil configurations appear to show the strongest correlations for transect P-11. The same observations made for transect P-05 can be recognized for transect P-11.

In the 4 m coil spacing category, the quadrature component of PRP orientation yields the most reliable signal readings. For 2 m coil spacing category quadrature component of the HCOP orientation records the most reliable signal readings. For 1 m coil spacing, however, HCOP quadrature readings are not conclusive as there is significant signal sharing for ice thicknesses above 1.6 m.

The overall assessment of the data suggests that there is a good consistent coherency in SIS performance. The data overlap between the two transects confirms this coherency.

An overall analysis of the Polarstern data based on signal quality and strength suggest that 4m PPR coil configuration yield the most reliable EM responses followed by 2 m and 1 m HCOP coil configurations. Although 1 m HCOP coil configuration displayed reliable data for transect P-05, transect P-11 did not show the same good quality results. This is due to the much smaller skin depth and therefore limited sensitivity at higher sea ice thicknesses. These limitations of the 1 m coil spacing should be considered when measuring sea ice with thicknesses of over 1.5 m.

5.4 Qikiqtarjuaq data

5.4.1 General observations

Qikiqtarjuaq sea ice is classified as land-fast sea ice (sea ice that is attached to the coastline). The sea ice condition of the study site is generally influenced by an early melt season. The ice in many areas is covered with snow that is extremely saturated with water (slush) and is obscured by a layer of fresh snow cover. The source of slush is predominantly snowmelt water and in some areas it is the sea water that infiltrates through sea ice cracks upward onto the sea ice surface, flooding the ice surface. Thus, for the most part, sea ice in Qikiqtarjuaq can be characterized by three distinct layers of snow and ice: the bottom sea ice layer, the water-saturated snow layer in the middle and the fresh snow layer on top. Five transects were established at different locations within the study sites. To validate EM measurements, drill-hole measurements were also taken along each transect.

5.4.2 Signal Sensitivity Analysis by Transects

Transect Q-10

Transect Q-10 consist of level sea ice with average bulk (snow and ice) sea ice thickness of approximately 1.18 m with standard deviation (SD) of 4.9 cm. Average snow cover depth for this transect is about 0.39 m with SD of 5 cm. According to the drill measurements, sea ice surface and thickness is fairly even along transect Q-10 (Fig. 5.8). EM data were acquired at 5- m spaced intervals. The variation in EM signals along transect Q-10 (Fig. 5.10) is consistent with the ice thickness variation (Fig. 5.9).

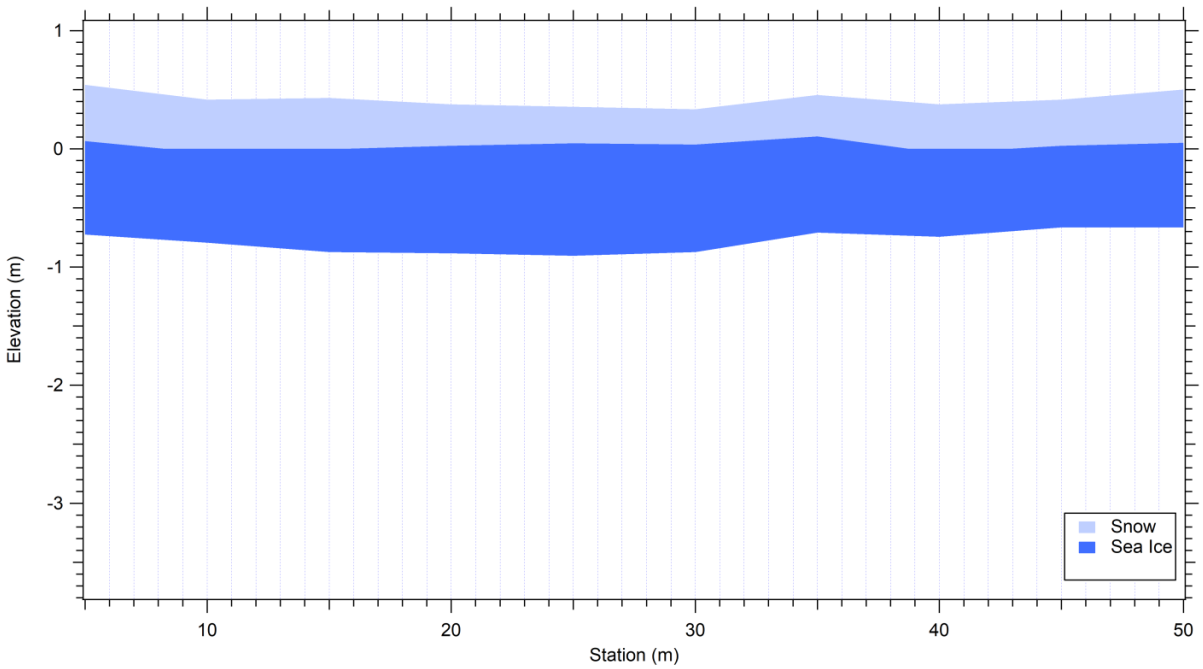

Fig. 5.9: Schematic presentation bulk sea ice thickness along transect Q-10. Drill-hole measurements were made at 5 m spaced intervals. Sea ice thickness is relatively even along the 100 m long transect. Drill-hole measurements were taken for only the first 50 m interval.

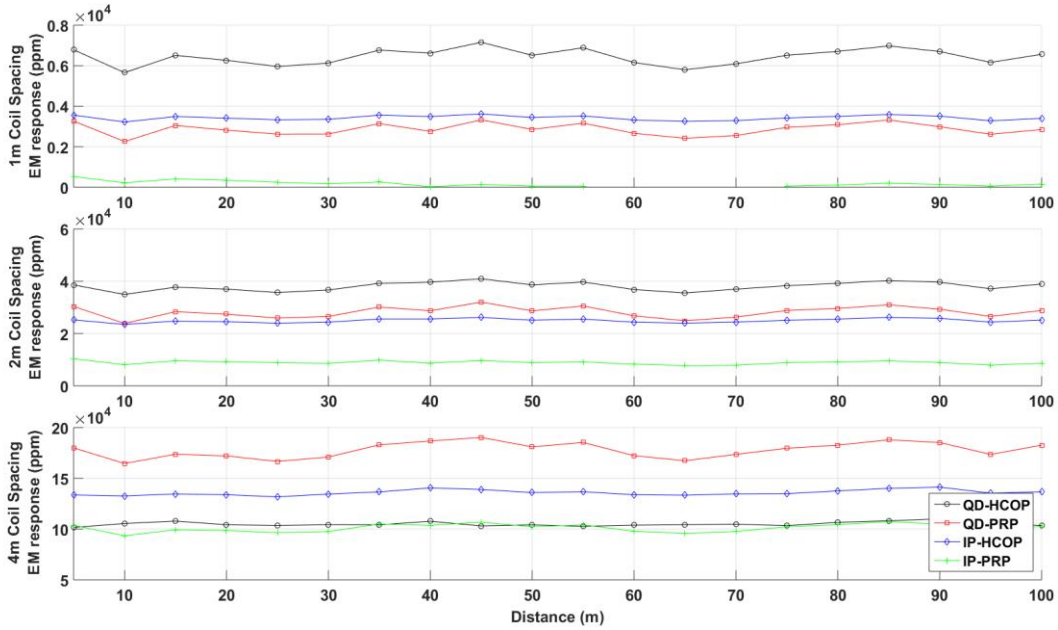

Fig. 5.10: EM signals of all SIS configurations along transect Q-10. Top: 1 m coil spacing configurations, middle: 2 m coils spacing configuration, bottom: 4m coil spacing configurations. SIS acquired data at 5 m spaced intervals.

By performing a basic signal analysis (Fig. 5.10 & Fig. 5.11), it is evident that 4 m coil spacing configurations yield the strongest signals returns followed by 2 m and 1 m coil spacing. The range of the measured signals decreases with smaller coil distance. The range of the EM signals collected at transect Q-10 is significantly smaller compared to Polarstern EM signals for all coil configurations. This can be explained by the thinner sea ice cover of the site and the small variation in sea ice thickness along the transect. This difference in signal range is expected to be valid for most of the data collected in Qikiqtarjuaq as sea ice is noticeably thinner for Qikiqtarjuaq transects compared to Polarstern transects.

A more in-depth evaluation of signals strength reveals that the quadrature signal response is strongest in PRP orientation and weaker in HCOP orientation for 4 m coil spacing configuration (Fig. 5.11). For 2 m and 1 m coil spacing configurations, however, HCOP quadrature responses are stronger than PRP quadrature responses (Fig. 5.11). The in-phase signal responses are stronger in HCOP orientation and weaker in PRP orientation regardless of which coil spacing is used (Fig. 5.11).

Figure 5.11 demonstrates that 4 m coil spacing PRP quadrature response is the strongest signal. For 2 m and 1 m coil spacings, HCOP quadrature signals are strongest. The weakest signal belongs to 1 m PRP coil configuration. In the pre-processing stage (data quality assessment), many of the 1 m PRP coil configuration signal readings were invalid with the rest of the data being dubious.

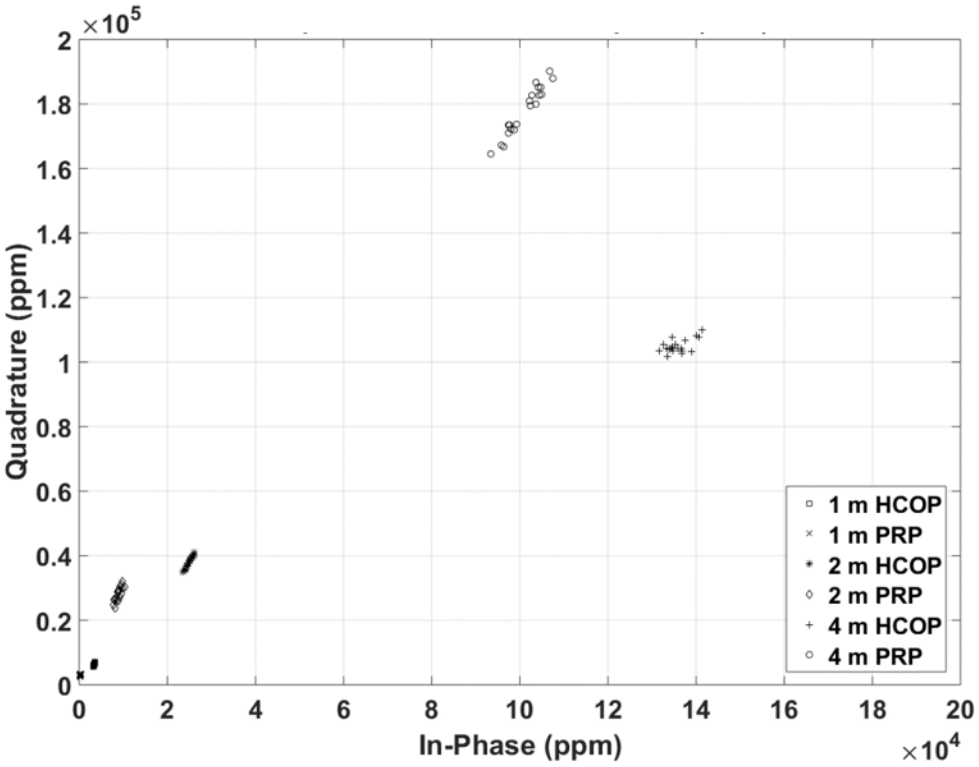

Fig. 5.11: Quadrature versus in-phase EM response of transect Q-10 for all coil spacings and orientations.

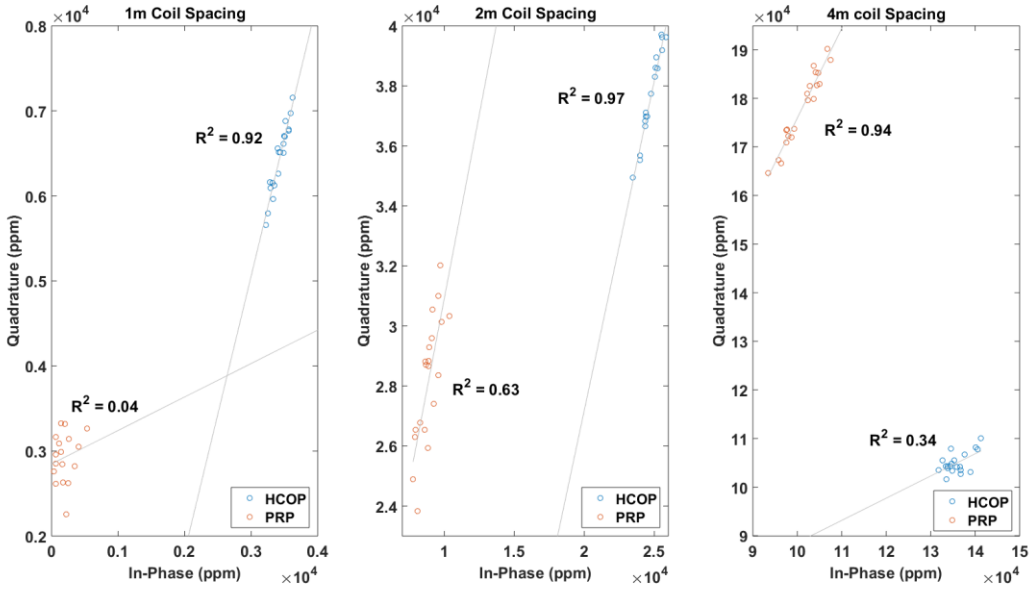

Fig. 5.12: HCOP and PRP, quadrature versus in-phase signals for 1 m coil spacing (left), 2 m coil spacing (middle) and 4 m coil spacing (right) for transect Q-10.

To identify which configuration yields the highest data quality, the correlations between signal components and their corresponding drill-hole sea ice thickness measurements were investigated. Ideally, a reliable configuration should show a strong correlation between in-phase and quadrature responses. A reliable signal component should show a strong correlation with its corresponding drill-hole measurements. Based on Fig. 5.12, strongest correlations between in-phase and quadrature readings belong to 1 m and 2 m HCOP configurations with R^2 values of 0.92 and 0.97 respectively, and 4m PRP coil configuration with an R^2 value of 0.94. These strong correlations may indicate that 4 m PRR configuration along with 2 m and 1 m HCOP coil configurations yield the highest quality data among all possible SIS coil configurations.

There is a non-linear exponential correlation between EM signals and sea ice thickness (Chapter 4). However, a look into EM signals to sea ice thickness correlations for transect 10 (Fig. 5.13), does not reveal any correlation between the two variables. This can be explained by the small range in sea ice thickness variation (1 m to 1.3 m) and sea ice slush content that cannot be efficiently resolved by SIS.

Although the correlation between EM signals and sea ice thickness is an exponential correlation (Fig. 4.3 & 4.4), a linear fit may be appropriate within this small sea ice thickness range.

To quantify EM signal to sea ice thickness correlation, linear regression is applied. The R^2 values are low but yet they are in line with the results observed with respect to configurations that yield the highest quality data. As noisy as the data may appear, the 1 m and 2 m HCOP configurations yield highest correlations within their coil spacing categories. The 4 m configuration, however, shows that in-phase signal in both PRP and HCOP yields highest data quality. The overall trend for most coil configurations shows increasing signal strength with an increase in sea ice thickness. However, this trend is dismissed for 1 m in-phase PRP signal. As stated before, data collected on this channel are not reliable.

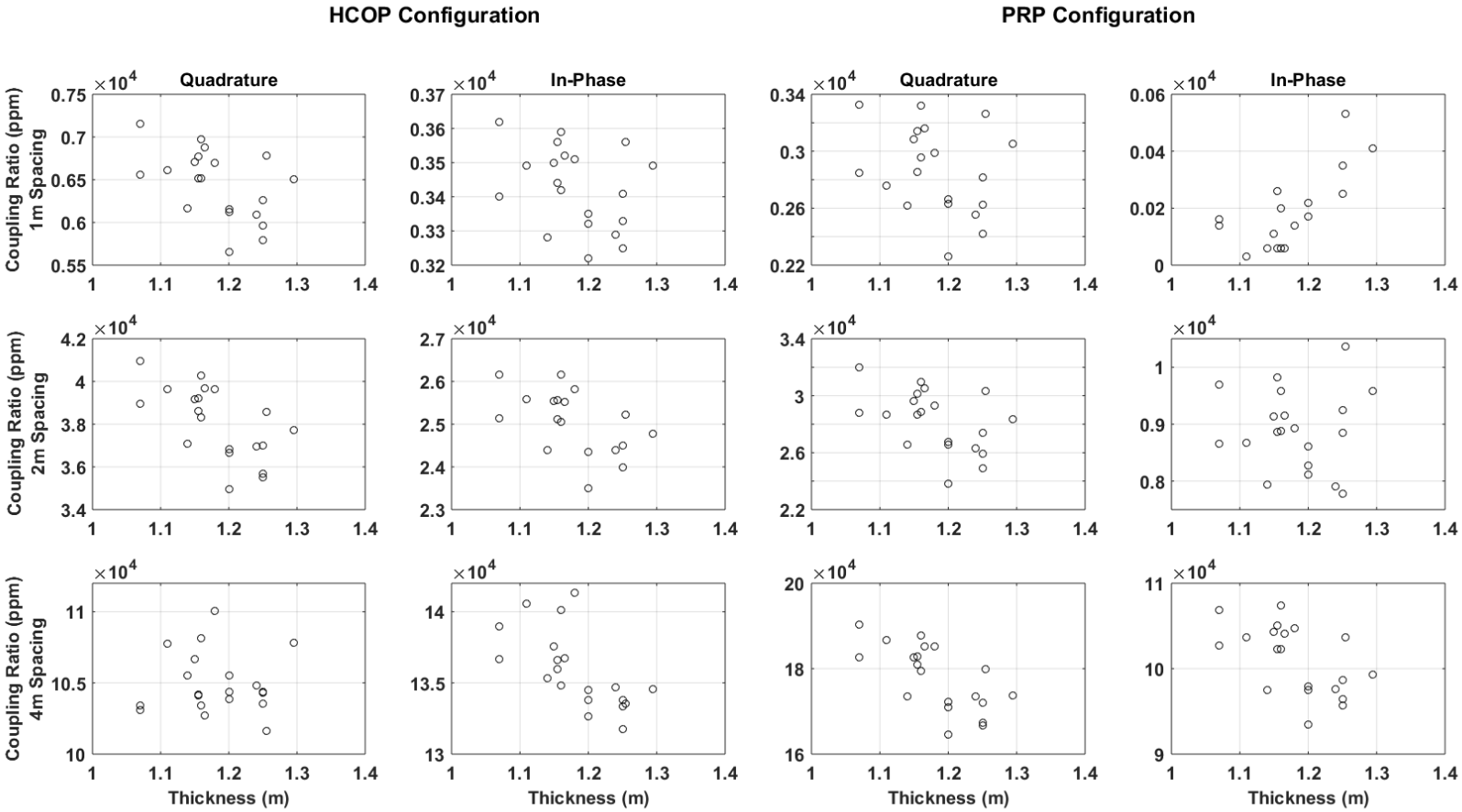

Fig. 5.13: Signal (quadrature and in-phase response) versus drill-hole sea ice thicknesses for transect Q-10.

Transect Q-11

Transect Q-11 is level sea ice covered with slush sections that are unevenly distributed along the transect. Slush is obscured by snow cover and is only visible when snow cover is disturbed. Average bulk sea ice thickness from drill data is approximately 0.91 m with a SD of 6.8 cm. Average snow cover depth is approximately 0.4 m with a SD of 3.4 cm. Drill-hole measurements were taken at 5 m spaced intervals for the first 45 m of the transect. An effort was also made to measure the depth of slush at the drill-hole locations. The slush depth ranged between 6 to 10 cm below snow depth. However, slush measurements are less accurate because determining the upper boundary of the slush layer proved to be difficult.

Signal readings for transect Q-11 (Fig. 5.14 & 5.15) are generally stronger relative to transect Q-10. Sea ice at this site is thinner relative to transect Q-10 which leads to stronger signal readings. Another factor leading to an increase in signal strength is the source of slush. If snow is saturated with conductive sea water seeping from under the sea ice, then higher conductivity of the bulk ice layer is expected, which leads to higher deceptive signal readings that are not a true representative of the actual sea ice thickness.

In general, signals behavior on transect Q-11 is very similar to transect Q-10 (Fig. 5.10). The range of the signals are very similar to transect Q-11, however, for the 2 m coil spacing configurations, transect Q-11 show partial overlap within the quadrature responses of HCOP and PRP orientations.

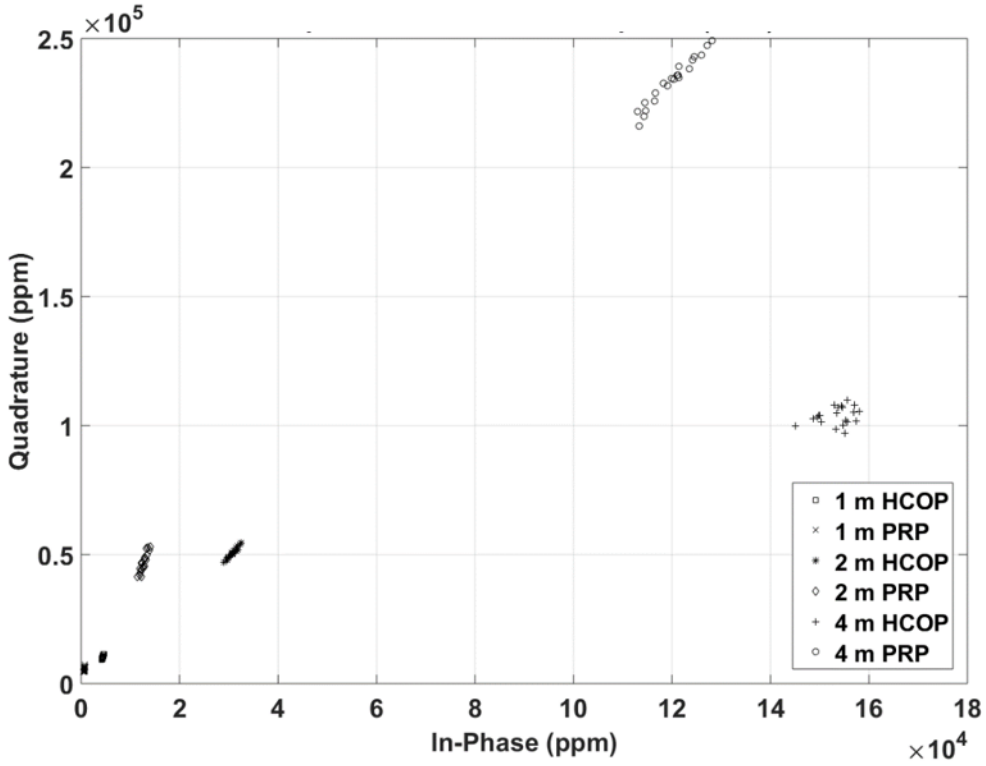

Fig. 5.14: Quadrature versus in-phase EM response of transect Q-11 for all coil spacings and orientations.

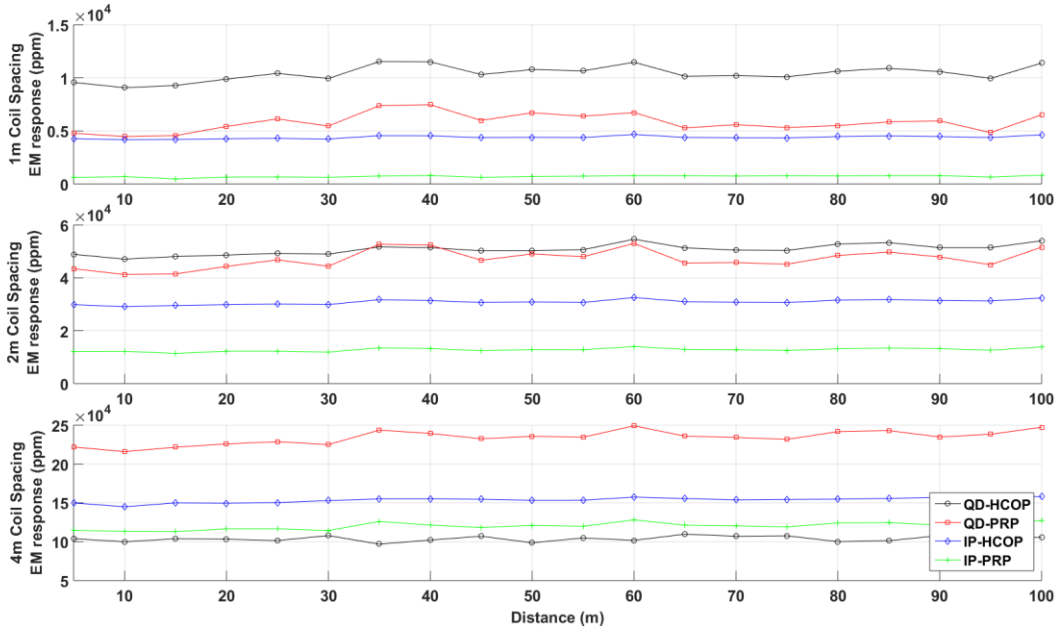

Fig. 5.15: EM response of all SIS configurations along transects Q-11. Top: 1 m coil spacing configurations, Middle: 2 m coils spacing configuration, Bottom: 4 m coil spacing configurations. SIS acquired data at 5 m spaced intervals.

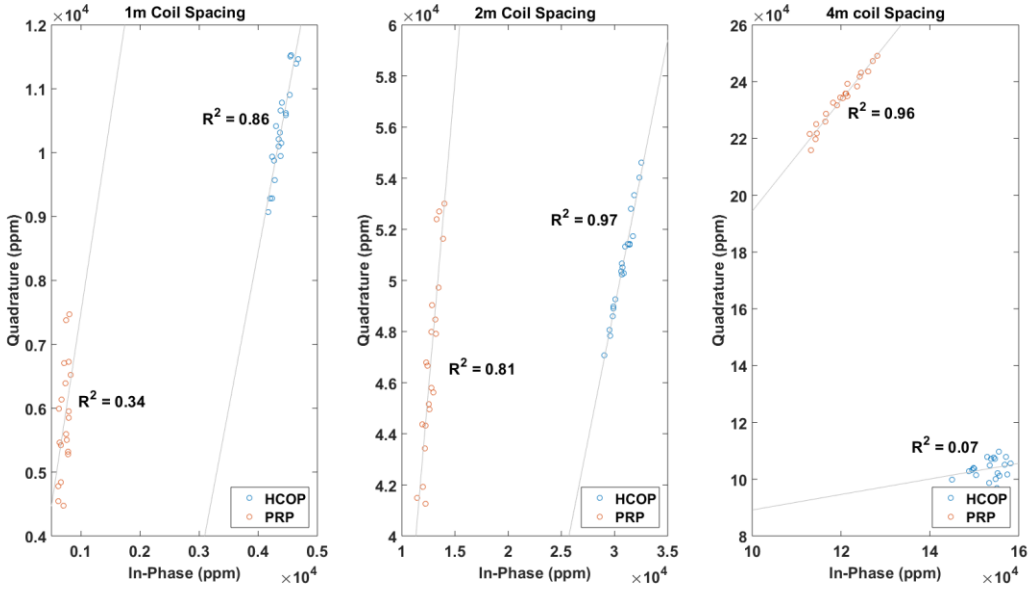

Fig. 5.16: HCOP and PRP, quadrature versus in-phase signals for 1 m coil spacing (left), 2 m coil spacing (middle) and 4 m coil spacing (right) for transect Q-11.

According to (Fig. 5.16) 4 m PRP (R^2=0.96), 2 m HCOP (R^2=0.97) and 1 m HCOP configurations (R^2=0.86) display the strongest correlations. However, no reliable conclusion can be made by analyzing signals based on signals to sea ice thickness correlations (Fig. 5.17). Calculated R^2 values for all signals are very low. Visual assessment of the plots reveals a very interesting pattern. It appears that contrary to the expectations, the signal strength increases with an increase in sea ice thickness. An explanation to this is most likely the presence of slush that has its source in seawater seepage. From the drill survey data, slush depth increases along the transect. The increase in ice thickness is accompanied by an increase in slush volume which in turn also increases bulk sea ice conductivity and therefore stronger signal readings.

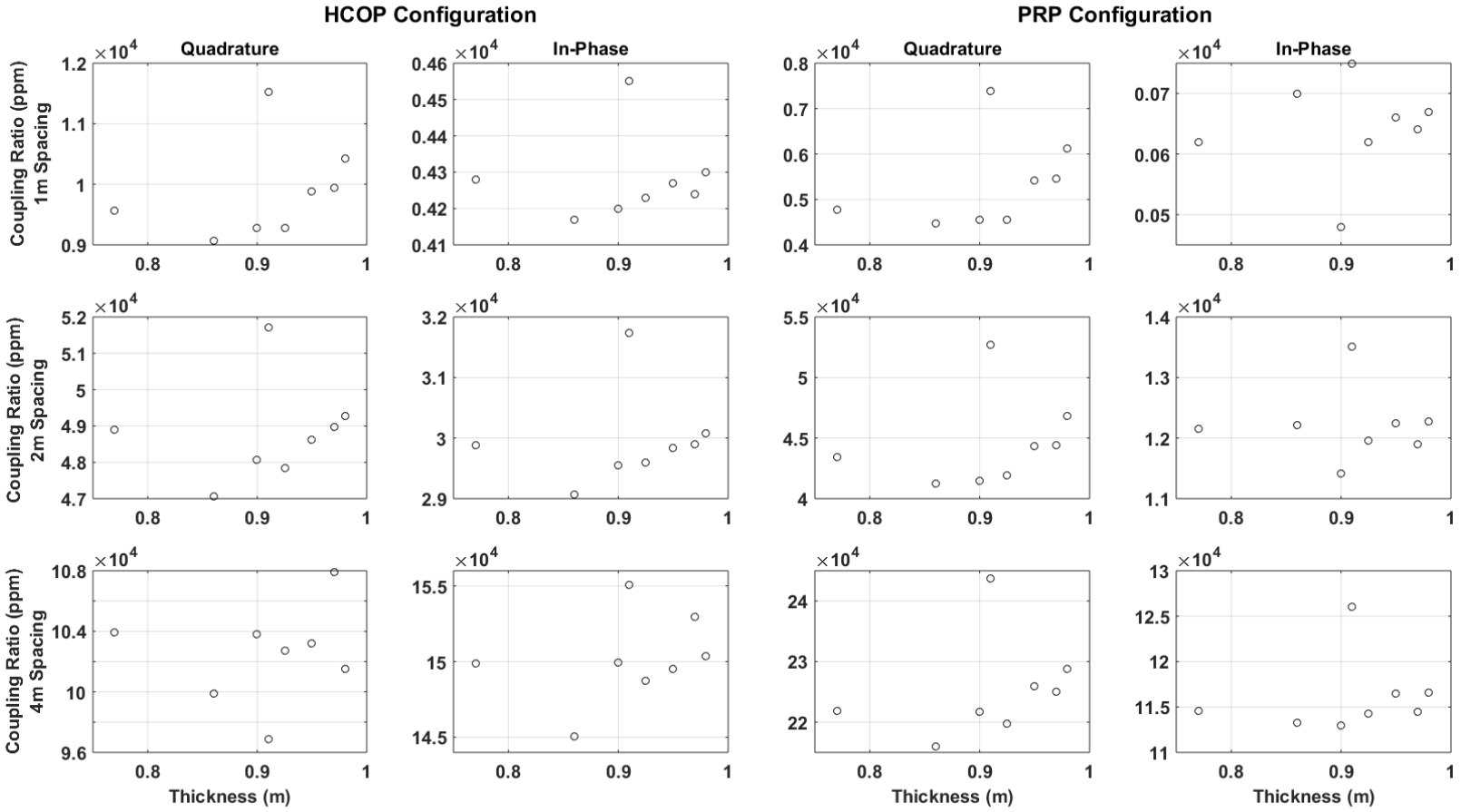

Fig. 5.17: EM signals (quadrature and in-phase response) versus drill-hole sea ice thicknesses for transect Q-11.

Transect Q-12

Transect Q-12 is located near the shoreline. Mean bulk sea ice thickness from drill measurements is about 1.4 m with a SD of 0.9 m. Sea ice at this location represents deformed sea ice formatiton. The ocean currents have pushed the sea ice towards the shoreline and as a result rafting of the sea ice occurred. Due to the geographical location of the site, sea ice deformations are not severe. However, the structure and complexity of the sea ice is significant and is confirmed by the difficulties faced during drill measurements. Unlike previous transects where sea ice surface was relatively flat, this site shows moderate but noticeable uneven sea ice surface structures. The transect stretches 100 m outward away from shoreline towards the sea. EM measurements were taken at 2 m spaced intervals. An effort was made to take detailed drill-hole measurements to cover the complexity of the ice structure of the site, however, due to the difficulty of the task, drill measurements were only taken for part of the transect (stations 0 to 38) at 2 m spaced intervals.

The signal behavior of transect Q-12 (Fig. 5.18 & 5.19) is very similar to previous transects, however, the signal strength is weaker for all configurations. The weaker signal is explained by the presence of relatively thicker sea ice thickness and the absence of slush areas. Another observation made is that 4 m HCOP configuration shows a linear data distribution and a strong signal correlation of R^2 =0.82 (Fig 5.19 & 5.20). The previous transects displayed a cluster distribution with very low R^2 values (Q-10 R^2=0.34, Q-11 R^2=0.07) for the same coil configuration.

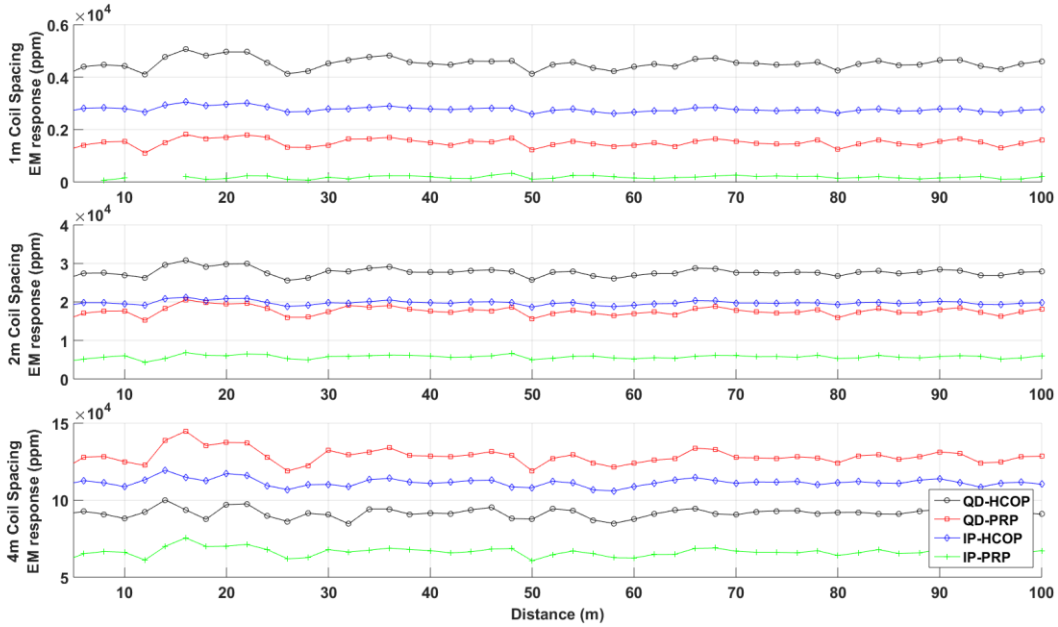

Fig. 5.18: EM response of all SIS configurations along of transect-Q-12. Top: 1 m coil spacing configurations, Middle: 2 m coils spacing configuration, Bottom: 4 m coil spacing configurations. SIS acquired data at 5 m spaced intervals.

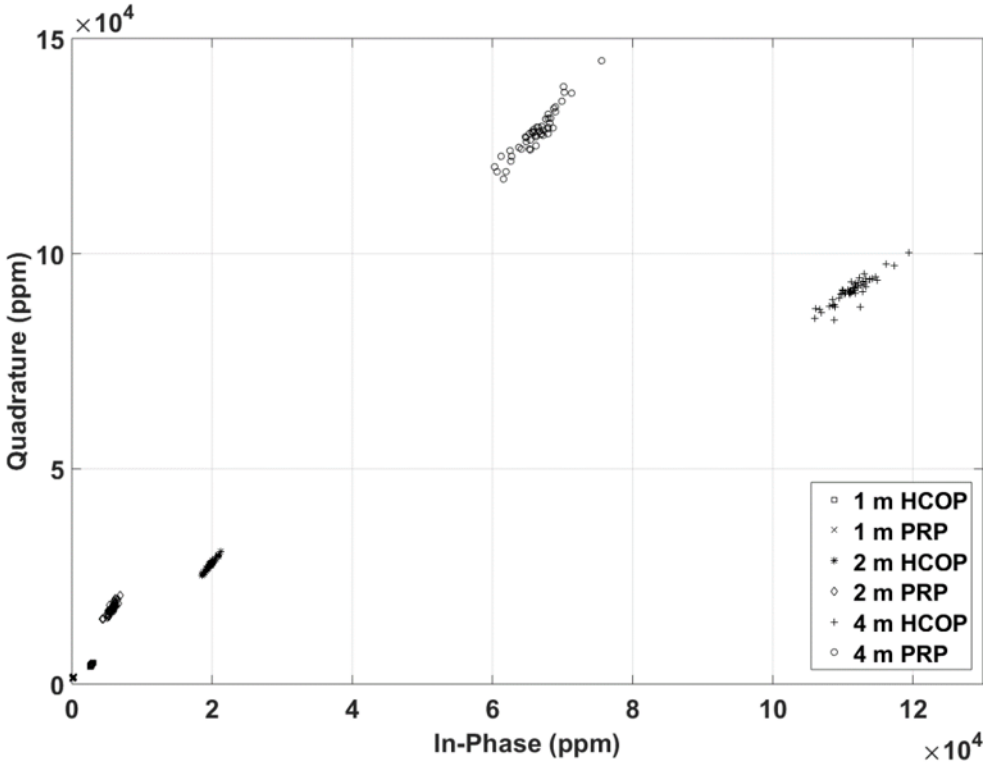

Fig. 5.19: Quadrature versus in-phase EM response of transect Q-12 for all coil spacings and orientations.

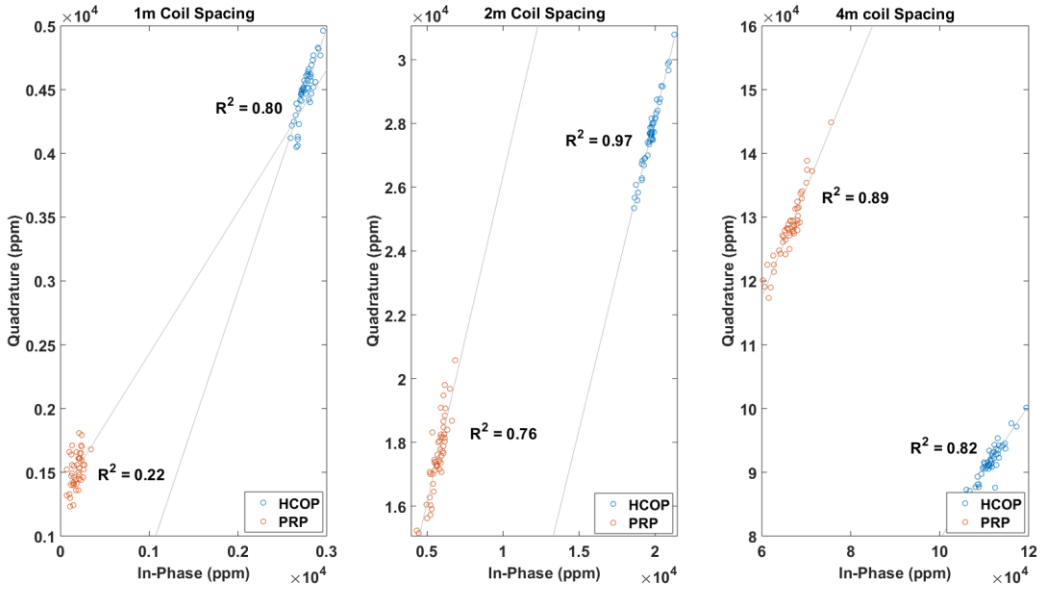

Fig. 5.20: HCOP and PRP, quadrature versus in-phase signals for 1 m coil spacing (left), 2 m coil spacing (middle) and 4 m coil spacing (right) for of transect Q-12.

Looking into signal to sea ice thickness correlation (Fig. 5.21), none of the coil configurations show a good correlation. In fact, although all lines show an overall increasing signal strength with decreasing sea ice thickness for most coil configurations; data appears to be randomly distributed and ambiguous. The narrow range in sea ice thickness and the complexity of the sea ice structure presents a poor correlation.

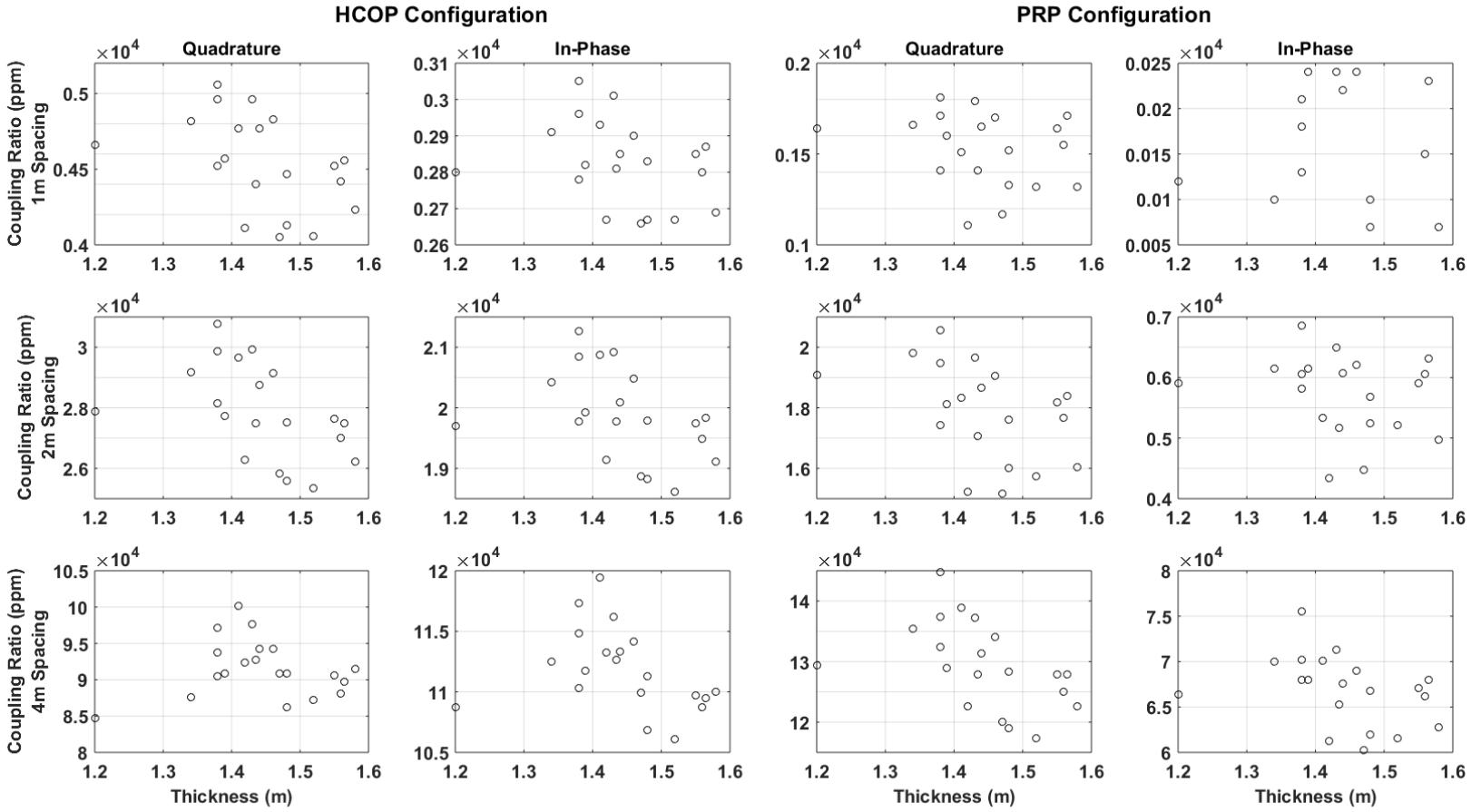

Fig. 5. 21: EM signal (quadrature and in-phase response) versus drill-hole sea ice thicknesses for transect-Q-12.

Transect Q-13

Transect Q-13 was established in an area known by the locals to have some of the thinnest sea ice in the region. Most of the study site was heavily flooded with seawater from a nearby ice hole augured the day before the survey operation and was re-opened for scoop-diving activity just before the survey operation was conducted. Slush condition got worse during the operation due to the ongoing flow of the sea water onto the ice surface. Survey operation was extremely difficult and slow due to the excessive slush volume in the area. Mean sea ice thickness from the drill data is approximately 1.19 m with SD 4.3 cm. Average snow depth is 0.46 m with SD of 2.8 cm. To check the repeatability of the EM data over transect Q-13, EM measurements were taken a second time retracing the transect from the last station to the initial starting point.

The EM data acquired on this transect obey the same general signal strength patterns observed in the previous transects, (Fig. 5.22). However, there is an interesting similarity between transect Q-13 and Q-11 which also contained slush volumes but to a lesser degree. There is a partial overlap of quadrature measurements between the higher signal range of 2 m HCOP configuration with the lower range of 2 m PRP configuration that can also be observed in line transect Q-11 (Fig. 5.14). This similarity may indicate that slush conditions cause this signal overlap in the 2 m HCOP and PRP quadrature readings. The difference in the overlaps may be associated with the difference in the sea ice thickness of the two sites and the degree to which the snow is saturated at each site. Transect Q-11 contained thinner sea ice volumes (mean of 0.91 m) compared to transect Q-13 (mean of 1.19 m). However, transect Q-13 snow cover is significantly more saturated.

Although sea ice at transect Q-13 is covered with high volumes of seawater slush, signals strength is still higher for transect Q-11. This indicates that the sea ice thickness is still the key factor influencing the signals strength at transect Q-13. The high-volume conductive sea water slush of transect Q-13 was not strong enough to effectively influence the response readings from sea water - ice boundaries.

Evaluation of in-phase to quadrature signal correlations (Fig. 5.24) for both forward and reverse surveys reveal that 4 m PRP configuration and 2 m HCOP configuration present strongest correlations, while the signal vs. depth correlation analysis (Fig. 5.25 & Fig. 5.26) display very weak correlations for all configurations. No reliable pattern can be observed in the signal to depth correlation plots (Fig. 5.25 & Fig. 5.26). In fact, data appears to be randomly

scattered. Narrow range in sea ice thickness and slush are the main reasons for this scatter behaviour.

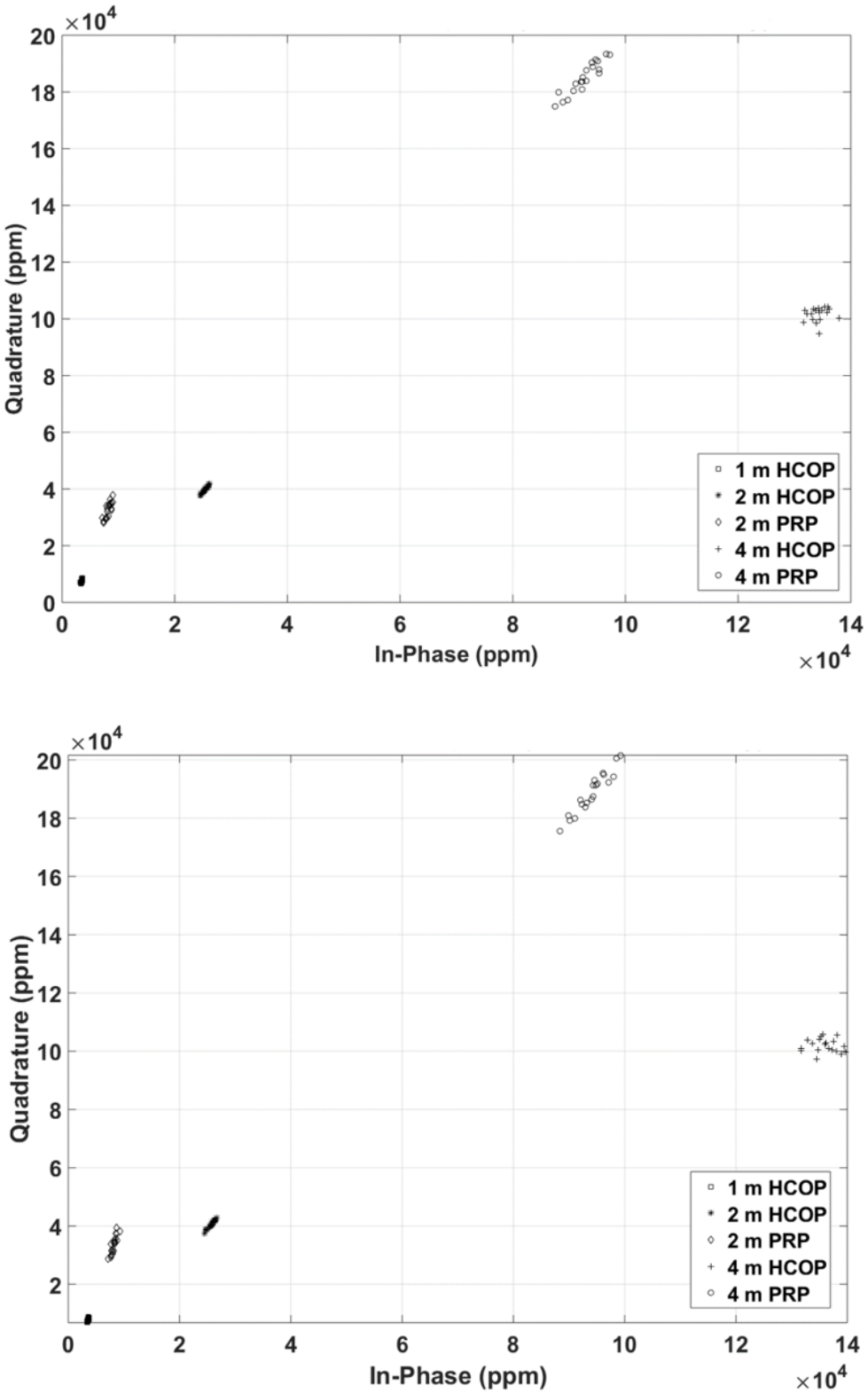

Fig. 5.22: Quadrature versus in-phase EM response of transect Q-13 for all coil spacings and orientations. The 1 m in-phase PRP data were invalid and not reliable to use.

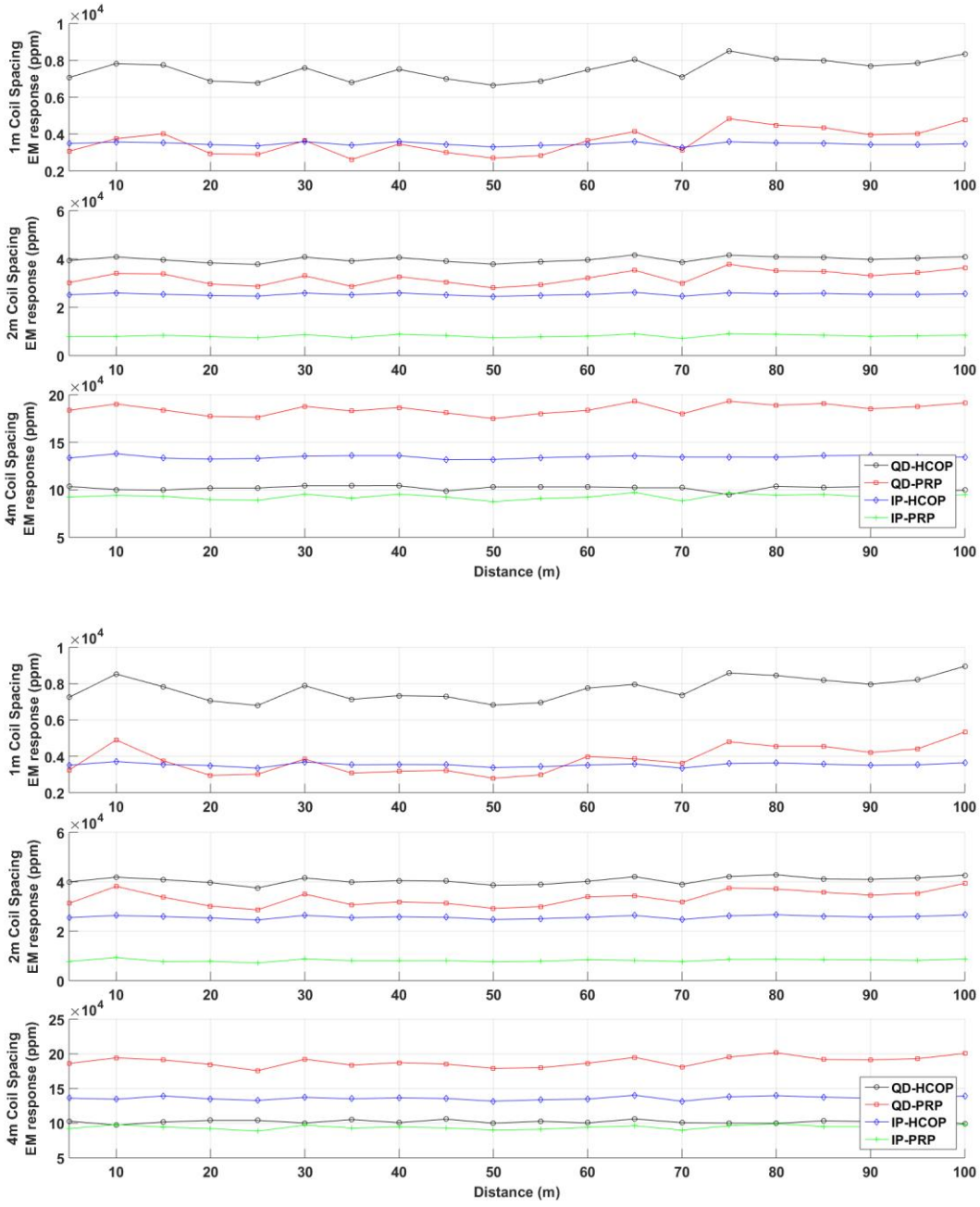

Fig. 5.23: EM response of all SIS configurations along transect Q-13. Top: 1 m coil spacing configurations, Middle: 2 m coils spacing configuration, Bottom: 4 m coil spacing configurations. SIS acquired data at 5 m spaced intervals.

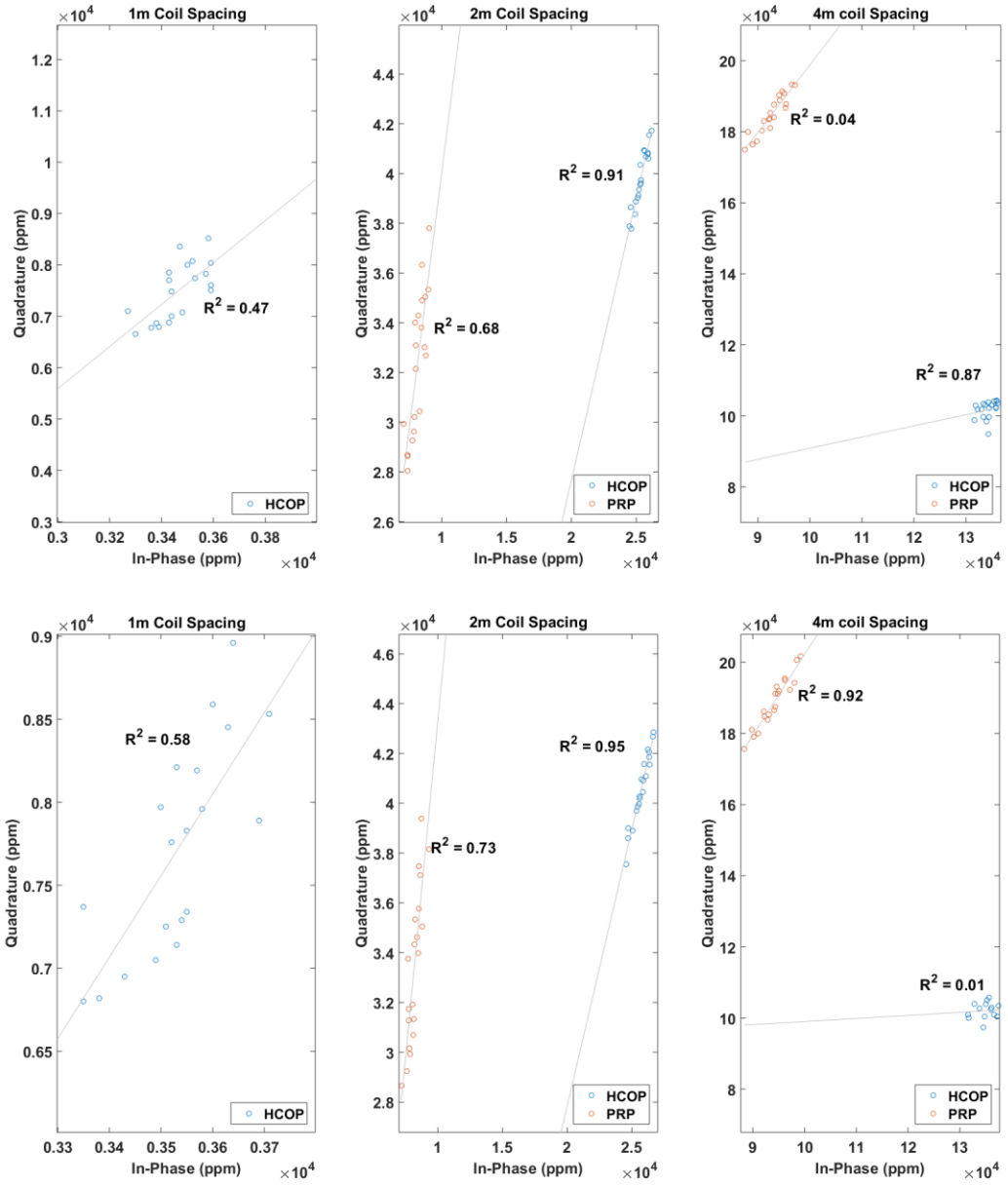

Fig. 5. 24: HCOP and PRP, quadrature versus in-phase signals for 1 m coil spacing (left), 2 m coil spacing (middle) and 4 m coil spacing (right) for transect Q-13. The 1 m in-phase PRP data were invalid and not reliable to use. Top: forward survey, Bottom: reverse survey.

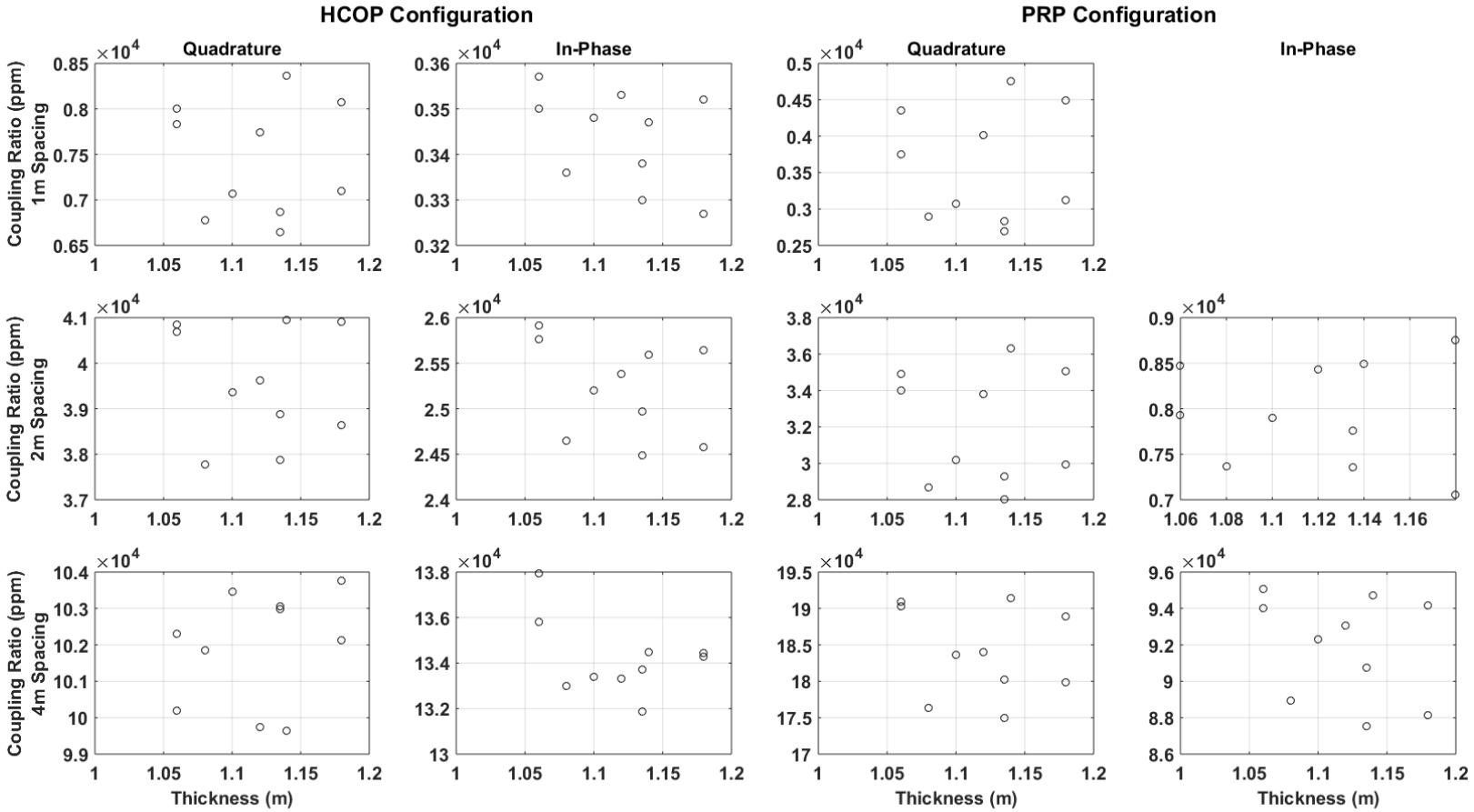

Fig. 5.25: EM signal (quadrature and in-phase response) versus drill-hole sea ice thicknesses for transect Q-13 (forward survey).

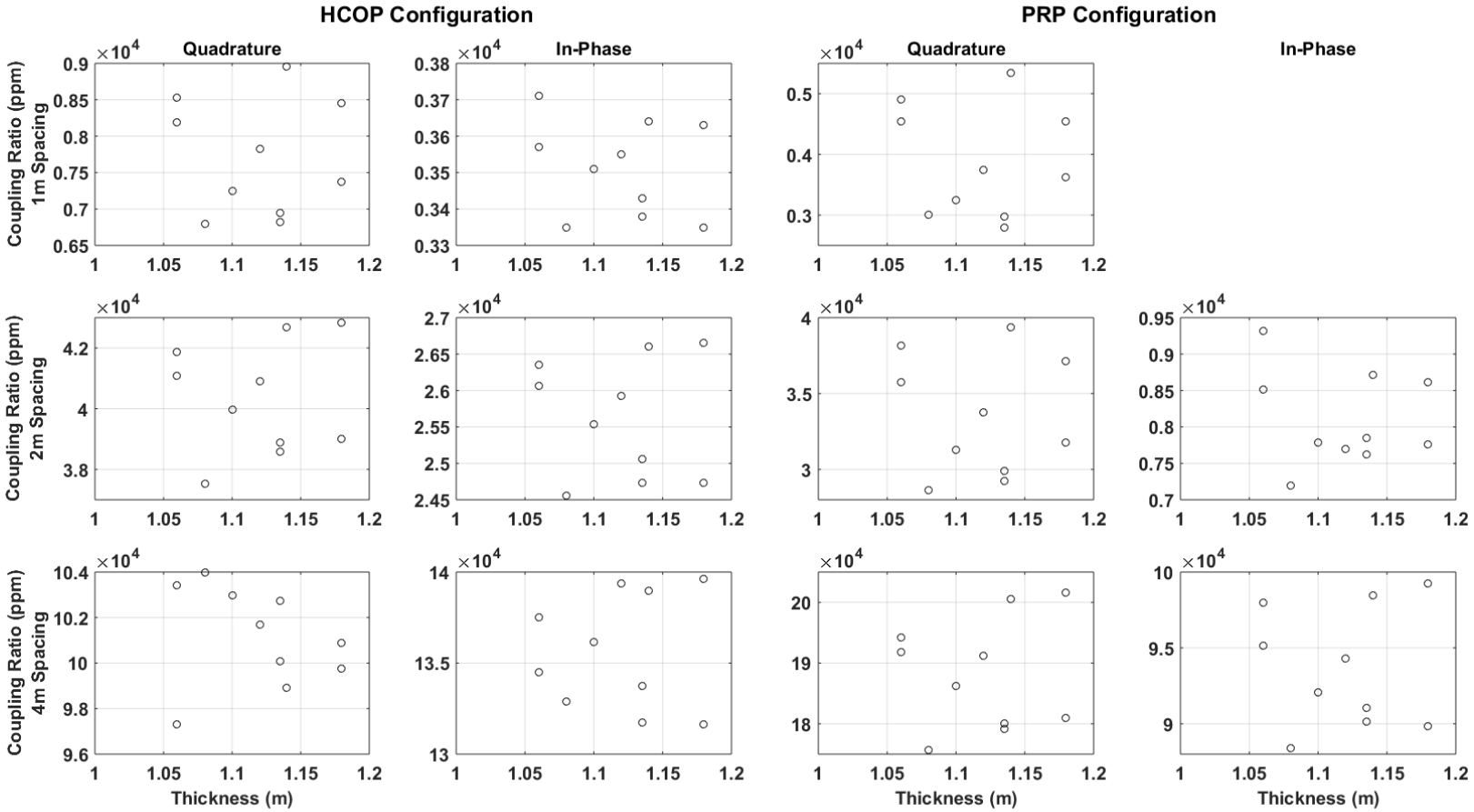

Fig. 5.26: EM signal (quadrature and in-phase response) versus drill-hole sea ice thicknesses for transect Q-13 (reverse survey).

Transect Q-14

Transect Q-14 is the longest transect (165 m) established over a very unique sea ice area. It stretches 165 m offshore of a small island outward towards an iceberg in a strait. Transect Q-14 consist of a variety of sea ice types encountered in previous transects (level ice, slush and rafted ice). It consists of uneven sea ice surface and slush condition from station 0 to station 20, level sea ice from station 30 to station 130, rafted sea ice from station 130 to station 135 and level sea ice from station 140 to station 160.

Average bulk sea ice thickness and snow cover was significantly greater compared to previous transects. Average sea ice thickness was approximately 1.53 m with SD of 0.88 m. Average snow cover was 0.47 m with a SD of 0.13 m. Similar to transect Q-13, a reverse survey was also performed to assess the repeatability of the EM data.

In addition, a water depth survey was also conducted at few locations to ensure water depth levels of this unique transect satisfy SIS operational requirements. Seawater depth standards for reliable SIS measurements might have not been satisfied for data collected at the starting points of the profile as SIS is not capable to operate over shallow seawater. From the water depth survey, the area at the starting point of the transect had depths of approximately 5 to 10 m. The possible presence of bedrocks and large boulders that were obscured by snow and ice can also explain the uncertainty of the data collected near the shoreline. It should be noted that due to the unique location of the site (located in a strait) the water currents were most likely strong enough to introduce significant errors in the water depth readings.

Similar to transect Q-14, in-phase 1 m PRP configuration data is noisy and unreliable. The reliability of some data points for some configurations was uncertain near the shoreline and at the site where there was evidence of sea ice rafting.

Complex sea ice structure along with sharp structural changes that especially occur in very short distance intervals add uncertainty to signal readings. The drill measurements show that at station 135, ice thickness is at its maximum thickness of 4.25 m and within 5 m (on station 140) ice thickness drops to 1.59 m. SIS may not be able to resolve this rapid change in sea ice thickness within such a small space interval (5 m). EM signals recorded are the averages of sea ice thicknesses within the footprint size of SIS coil spacings and therefore, unable to reproduce abrupt changes in sea ice thickness conditions and according point measurements at drill sites.

Fig. 5.27 shows SIS signal to sea ice thickness correlations for all configurations before removal of uncertain data points (stations 0 and 10 located near the shoreline) and stations 130 and 135. SIS EM readings over stations 130 and 135 (rafted sea ice section) introduce two major outliers to the EM data. Since there is a large gap between these two signal readings and the rest of the data acquired over this transect, it is difficult to validate the accuracy of these signal readings merely based on graphical and statistical analysis.

EM Signals behaviour for transect Q-14 (Fig. 5.28 & Fig. 5.29) is generally similar to all other transects. 4 m coil spacing configuration yield strongest signals followed by 2 m and 1 m coil spacing configurations. For 4m coil spacing configurations, the in-phase signal is strongest in HCOP orientation and weakest in PRP orientation, while the quadrature response signal is strongest in PRP orientation and weakest in HCOP orientation. For 1 m and 2 m coil spacing configurations, in-phase and quadrature signal responses are both strongest in HCOP orientation and weakest in PRP orientation.

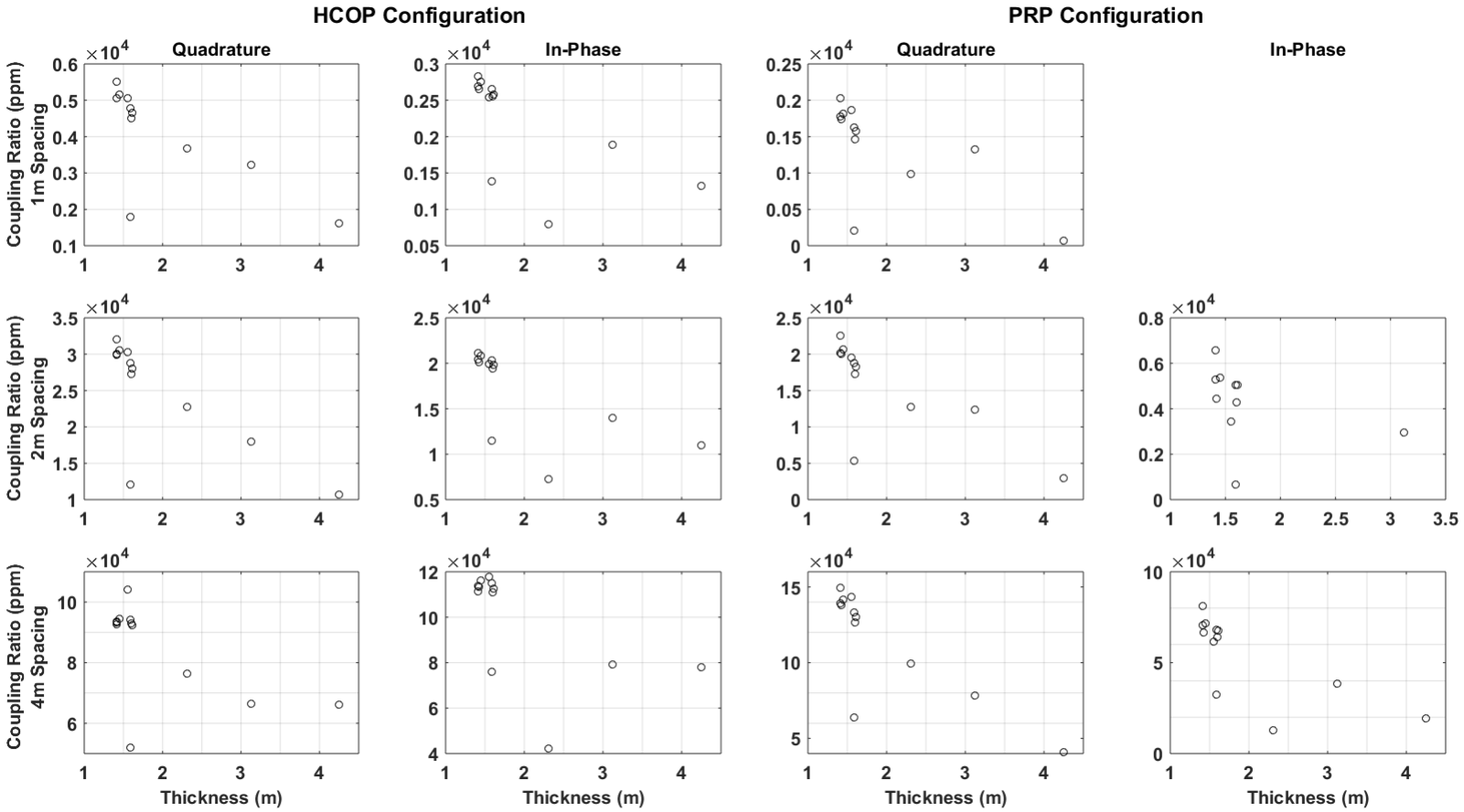

Fig. 5.27 EM signal (quadrature and in-phase response) versus drill-hole sea ice thicknesses for transect Q-14 from the pre-processing stage. Outliers belong to near shoreline zone and rafted sea ice section.

Determining highest signal quality configuration based on signal correlations (Fig. 5.30) 4 m PRP coil configuration, 2 m and 1 m HCOP coil configurations show the strongest R^2 values. Signal to sea ice thickness correlations are very poor (Fig. 5.31 & Fig. 5.32) and not conclusive. This can be explained by the combined contribution of slush, small sea ice thickness range (0.79 m to 1.18 m) and insufficient sample data points.

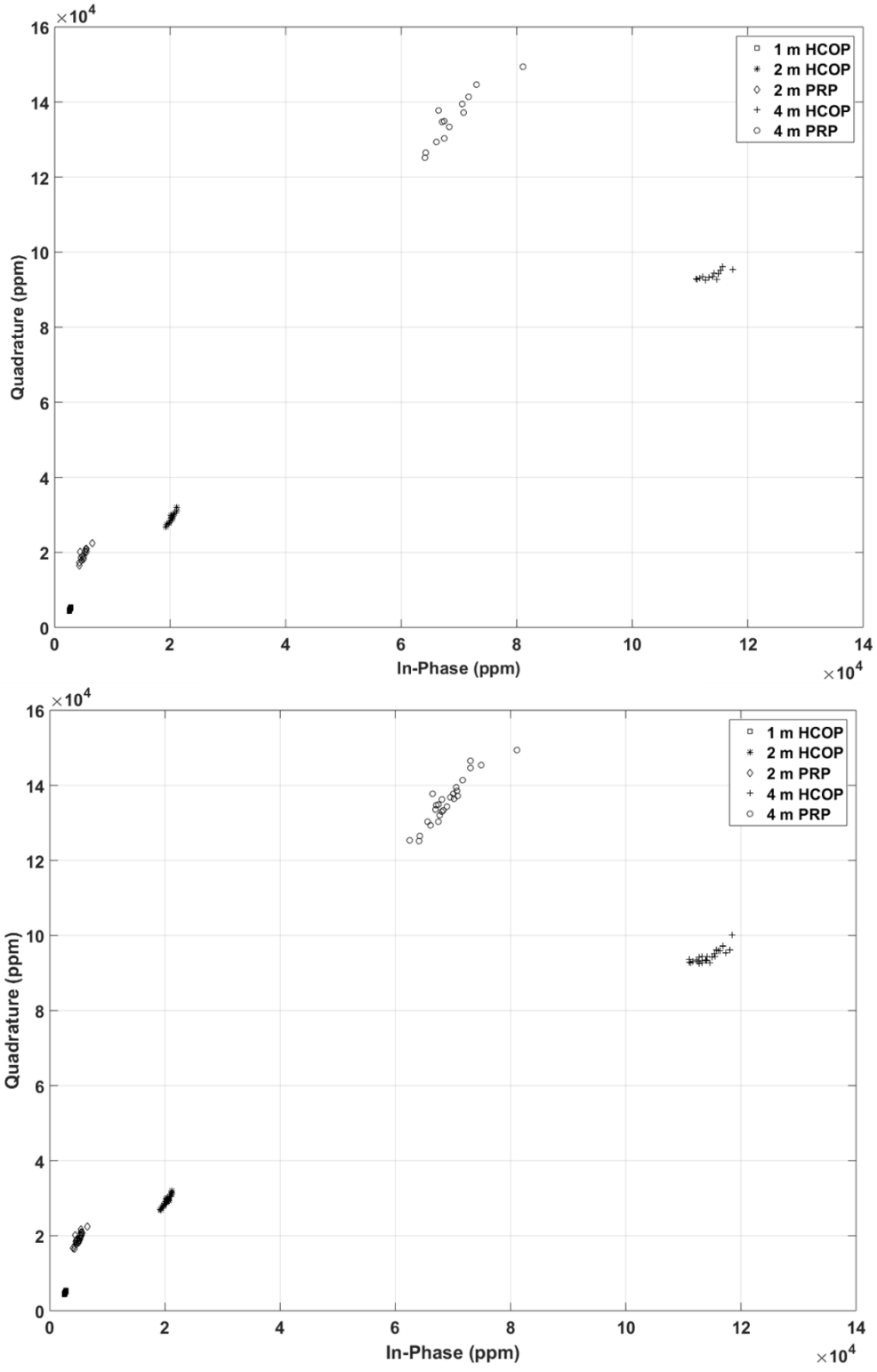

Fig. 5.28: Quadrature vs in-phase EM response of forward (top) and reverse survey (bottom) of transect Q-14.

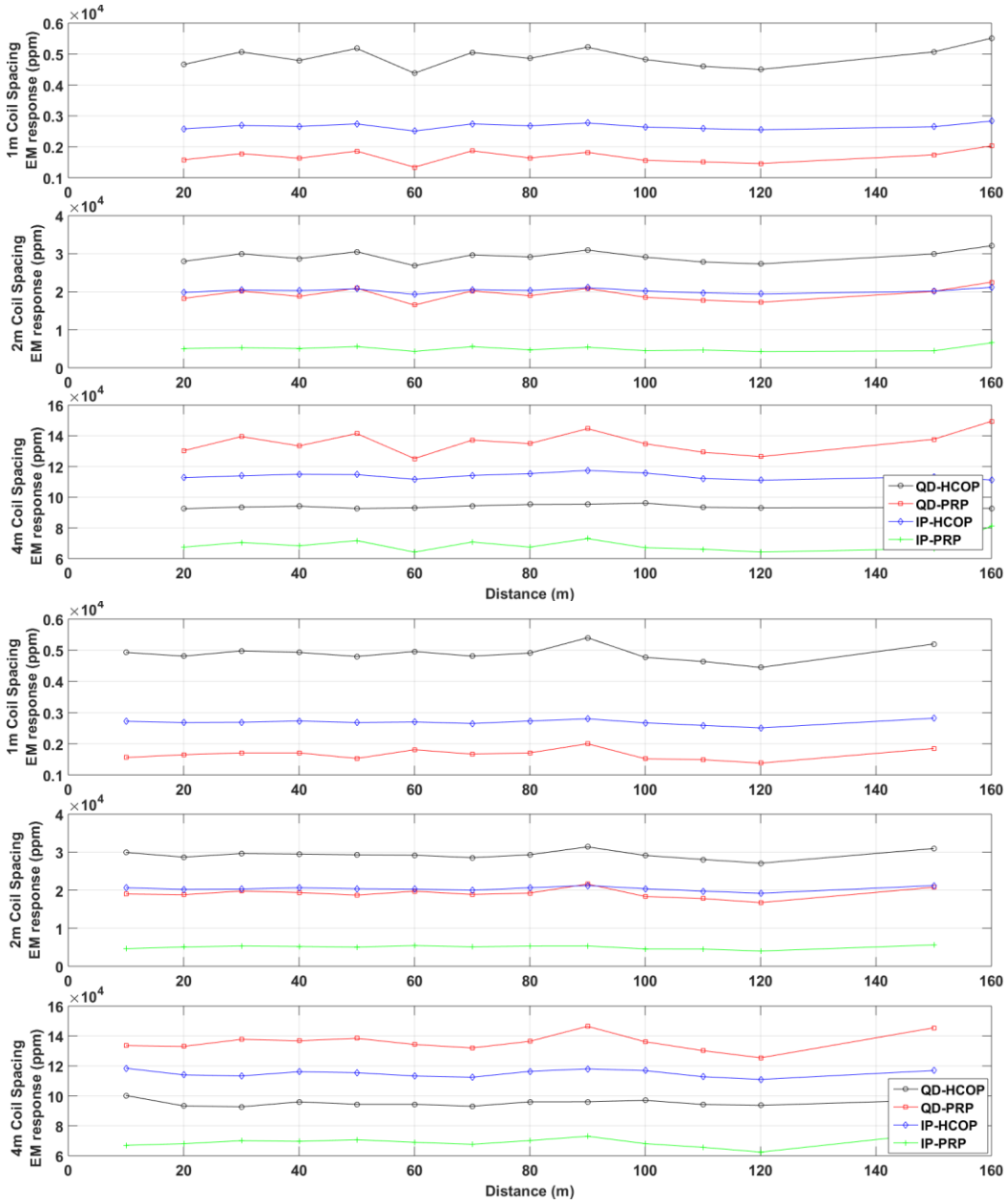

Fig. 5.29: Signal readings for all coil configurations along transect Q-14. Top: forward survey, Bottom: reverse survey. Unreliable data was removed.

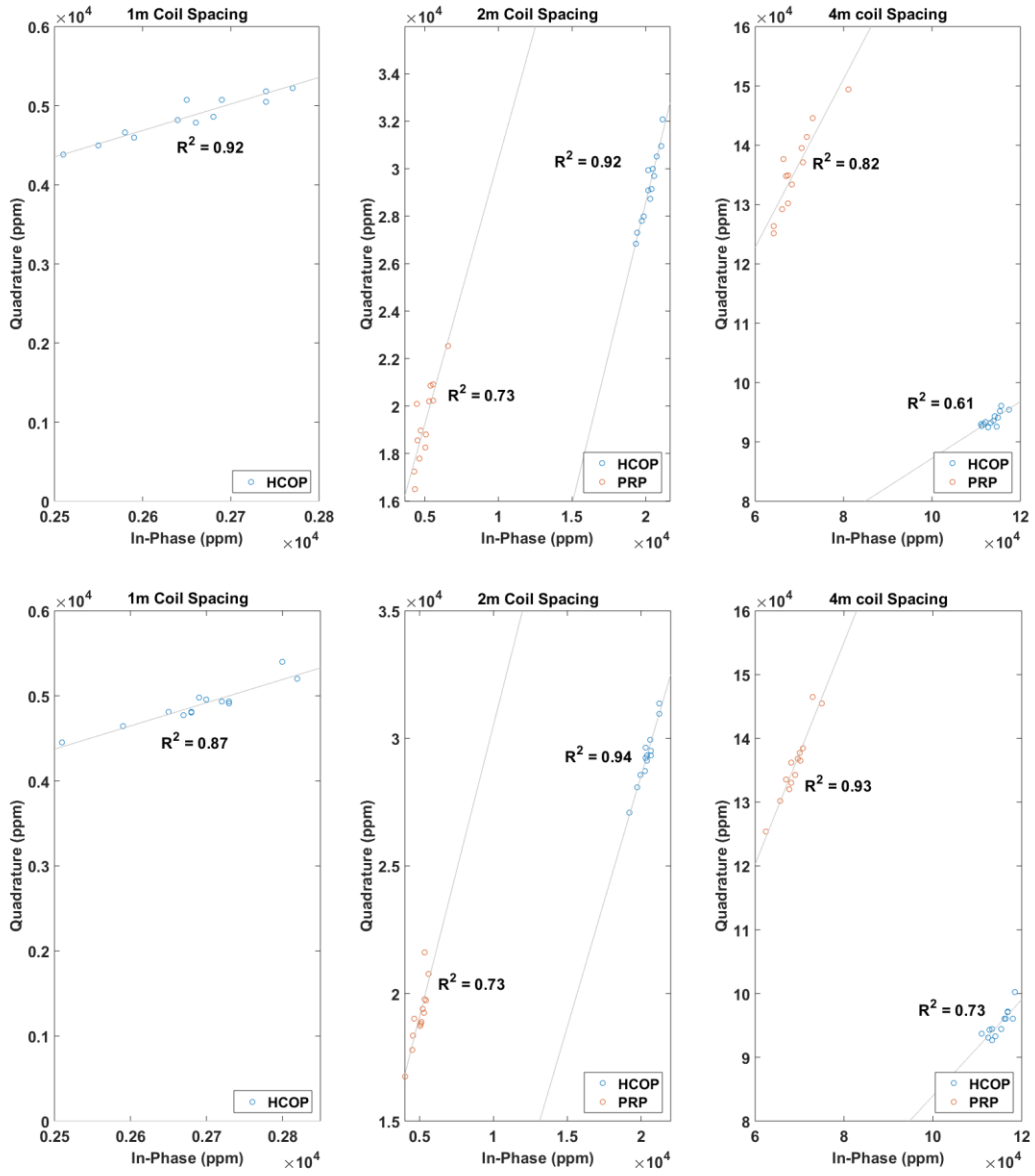

Fig. 5.30: HCOP and PRP, quadrature versus in-phase signals for 1 m coil spacing (left), 2 m coil spacing (middle) and 4 m coil spacing (right) for transect Q-14. The 1 m in-phase PRP data were invalid and not reliable to use. Top: forward survey, Bottom: reverse survey.

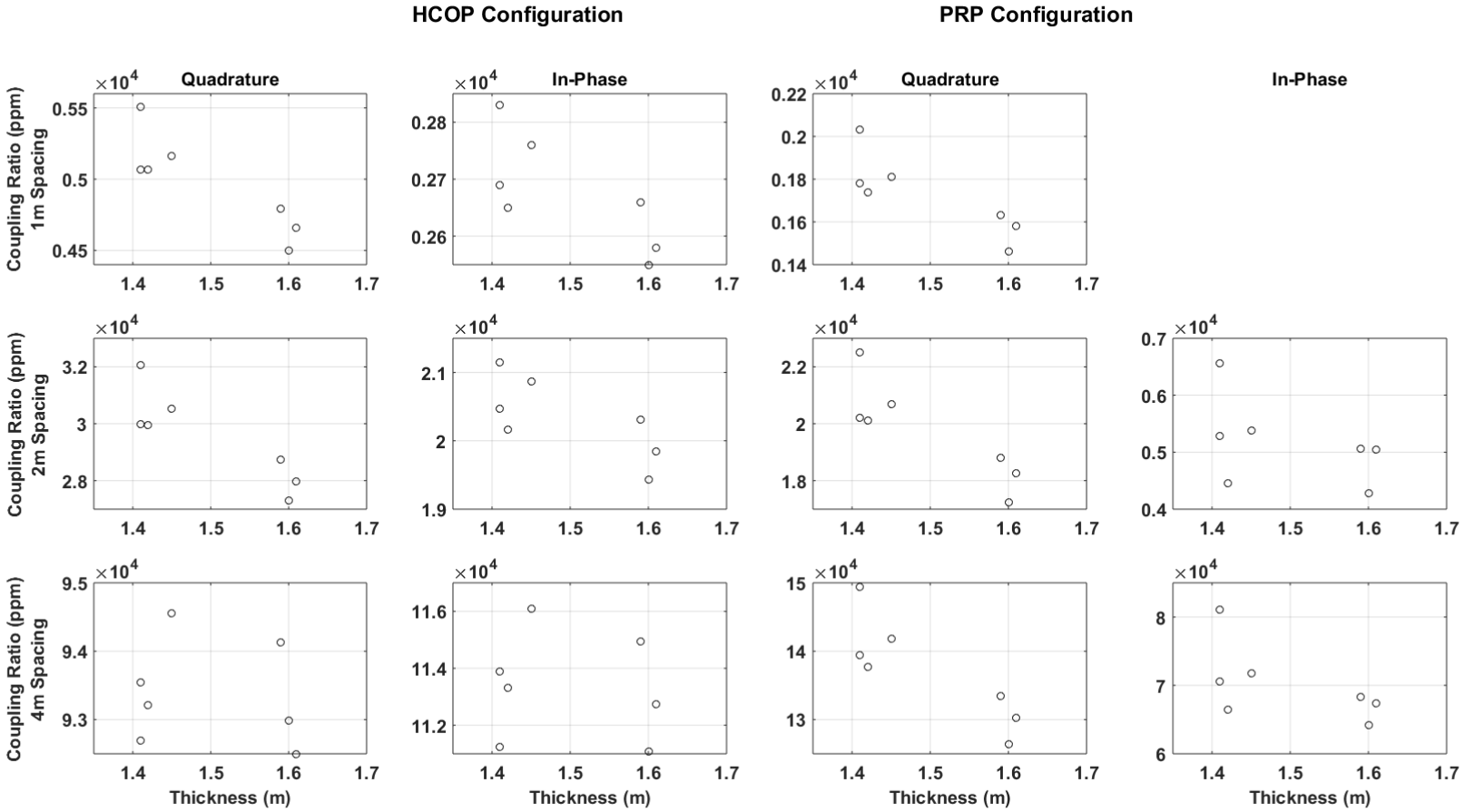

Fig. 5.31: EM signal (quadrature and in-phase response) versus drill-hole sea ice thicknesses for transect Q-14 forward survey.

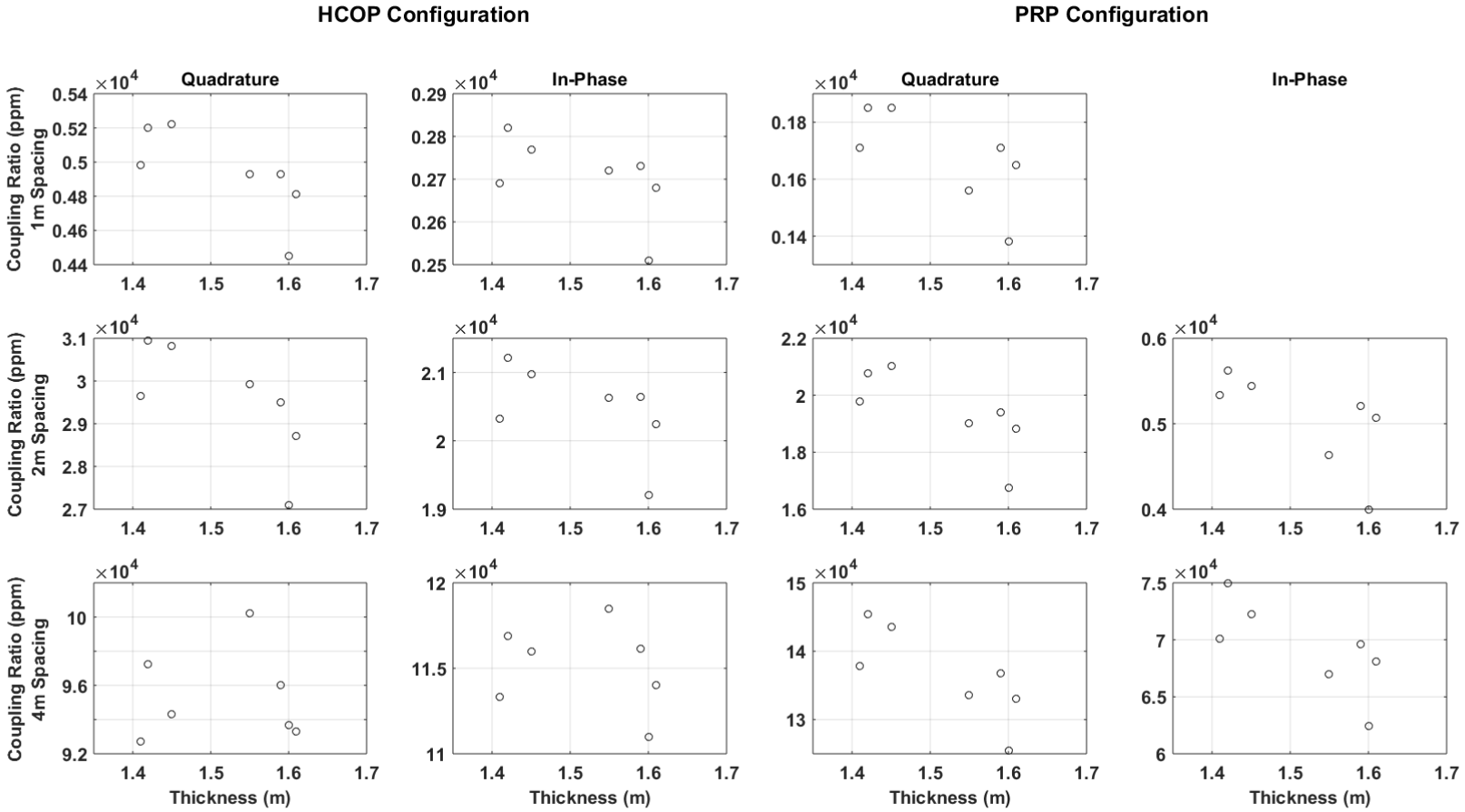

Fig. 5. 32: EM signal (quadrature and in-phase response) versus drill-hole sea ice thicknesses for transect Q-14 reverse survey.

Qikiqtarjuaq Overall

Examination of the EM data collected from Qikiqtarjuaq indicates that 4 m coil spacing configuration display strongest signal returns (highest ppm values) followed by 2 m and 1 m coil spacing configurations (Fig. 5.33). This is in agreement with the theoretical models. It is also evident that slush conditions and volume have a notable impact on the signal strength

Calculated mean sea ice thickness and snow cover of all transects are presented in Table 5.4. From the drill data, Q-12 and Q-14 have the greatest sea ice thicknesses. Transects with relatively greater mean sea ice thickness (Q-12 & Q14), display weaker signals for all coil configurations. According to Fig. 5.33, EM signals acquired over transect Q-12 and Q-14 show a very good consistency for most coil configurations. However, 1 m HCOP and 2 m PRP coil configuration show two distinct responses for these two transects. The main reason causing this distinct signal behaviour of the two transects is most likely the complex structure of transect Q-12 relative to transect Q-14. Transect Q-12 consisted of relatively uneven sea ice structures containing cavities that may be filled with sea water. This increases bulk sea ice conductivities contributing to relatively stronger signal readings.

Transects Q-10 (mean: 1.18 m, SD: 0.49) and Q-13 (mean: 1.19 m, SD: 0.044) have almost equal mean sea ice thickness. However, the signal signatures for these transects can easily be distinguished from each other by 1 m HCOP, 2 m and 4 m PRP coil configurations (Fig. 5.34). This may imply that sea ice thickness is not the only factor influencing EM signals on these transects. Transect Q-13 contain significant slush volume over the sea ice. The presence of this slush volume may be the reason for the difference between the two transects signal pattern. It appears that 2 m HCOP is the most stable coil configuration when sea ice is influenced by the complex structure and slush conditions.

SIS recorded strongest EM signals on Transect Q-11 for all coil configurations. This transect consisted of thinnest sea ice surveyed among all other transects (mean: 0.91, SD: 0.068). Transect Q-11 was also covered with significant slush volume. Thin sea ice combined with large slush volumes contributed to the high signal readings of this transect.

The 4 m spacing HCOP coil configuration shows a very narrow range of quadrature readings versus a wide range of in-phase readings for all of the five transects surveyed. This is especially more problematic for transect Q-10, Q-11, and Q-13 where they mostly share the same range of quadrature readings and the signal readings are distributed in a cluster. This implies that 4m

HCOP configuration is most likely not suitable for sea thin sea ice conditions where sea ice is covered with saturated snow cover.

Table 5.4: Mean and standard deviation of sea ice thickness and snow depth of all transects from drill-hole surveys.

	Q-10	Q-11	Q-12	Q-13	Q-14
Bulk sea ice mean thickness & SD	1.18 0.049	0.91 0.068	1.44 0.09	1.19 0.044	1.53 0.88
Snow depth mean & SD	0.39 0.05	0.42 0.034	0.15 0.08	0.46 0.031	0.44 0.08

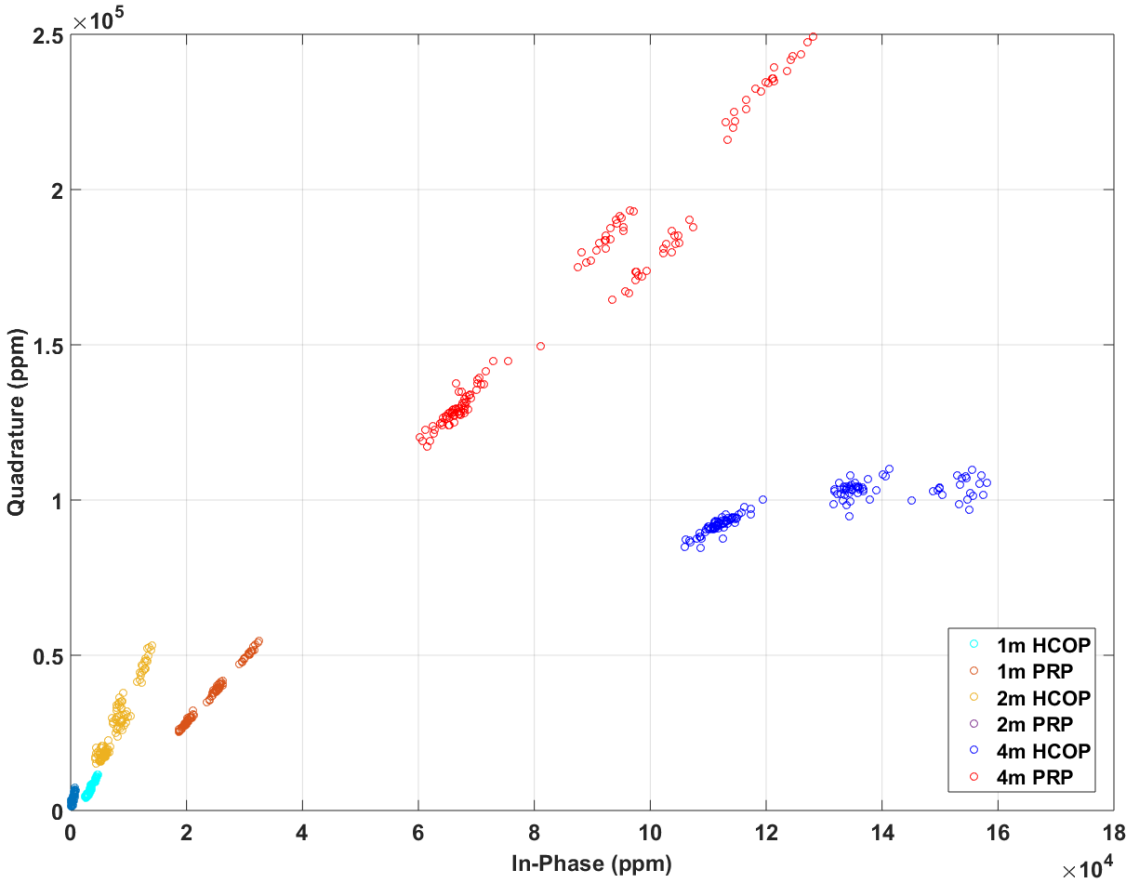

Fig. 5.33: Quadrature versus in-phase response of Qikiqtarjuaq field data. EM data for all coil spacings are included.

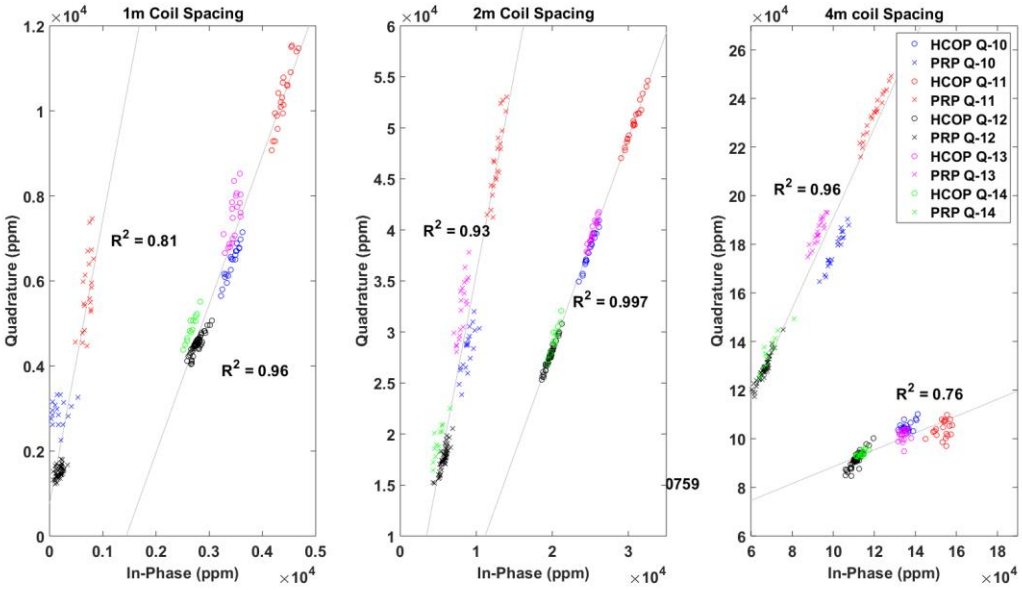

Fig. 5.34: Quadrature vs in-phase response correlation as a function of coil spacing. There are no data for 1 m PRP coil configuration for transects Q-13 and Q-14

Table 5.5: Calculated R^2 coefficients (in-phase to quadrature correlations) as a function of coil spacing

	Qikiqtarjuaq	
Configuration	HCOP	PRP
1 m spacing	0.96	0.80
2 m spacing	0.99	0.93
4 m spacing	0.75	0.96

The sea ice thickness range and variability of Qikiqtarjuaq region is considerably smaller when compared to the Polarstern region. The quantity of collected drill-hole measurements at Qikiqtarjuaq is also noticeably fewer compared to Polarstern. These facts combined with saturated snow conditions contribute to the relative dispersity of EM data in Fig. 5.34. It also explains why the expected signal to sea ice thickness non-linear correlation (Chapter 4) is not apparent in Fig. 5.35.

Signal to sea ice thickness correlations for the entire Qikiqtarjuaq data is acceptable for most coil configurations. However, when making an assessment based signal to sea ice thickness, the distinct signal distributions of transect Q-10 and Q-13 should be also recognized (Fig. 5.35). This is especially more evident for 4 m and 2 m PRP coil configuration where transect Q-10 and Q-13 form two distinct cluster of data points on the plots (Fig. 5.35).

Under linear correlation assumption and calculating R^2 coefficients, 4 m PRR, 2 m, and 1 m HCOP configuration yield the highest quality data compared to other configurations.

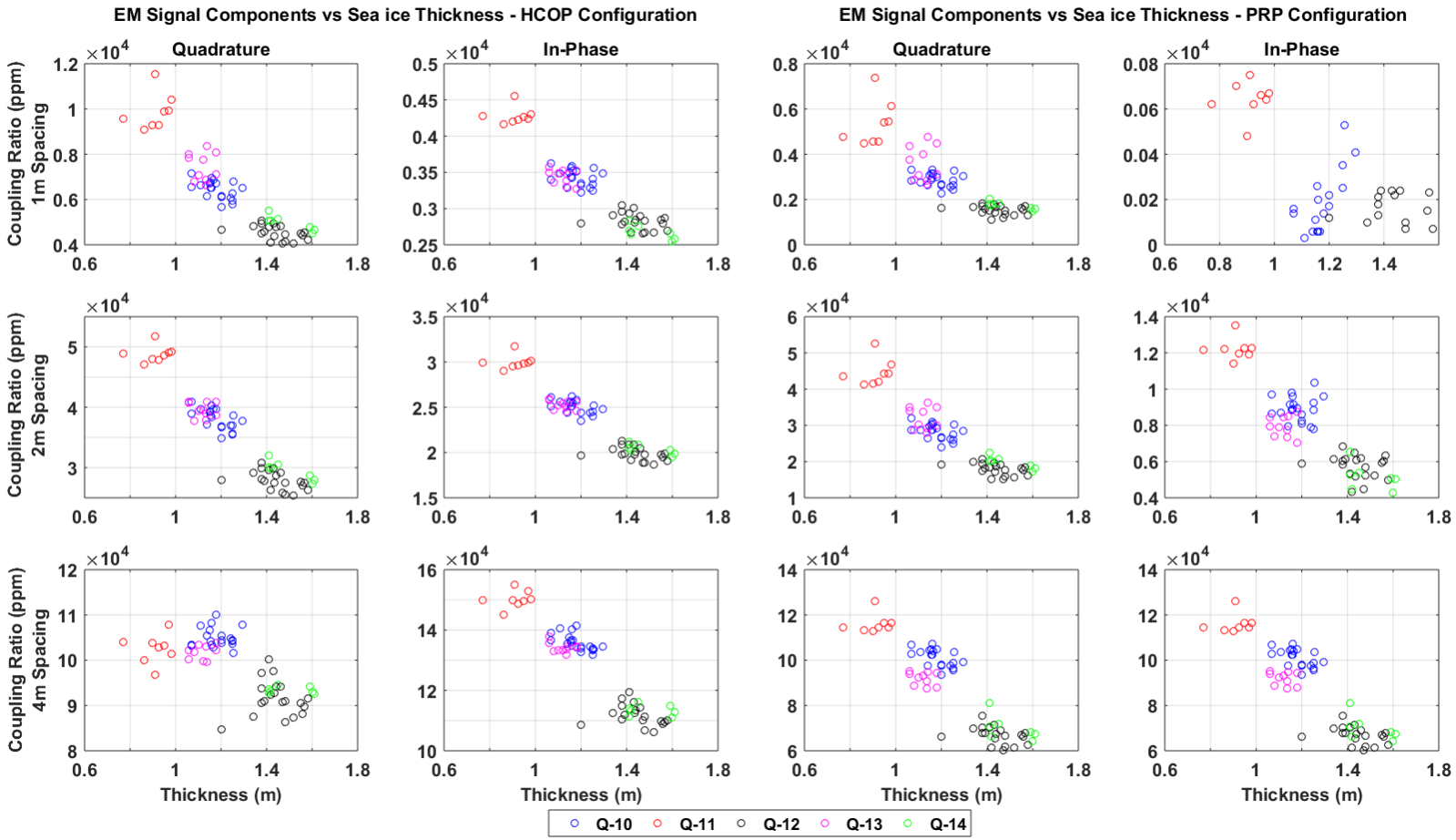

Fig. 5.35: Signal to sea ice sea thickness correlations of Qikiqtarjuaq data. Each transect is displayed with a unique colou

5.4.3 Collective signal Evaluation of Polarstern and Qikiqtarjuaq

Collective EM signal evaluation of both study regions (Polarstern and Qikiqtarjuaq) suggests that there is an acceptable coherency between the two data sets for 2 m and 4 m coil spacing configurations. Qikiqtarjuaq consists of thinner sea ice and narrow range in sea ice thickness, hence constituting the upper range of the EM data (Fig. 5.36 & 5.37). Polarstern consists of thicker sea ice with a significantly wider range in sea ice thickness and as a consequence forms the widest range in EM data (Fig. 5.36 & 5.37). 1 m coil spacing configuration possesses the noisiest data set. In 2 m coil spacing configuration, the HCOP configuration looks decent however the PRP configuration looks very noisy. For 4 m coil spacing the results show strong correlations in both HCOP and PRP configurations, however, the upper range of the HCOP quadrature readings is uncertain as there is a significant overlap between the quadrature readings (Fig. 5.37).

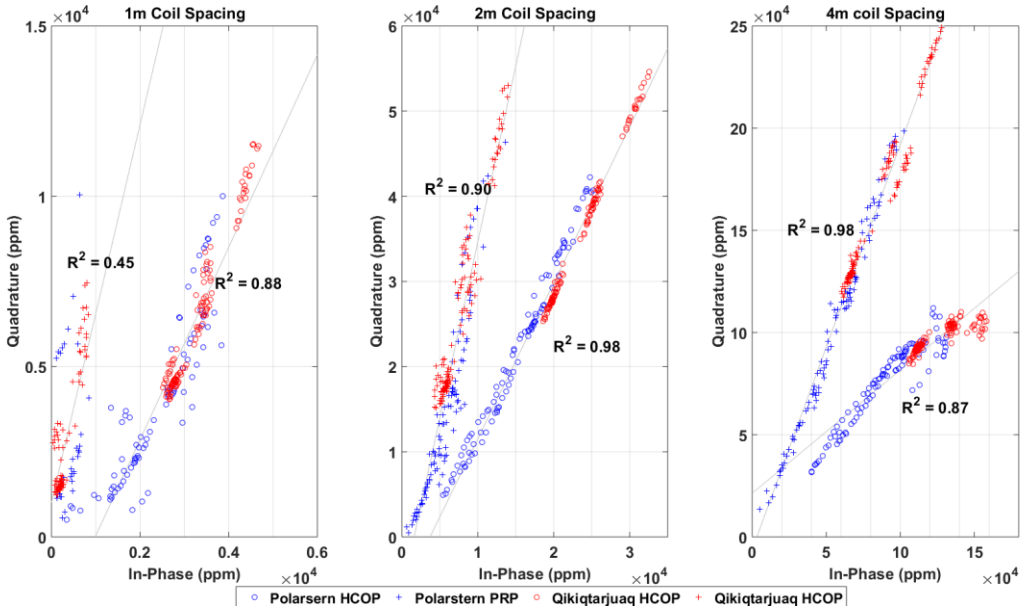

Fig. 5.36: The correlations between quadrature an in-phase response of both study sites are demonstrated as a function of coil spacing. The red data points depict Qikiqtarjuaq EM data. The blue data points depict Polarstern EM data.

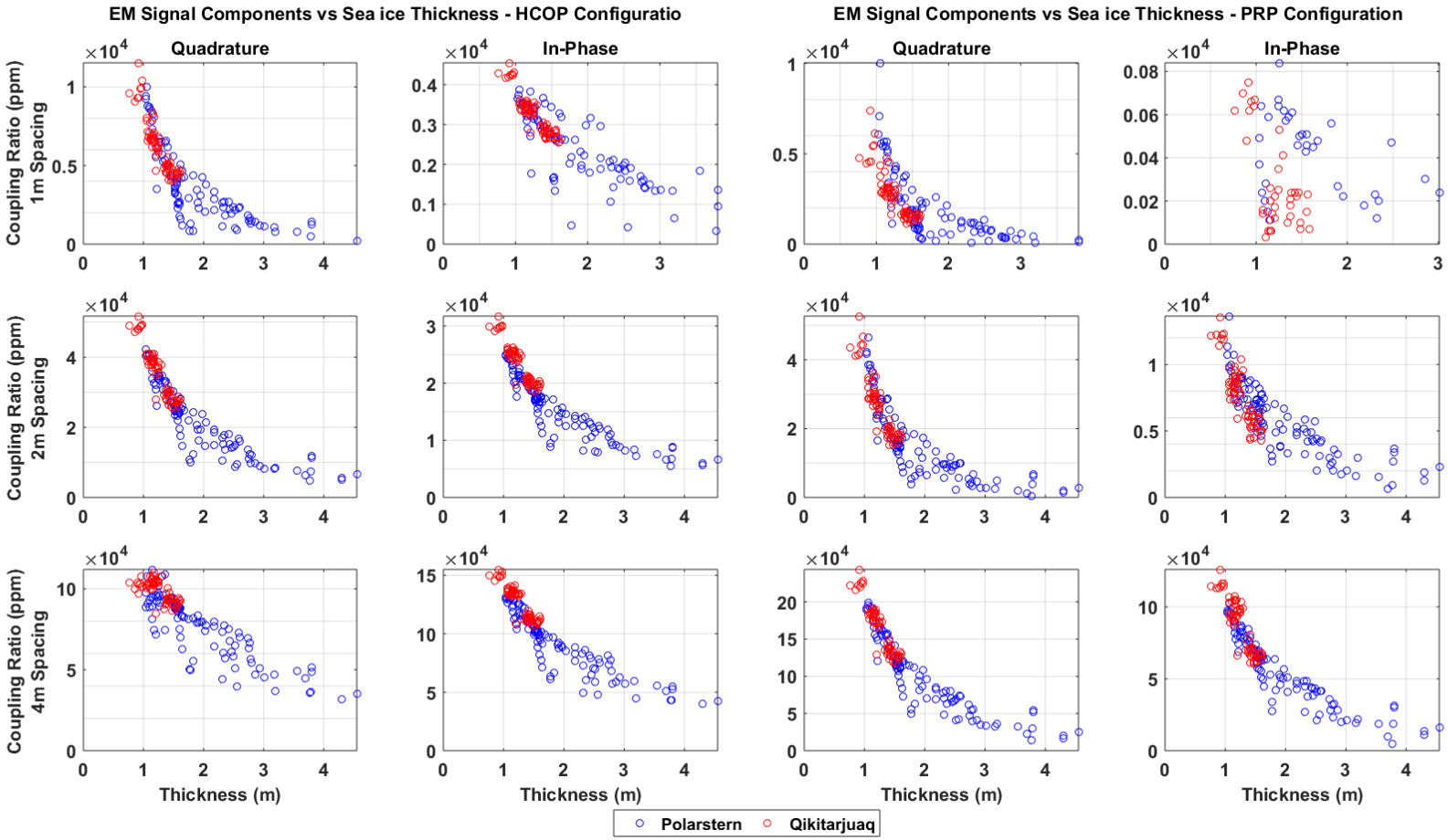

Fig. 5.37: Signal to sea ice thickness correlations for entire EM data collected at both study sites.

Investigating signal to sea ice thickness correlations of the entire EM data collected, it is evident that the signals from the two study regions are comparable and that conclusions agree.

In 1 m coil spacing category, quadrature HCOP configuration appears to yield the strongest signal and decent signal to sea ice thickness correlation. However, there is a significant ambiguity in the signal readings for the ice thickness in the range of 1.6 m to 2.5 m. Data that is responsible for this ambiguity is from transect P-11, Polarstern study area. Removing transect P-11 will significantly improve signal correlations for all configurations.

In the 2 m, coil spacing category both HCOP quadrature configuration and PRP quadrature configuration appear to yield the highest quality data. Both configurations show strong signal readings with the widest range and fairly good correlation to sea ice thickness. The ambiguity observed in 1 m HCOP quadrature configuration is improved in these configurations.

In the 4 m coil spacing category the PRP configuration yields strongest signals with a much-improved signal to sea ice thickness correlations. The signal range is also widest in PRP configuration compared to HCOP configuration. The quadrature PRP component offers the most reliable signal responses in this coil spacing category.

5.5 Conclusion

The sensitivity of SIS coil configurations was investigated by performing graphical and statistical analysis on experimental field data collected from two distinct sea ice study regions. Polarstern EM data displayed a significantly wider range of EM responses for all coil configuration compared to Qikiqtarjuaq. This was due to considerably thicker sea ice volumes of Polarstern survey transects.

The results revealed that EM signals are influenced by ridged sea ice, melt-ponds and slush covered sea ice types. All coil configurations show effective influence over melt-ponds displaying stronger signal readings (transect P-05). Quadrature signal component is the most sensitive signal component to melt pond. The size of the melt pond and its salinity influences the magnitude of the EM responses. The exact nature of the EM interaction with the melt pond cannot be characterized by the limited data available in this study.

Slush volumes do influence SIS EM response readings; however, seawater at sea ice – seawater interface has the dominant influence on the EM responses over thin sea ice. The EM response influence from slush ice depends on the sea ice thickness (SIS distance to sea ice – sea water interface) and source and magnitude of snow saturation. The thinner the sea ice is the less influence the slush volume has over the EM measurements. According to Fig. 5.35, 4 m and 2 m PRP coil configuration and 1 m HCOP coil configuration appear to be the most sensitive coil configurations to snow saturation. Therefore, further analysis of slush influence on EM responses should be focused on the aforementioned coil configurations.

Evaluation of experimental field data indicates that 4 m coil spacing yields the strongest EM responses relative to 2 m and 1 m coil spacings. Likewise, 1 m coil spacing yields weakest EM responses and significantly shorter range in EM responses. Within 4m coil spacing configurations, the quadrature signal component of PRP coil orientation yields the best quality data. For 2 m and 1 m, coil spacing configuration the quadrature signal component yields the highest quality data in the HCOP orientation. 1 m coil spacing coil configurations tend to be the least stable coil configurations displaying too many response errors, with in-phase PRP orientation being the most problematic of all.

6 Inversion Results

6.1 Introduction

This chapter focuses on the retrieval of sea ice thickness estimates through the inversion of SIS field data. SIS is supplied with its own inversion software package, called SISinvert, which was used to estimate sea ice thickness inversions in this research.

The aim of this chapter is to evaluate the capability and accuracy of SISinvert for the estimation of sea ice thickness values for different sea ice types and to determine what coil configuration(s) (data component(s)) provide the most accurate inversion results.

6.2 SIS Inversion Method

Computation of EM inverse problems requires the utilization of numerical techniques. There are several methods commonly used to invert EM data, including Marquardt-Levenberg (Levenberg 1944; Marquardt 1963), singular value decomposition (SVD) (HUANG and Palacky 1991; Golub and Reinsch 1970) and the Occam's method (Constable et al. 1987). The inversion algorithm used by SISinvert is explained in detail by Holladay (1980). A short summary of the inversion procedure is given here. Figure 6.2 shows a flow chart of the inversion process.

Inversion (inverse problem) attempts to reconstruct an earth model from a set of finite field observations. The process generally begins with the introduction and parameterization of an idealized starting model. A model is characterized by two sets of parameters; parameters that describe physical properties of a half-space, e.g. layer thickness, conductivity and permeability, and parameters that characterize the EM system (e.g. SIS) used to acquire the field data. A half-space model is an n-layered earth model consisting of a fixed number of layers (normally a two-layer model consisting of a sea ice layer and a seawater layer) with each layer assumed to have a finite thickness (*t)* and conductivity (σ), except for the bottom layer which has infinite thickness. The magnetic permeability (μ) of all layers is assumed to be that of free space ($\mu_i = \mu_0$). The

EM system parameters (SIS parameters) include transmitter height (h_t), receiver height (h_r), coil spacing (s), operating frequency (f) and pitch and roll of the instrument.

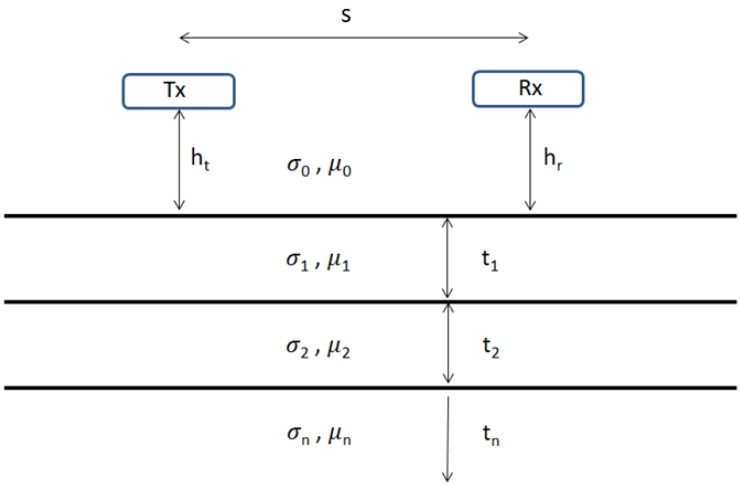

Fig. 6.1: Illustration of an n-layer earth model with transmitting (Tx) and receiver (Rx) coils. Typically, a 3-layer model (air, sea ice and sea water) is used in sea ice EM inversions.

Parameterization is followed by forward modeling. The forward model is a mathematical presentation of the observed EM response. It describes the relationship between model parameters and the expected EM response for any multi-layer model and predicts the expected EM response when adequate model parameters are used. The non-linear relationship between model parameters and the EM response is expressed by Hankel transform integrals (Equations 2.9 & 2.10). Computation of these integrals is based on the Gauss-Laguerre integration method. Gauss-Laguerre is a standard numerical technique to approximate integrals. Given starting model parameters, SISinvert uses the Gauss-Laguerre integration method to compute a forward model.

To estimate sea ice thickness and conductivity via inversion, the synthetic data generated by the forward model are compared to the observed EM data. The difference (errors) between the two datasets is minimized iteratively. In each iteration, the forward model is varied (sea ice thickness and conductivity) until an acceptable misfit is accomplished where no further significant improvement can be made. To accomplish this task an iterative least-squares non-linear regression algorithm, which utilizes the Marquardt-Levenberg algorithm and singular value decomposition (SVD) method, is used.

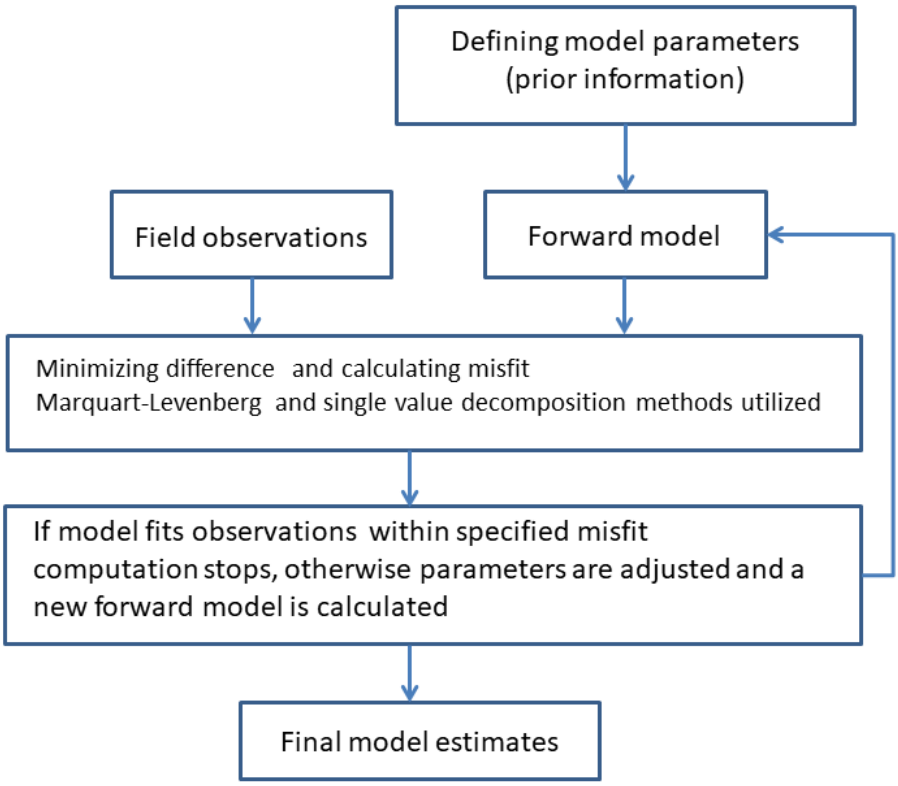

Fig. 6.2: General schematic of SISinvert's inversion process.

6.3 Field data inversion procedure and structure

The inversion algorithm utilizes prior knowledge (starting model parameters) to reduce the potential for the final model to converge on false sea ice thickness estimates. Therefore, a starting model is important in characterizing the adequate range of predicted sea ice thickness estimates.

The starting model should be representative of the sea ice properties being profiled. However, for the transects considered in this study, the sea ice formations and sea ice structure varied both between transects and also within transects. This implies that a single starting model may not be suitable for all transects. Taking this into consideration, and after testing numerous models, a

total of four staring models were proposed to accommodate the variability of sea ice physical properties along the transects (Table 6.1). A two-layer half-space model, consisting of a sea ice layer over top of a seawater layer, was chosen to be the basis of all starting models. The conductivity values assigned to each layer are shown in Table 6.1. The sea ice layer is restricted to single sea ice conductivity (models 1 to 2) or to a range of conductivities (models 3 to 4). The seawater layer is assigned a single conductivity value of either 2.55 (average seawater conductivity in the Arctic region).

Table 6. 1: List of starting models used. SISinvert uses a starting conductivity value to run the inversion. This value was assigned to be the lowest conductivity value in models that use a range of conductivities (m3-m4).

Starting model	Sea ice conductivity (S/m)	Seawater conductivity (S/m)
m1s	0.01	2.55
m2s	0.001	2.55
m3s	0.01-0.15	2.55
m4s	0.001-0.15	2.55

As discussed in Chapter 4, each coil configuration has its own unique footprint and depth sensitivity. The variability in the signal strength of different coil configurations shown in Chapter 5 confirms theoretical models to some extent, acknowledging that some coil configurations yield better data quality over others under different sea ice types.

In the inversions, coil configuration and quality of field data used will generate different results. For each coil spacing, SIS measures four unique signal data components (i.e. IPzz, QDzz, IPzx, and QDzx). Inversion can be performed using a single data component or a combination of multiple data components (up to a maximum of four components). All possible data inputs for an inversion are listed in Table 6.2. Utilization of multiple data components for the inversion may provide a more comprehensive insight regarding sea ice types. This is particularly valuable if general sea ice types are known as each coil configuration may behave differently to different sea ice type (e.g. slush sea ice versus level sea ice type).

Table 6.2: List of all possible inversion data input components used in the inversions.

Inversion data input	Inversion data input
1 component	IPzz, QDzz, IPzx or QDzx
2 components	IPzzQDzz, IPzzQDzx, IPzzIPzx, IPzxQDzz, IPzxQzx or QDzzQDzx
3 components	IPzzQDzxIPzx, IPzzQDzzIPzx, IPzzQDzzQDzx or QDzzQDzxIPzx
4 components	IPzzQDzzIPzxQDzx

6.4 SIS Inversion results

The accuracy of the inversion results is primarily assessed based on the calculation of root mean square errors (RMSE), which is a measure of the deviation between predicted sea ice thickness results of the inversion models and the in situ sea ice thickness measurements carried out at drill holes.

The relative error for drill hole measurements is about 2 cm (Eicken 2009) and therefore have insignificant influence on the RMSE values. However, as stated in chapter 5, the measured EM response is not a point measurement. It is rather an average EM response from a circular area (footprint that is several meters in diameters and increases with increasing ice thickness) directly below the instrument. Therefore, inverted sea ice thickness represents the average sea ice thicknesses of the area directly below the instrument. An important assumption made here is that the sea ice drill-hole measurement taken directly below SIS at each station is equal to the average sea ice thickness of the footprint area. This assumption may introduce some uncertainty in the RMSE values; however, quantifying this uncertainty is not simple and requires a separate study that is out of the scope of this research. Such study would require multiple drill hole measurements taken within the footprint area of the EM instrument and using their mean value for the uncertainty analysis.

RMSE values of all survey transects are presented in Tables 6.7 to 6.12 in Appendix A. Inversion trials with the lowest RMSE values are considered to give the most accurate sea ice thickness results. A list of data components that generate the most accurate sea ice thickness inversion results (low RMSE values) is given in Table 6.3.

Table 6.3: Data components that generated the most accurate sea ice thickness inversion results (lowest RMSE values). Numbers in brackets are RMSE values in meters.

Transect	Data input	4 m coil spacing	2 m coil spacing	1 m coil spacing
P-05	**1 component**	QDzx (0.14)	QDzz (0.13)	QDzz (0.16)
	2 components	QDzzQDzx (0.14)	IPzzQDzz (0.13)	IPzzQDzz (0.15)
	3 components	IPzzQDzzQDzx (0.14)	IPzzQDzzIPzx (0.15),IPzzQDzzQDzx (0.16)	NA
	4 components	IPzzQDzzIPzxQDzx (0.17)	IPzzQDzzIPzxQDzx (0.17)	
P-11	**1 component**	QDzx (0.36)	QDzz (0.38)	NA
	2 components	QDzzQDzx (0.37)	IPzzQDzz (0.38)	NA
	3 components	IPzzQDzzQDzx (0.42)	IPzzQDzzQDzx (0.38)	NA
	4 components	IPzzQDzzIPzxQDzx (0.42)	IPzzQDzzIPzxQDzx (0.39)	NA
Q-10	**1 component**	QDzx (0.05)	QDzz (0.05)	QDzz (0.05)
	2 components	QDzzQDzx (0.05)	IPzzQDzz (0.05)	IPzzQDzz (0.06)
	3 components	IPzzQDzzQDzx (0.04)	IPzzQDzzQDzx (0.05)	IPzzQDzzQDzx (0.07)
	4 components	IPzzQDzzIPzxQDzx (0.05)	IPzzQDzzIPzxQDzx (0.06)	NA
Q-11	**1 component**	QDzx & IPzz (0.09)	QDzz & Ipzz (0.08)	IPzz (0.08)
	2 components	QDzzQDzx (0.08)	IPzzQDzz (0.08)	QDzzQDzx (0.09), IPzzQDzz(0.11)
	3 components	IPzzQDzzQDzx (0.08)	IPzzQDzzIPzx (0.08)	IPzzQDzzQDzx (0.13)
	4 components	IPzzQDzzIPzxQDzx (0.09)	IPzzQDzzIPzxQDzx (0.09)	NA
Q-12	**1 component**	QDzx(0.17)	IPzx (0.13), QDzz (0.14)	QDzz & Ipzz (0.13)
	2 components	IPzzQzx (0.12)	IPzzQDzz & QDzzQDzx (0.15)	IPzzQDzz (0.13)
	3 components	IPzzQDzzQDzx (0.18)	IPzzQDzzIPzx (0.15)	IPzzQDzzQDzx (0.18)
	4 components	IPzzQDzzIPzxQDzx (0.22)	IPzzQDzzIPzxQDzx (0.23)	NA
Q-13	**1 component**	QDzx (0.07)	QDzz (0.06)	QDzz (0.11)
	2 components	QDzzQDzx (0.07)	IPzzQDzz (0.06)	IPzzQDzz (0.07)
	3 components	IPzzQDzzQDzx (0.07)	IPzzQDzzIPzx (0.07)	IPzzQDzzQDzx (0.10)
	4 components	IPzzQDzzIPzxQDzx (0.07)	IPzzQDzzIPzxQDzx (0.06)	NA
Q-13	**1 component**	QDzx (0.07)	QDzz (0.06)	QDzz (0.11)
	2 components	QDzzQDzx (0.07)	IPzzQDzz (0.06)	IPzzQDzz (0.07)
	3 components	IPzzQDzzQDzx (0.07)	IPzzQDzzQDzx, IPzzQDzzIPzx (0.07)	IPzzQDzzQDzx (0.10)
	4 components	IPzzQDzzIPzxQDzx (0.07)	IPzzQDzzIPzxQDzx (0.06)	NA

According to RMSE values (Table 6.3) alone, it appears that using a single quadrature data component is generally sufficient to provide accurate inversion results without any need to use multiple data inputs that also yield very similar low RMSE values. For the Polarstern transects, where sea ice is thicker, the 4m coil spacing QDzx data component yielded the lowest RMSE

values. For the Qikiqtarjuaq transects, where sea ice is thinner, the 2 m coil spacing QDzz or IPzz data components yielded the lowest RMSE values.

RMSE value is a good indicator of the overall agreement between the inverted and observed sea ice thicknesses along a whole transect but it does not provide any information as to where most of the errors occur along each transect. This is an important piece of information that distinguishes data component combinations with similar RMSE values from each other. As indicated in Table 6.3, most data component combinations yield very similar low RMSE values. Although the RMSE values appear to be similar, the error distribution along a transect is often variable between data component combinations. This difference in error distribution along a transect is attributed to the difference between different coil configuration sensitivities and the sea ice conditions of the transect being surveyed. Therefore, in addition to RMSE values, graphical analyses of error distributions are also used to determine data components that yield the most accurate inversions of sea ice thickness.

A particular data component may prove to be superior over other data components by providing a more accurate inversion result over certain sea ice (e.g. over level ice or over ridged ice). Surveyed transects are therefore grouped and analyzed based on five sea ice types observed in the field surveys, Table 5.1.

The effect of starting models on inversion results depends on the number of data components used in the inversions. For one data component, the inversion results are generally similar and converge to the same sea ice thicknesses. However, as the number of data components increase the results begin to diverge more.

6.4.1 Level sea ice

Transect Q-10 consists of the simplest sea ice type. According to the drill measurements, the sea ice surface and thickness were fairly even along this transect (Fig 5.11). As shown in Table 6.3 all of the selected inversion input data components (single and multiple data components) yield similar low RMSE values. Since this transect is fairly level, it is reasonable to expect results that demonstrate uniform sea ice thickness error distribution along this transect. Examining the error distribution along transect Q-10 reveals that single, paired and three input data component combinations of 4 m and 2 m coil spacings yield the most accurate and reliable sea ice thickness estimates. Since the RMSE errors are low and the error distribution is more or less uniform along most of this transect, it is reasonable to use 2 m coil spacing QDzz or IPzzQDzz data components for the most accurate results over level first-year ice. Figure 6.3 illustrates sea ice thickness inversion results using the 2 m coil spacing QDzz single data component. All four models converge to the same result (RMSE = 0.05). The error distribution is also uniformly very low for the most part of the transect.

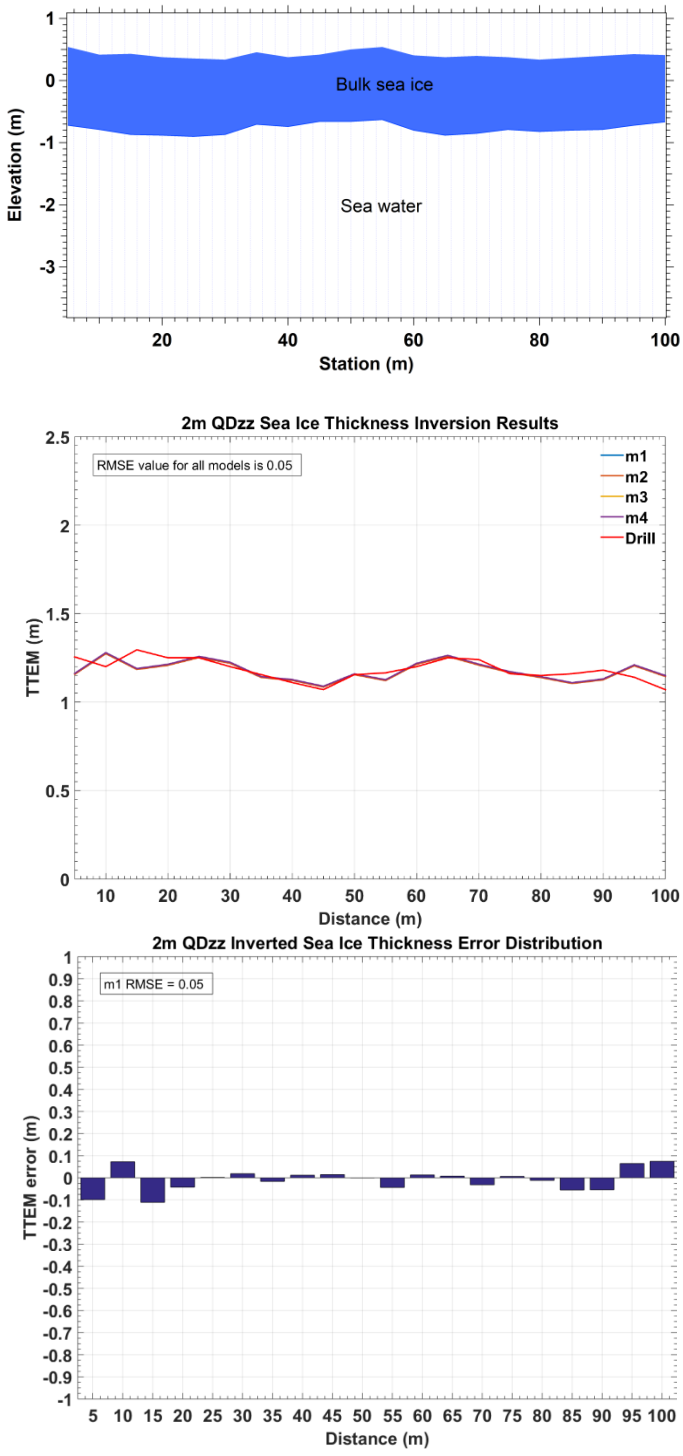

Fig. 6.3: Top: Sea ice and snow thickness along transect Q-10, as observed from drill hole and snow probe measurements taken at 5 m intervals. Middle: Inverted sea ice thickness results using a single 2 m QDzz signal component. All starting models converge to the same result. Bottom: Error distribution of the inverted result.

6.4.2 Ridged sea ice

Transects P-05 and P-11 contain the thickest sea ice formations (Fig. 6.4), consisting of ridged sea ice type at the center of the transects that gradually flatten out to level sea ice type towards the ends of the transects. According to the in situ drill measurements, transect P-05 has a mean sea ice thickness of 1.76 m with a standard deviation (SD) of 0.63 m. The mean and standard deviation of sea ice thickness for transect P-11 are 2.21 m and 0.94 m, respectively. EM instruments tend to underestimate sea ice thickness of ridged sea ice by as much as 50%. This is because the ridge keels have higher porosity making it more conductive relative to uniform solid sea ice structure. Moreover, because of the geometrical structure of ridged sea ice, the EM footprint is not just influenced by ridged sea ice but also by thinner sea ice surrounding it. This makes the average signal readings at the ridge zone more sensitive to sea-water influence.

Regardless of which data component(s) is used in the inversions, results indicate that RMSE values are much greater for P-11 than for P-05. This is attributed to the more complex structure of the sea ice along transect P-11. According to drill measurements, the ridged ice along transect P-11 shows substantial variability in the draft of the ridge keel compared to P-05. Due to the relatively large footprint of the EM sensor, SIS cannot resolve the variability of the ice thickness across this ridge. The error distributions are greatest where there are sharp changes in sea ice thickness along the transect. This is evident for P-11 where keel structures are very sharp (Fig. 6.4).

Considering Table 6.3 and examining the error distribution along the two transects it is observed that using single or paired data components gives reasonably accurate and reliable results to sufficiently map the entire sea ice thickness profile of both transects. An attempt was made to determine if using multiple data components can improve results for ridged ice sections. However, none of the multiple data components improved results.

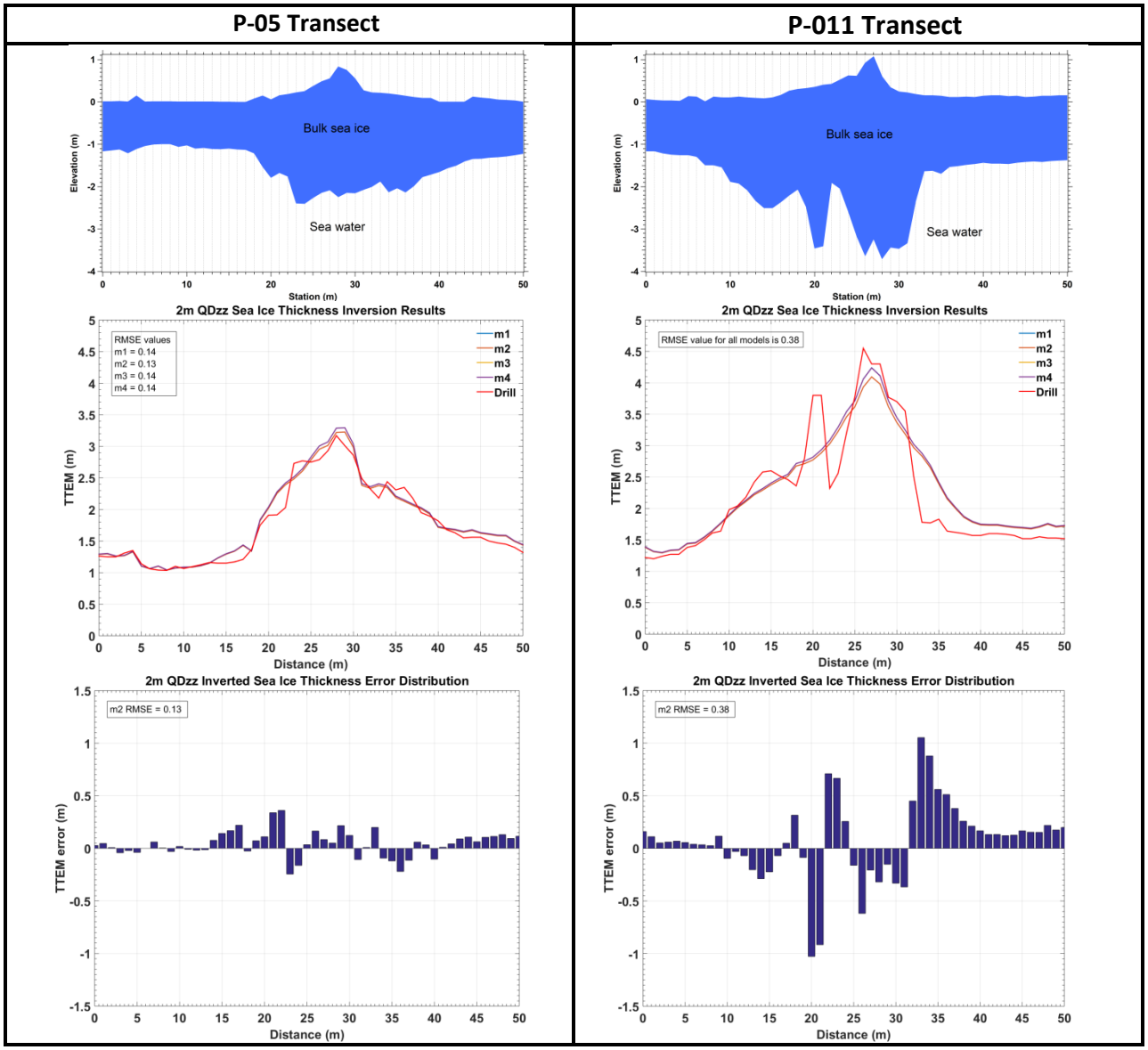

Fig. 6.4: Top: Schematic presentation of sea ice thickness along transects P-05 (left) and P-11 (right). Sea ice thickness measurements are from drill-hole surveys performed at 1 m spaced intervals. Mid-sections of the profiles are ridged sea ice structure on the surface and keel at the bottom. Middle: Inverted sea ice thicknesses of the most accurate data component. Bottom: Error distribution of the most accurate model.

6.4.3 Rafted sea ice

Transect Q-12 is covered with rafted sea ice. Drill measurements taken at 2 m distance intervals show an average bulk sea ice thickness of 1.44 m with a standard deviation of 0.9 m. Rafted sea ice pieces have created sharp and erratic small-scale surface irregularities. In some areas of the transect, the size of surface irregularities is even smaller than the footprint size of 1 m coil spacing. The internal sea ice structure is also extremely complex.

Graphical analysis of inverted sea ice thicknesses reveals that with the exception of 4 m IPzzQDzx inversion results (Fig. 6.5), the predicted sea ice thicknesses are commonly overestimated for all coil configurations and models. As shown in Table 6.3, the most accurate result is also generated by 4 m IPzzQDzx (RMSE of 0.12). All other 4 m input data combinations yield relatively higher RMSE errors. Subsequently, 1 m and 2 m single data component inversion results shown in Table 6.3 yield the lowest RMSE values.

As stated before, both sea ice surface and internal structure are very complex and fluctuate rapidly within short distances. The overestimation of inverted sea ice thicknesses may be explained by the ratio of instrument's footprint size relative to rapid fluctuation in sea ice structure, frequency of drill-hole measurements and uncertainty in instruments height above the sea ice surface.

Longer coil spacing covers a larger area of sea ice (larger footprint). The EM response measured is an average response of the area under the instrument. Therefore the discrepancy between the inverted sea ice thicknesses and drill measurements (RMSE values) is larger for longer coil spacings as is generally observed in Table 6.3. The distance interval the drill-measurements were taken (2 m intervals) may be too large to effectively represent the sea ice fluctuations. Lastly, the complex sea ice surface structure and uneven snow distribution along transect Q-12 generate greater uncertainty in instruments height above the sea ice surface. Actual instrument height above sea ice surface is most likely higher than what is used in the inversions. This leads to significant error (up to 0.2 m) and overestimation of inverted sea ice thicknesses for this particular sea ice type.

Overall, more data is required to make a reliable assessment of SIS performance over rafted sea ice. Evaluation of available data (transect Q-12) suggests that utilization of 4 m IPzzQDzx

yields most accurate results followed by 1 m and 2 m single coil data components indicated in Table 6.3.

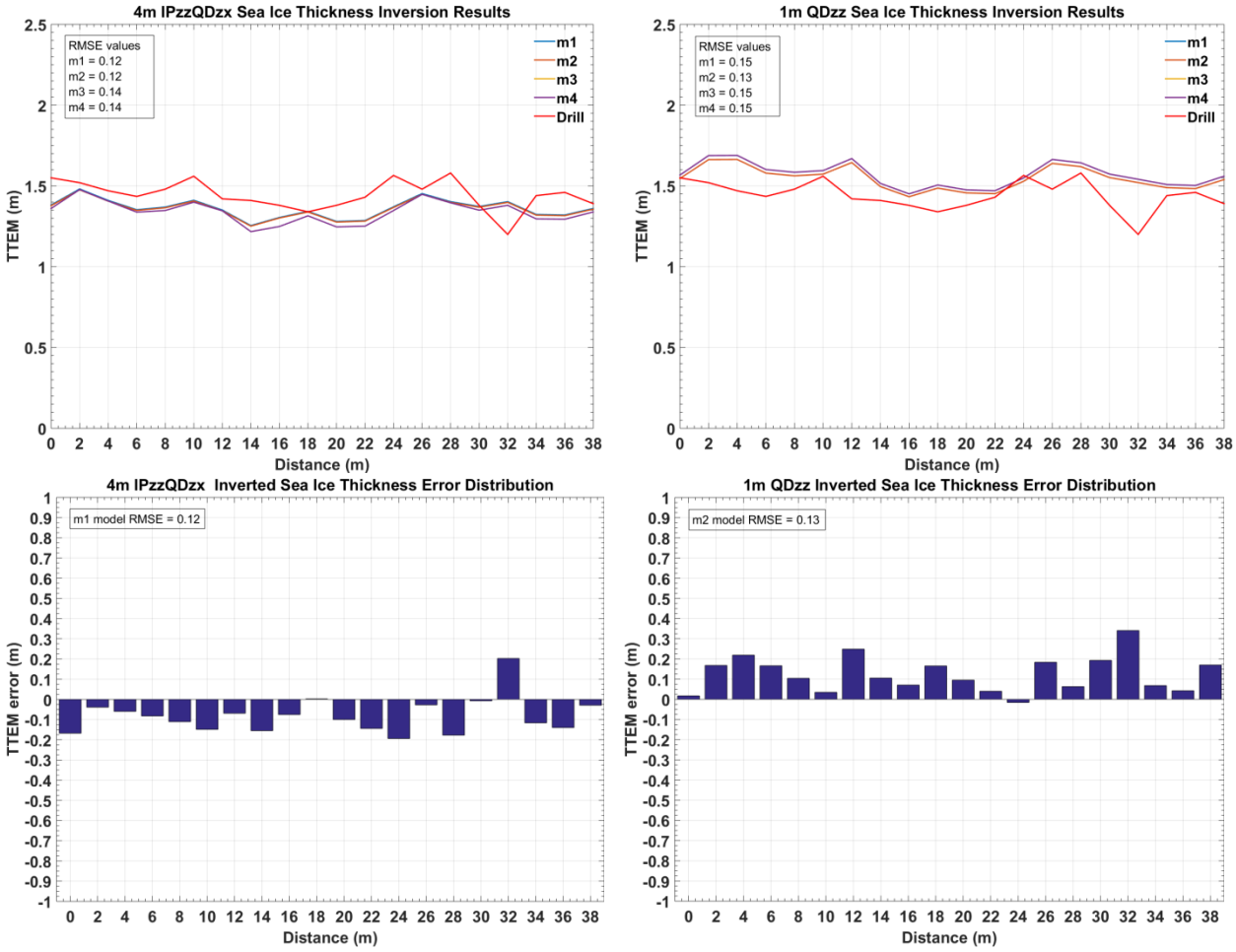

Fig. 6.5: 4m IPzzQDzx (right) and 1m QDDzz (left) inversion results of transect Q-12. Top plots show predicted sea ice thicknesses. Bottom plots represent error distributions.

6.4.4 Melt pond

As previously discussed (Chapter 5.3), the level sea ice on either side of transect P-05 contains two frozen melt ponds (Fig. 5.2). Furthermore, it was shown that the EM readings from all coil configurations were influenced (stronger signal readings) by the larger melt pond that extends from station 7 to 16 (Fig. 5.3).

A two-layered and a four-layered earth model were utilized for the inversion of sea ice thicknesses. In the two-layered earth model, the frozen melt pond and the sea ice below the melt pond were collectively grouped into one single layer (bulk sea ice). Here, the objective of a two-layered earth model is only limited to estimating the depth of the sea ice – sea water interface (bulk sea ice thickness). It does not provide any information about the melt pond.

The inversion results from two-layered earth models generally show a very good agreement between the inverted sea ice thicknesses and the drill-hole data. The most accurate results are generated with 4 m QDzx (RMSE = 0.14) and 2 m QDzz (RMSE = 0.13) single coil components which also yield strongest EM responses in their coil spacing categories (Fig. 6.6).

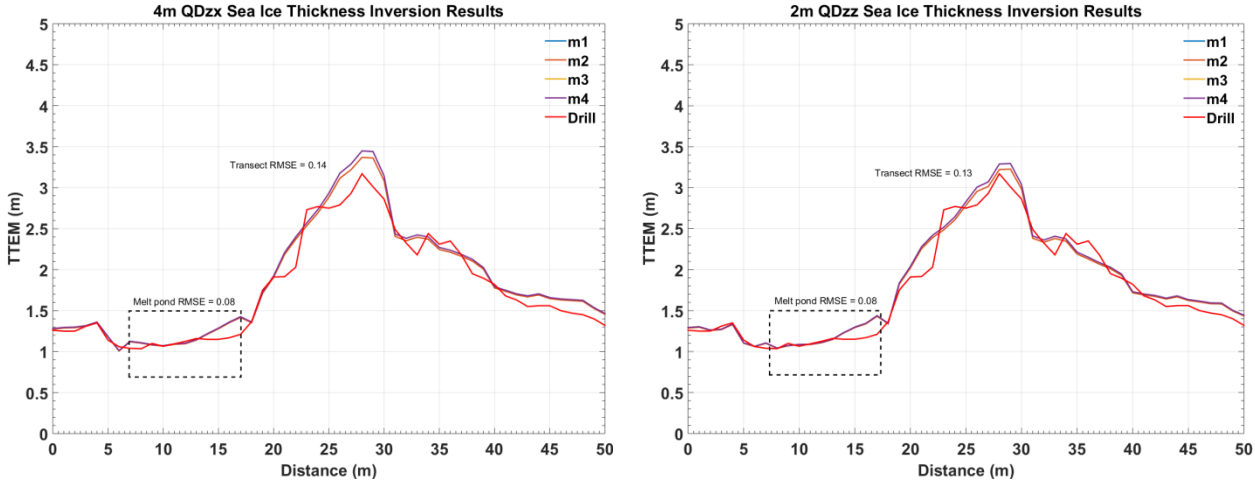

Fig. 6.6: Two-layer model sea ice thickness inversion results of 4 m QDzx and 2 m QDzz data components of transect P-05. The line segments in rectangle represent the melt pond section of the transect.

In a four-layered earth model (Fig. 6.7), the snow and ice covering the melt pond were collectively grouped into a single layer. The frozen pond forms the second layer of the model.

The sea ice below the melt pond and the seawater from the third and fourth layers of the four-layered earth model subsequently.

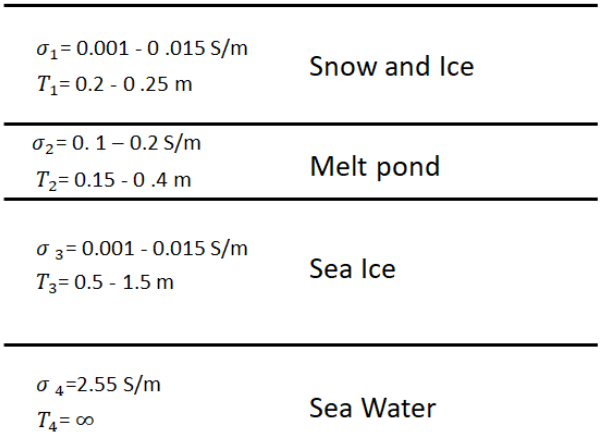

Fig. 6.7: Schematic diagram of the four-layered model used for melt pond section inversions.

Since the sea ice – sea water depth can be determined using a two-layer earth model, the primary goal of using a multi-layered earth model was to specifically estimate the melt pond depth. Nerveless, accurate thickness estimation of the ice layers below and above melt pond would also be ideal.

According to the four-layered earth model inversion results, 1 m IPzzQDzzQDzx yielded the most accurate melt pond thicknesses with the lowest RMSE value being 0.06 (Fig. 6.8). The estimates for top sea ice cover thicknesses were also very good (RMSE = 0.02). The least accurate layer thickness estimates were for the bottom sea ice layer with the lowest RMSE of 0.15. In general, the accuracy of the results decreased from top to bottom layers for all coil configurations. However, 1 m coil spacings showed relatively lower RMSE values compared to 2 m and 4 m coil spacings.

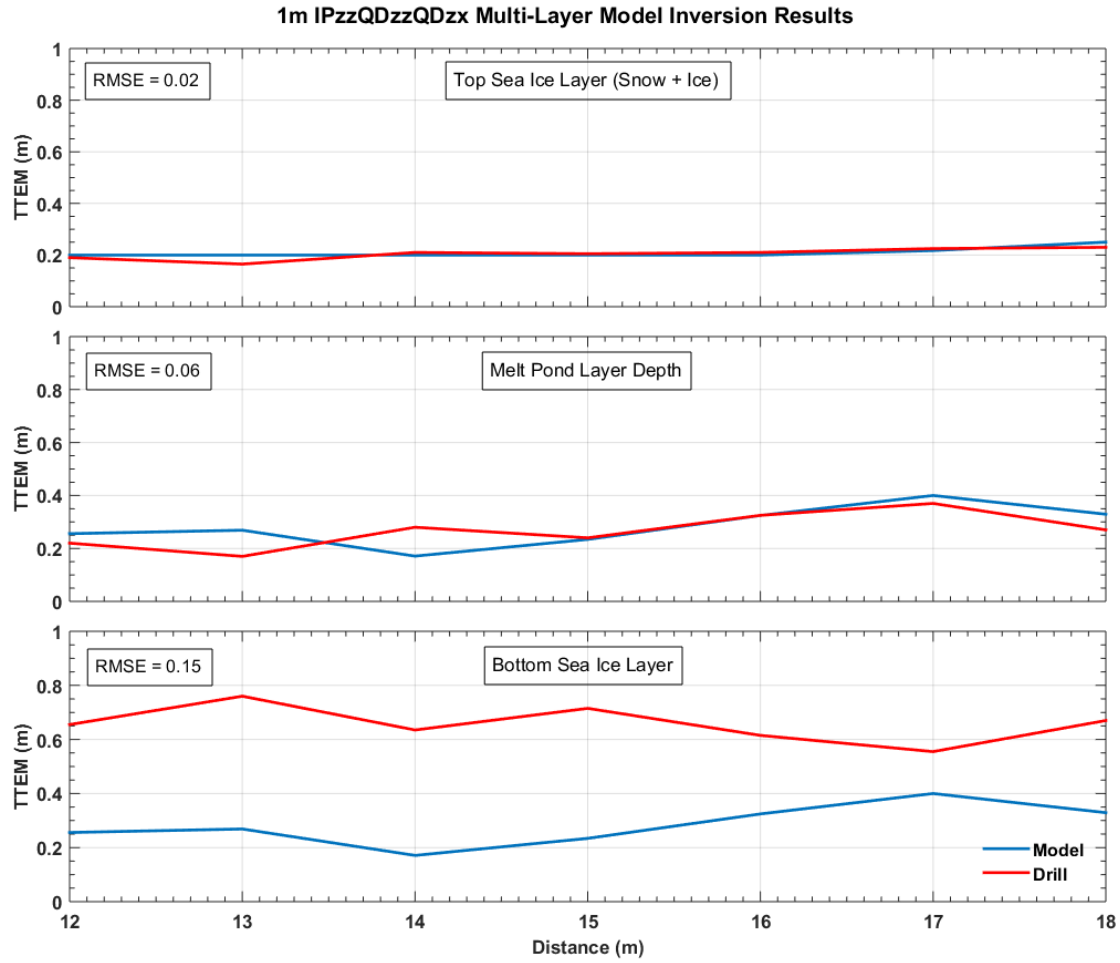

Fig. 6.8: 1 m IPzzQDzzQDzx inversion results using a four-layered earth model for Transect Q-12 melt pond section. The accuracy of the inverted thicknesses decreases from top to bottom layers.

Overall, utilization of a two-layered earth model with single data component inversion input (4 m QDzx and 2 m QDzz) provided accurate estimates for the sea ice – sea water interface depth of a melt pond covered sea ice. Furthermore, employment of a four-layered model and using multi-data component of 1 m coil spacing (1m IPzzQDzzQDzx) proved to accurately estimate not only the melt pond but also the ice layers above and below the melt pond.

6.4.5 Slush covered sea ice

Transects Q-11 and Q-13 consist of thin (~1 m) level sea ice covered with slush sections that are unevenly distributed along the transects. Unfortunately, the exact extent and depth of the slush sections could not be fully documented for transect Q-13 due to undesirable field conditions, uncertainty in detecting exact slush-snow boundaries and time constraints of the transect survey. Working on slush sea ice condition was physically very demanding.

Inversion of slush covered sea ice section of transect Q-11 was performed using both a two-layered earth model and a four-layered earth model. However, since there are no reliable slush drill-hole measurements available for transect Q-13, only a two-layered earth model was used for the inversions of this transect to estimate bulk sea ice thickness (sea ice – sea water interface depth).

Transect Q-11

For transect Q-11, drill-hole measurements were taken at 5 m intervals from station 0 to 35. During the drill measurements, the presence of slush on top of the sea ice was noted from stations 20 to 35. The exact starting point of the slush is not known but is approximated to be between stations 15 and 20.

Graphical analysis of two-layered earth model inversions indicates that the predicted sea ice thicknesses are overestimated between stations 0 to 15 m and are underestimated from stations 15 to 35 m (Fig. 6.9). The underestimated sea ice thicknesses coincide with the slush segment of the transect. This underestimation can be explained by the higher bulk conductivity of the slush and snow-covered sea ice. High conductivity seawater mixed with the snow-cover overlying the sea ice increases the bulk sea ice conductivity. Higher conductivity values lead to stronger EM signals and hence the underestimation of sea ice thickness.

Evaluation of inverted sea ice thicknesses using original starting models reveals that single, paired and three data component combinations at 2 and 4 m coil spacings give best inversion results (Table 6.3). The RMSE values are low and the error distribution on either side of station

15 is at its minimum and uniformly distributed. Figure 6.8 shows an example of the inversion results using paired data components for 2 coil spacing.

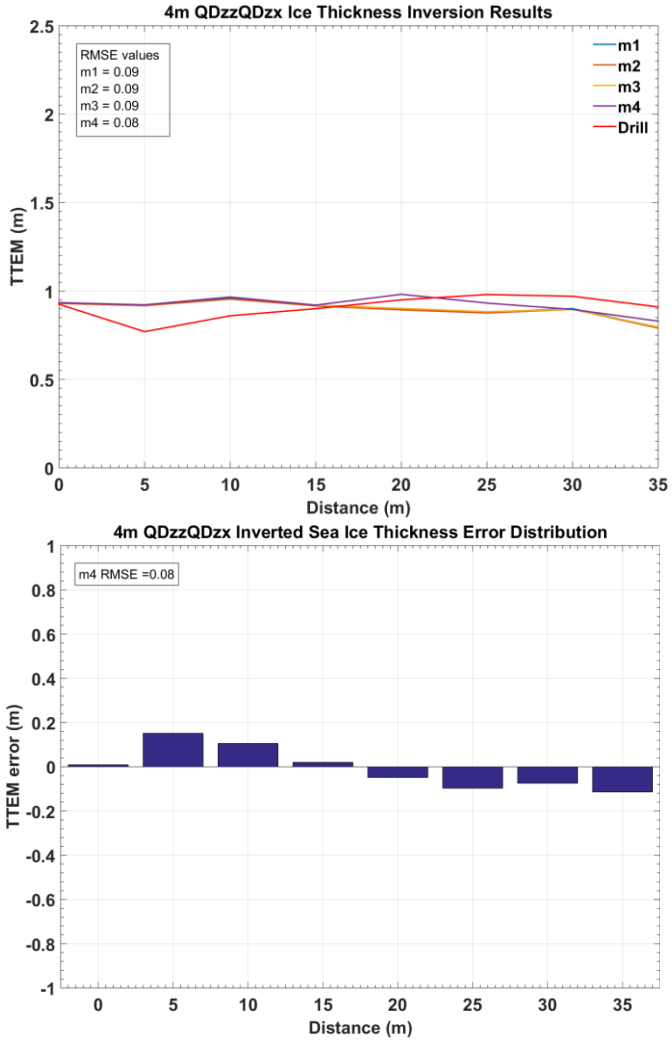

Fig. 6.9: Transect Q-11 example inversion result for 4 m QDzzQDzx paired signal component. Top plot show predicted sea ice thicknesses for all four two-layer models. Most models converge to the same result. The bottom plot presents the error distribution from station 0 to station 35 for the m4 model (model with lowest RMSE). As illustrated in the plots sea ice thicknesses are overestimated from station 0 to station 15 and underestimated from station 15 to station 35 where slush sea ice is present.

The sea ice conductivity values of the original four starting models may not be suitable for inversion of data acquired over slush-covered sea ice as the bulk sea ice conductivity of slush-covered sea ice is presumably much higher than that of dry snow-covered sea ice. In an attempt

to improve the sea ice thickness estimates for the slush segment, the conductivity parameter of the sea ice layer in the staring models was increased (Table 6.4). Inversion results generated from adjusted models significantly improved sea ice thicknesses of slush segment (Table 6.5, Fig. 6.10).

Table 6.4: Starting models generated for slush sea ice inversions. The sea ice conductivity values were increased relative to the original (slush-free) starting models presented in Table 6.1. The conductivity values were allowed to iterate between 0.001 S/m to 0.3 S/m.

Starting model	Sea ice conductivity (S/m)	Seawater conductivity (S/m)
m1s	0.05	2.54
m2s	0.1	2.54
m3s	0.15	2.54
m4s	0.2	2.54

The RMSE values of the new inversion models were calculated (Table 6.12 in the appendix), and the lowest RMSE values were selected for accuracy analysis (Table 6.5). Inversion results generated from the adjusted starting models show significant improvement in the accuracy of the inverted sea ice thicknesses. The deviation between the drill measurements and inverted sea ice thicknesses decreased for all data components. Evaluation of the RMSEs reported in Table 6.5 indicates that 4 m and 2 m coil spacings results for single, paired and three component data yield the most accurate, reliable estimates of sea ice thickness. Figure 6.10 demonstrates the inversion improvements for the 2 m IPzzQDzz data component. The RMSE value for this particular data component decreased significantly from 0.09 m to 0.02 m. The maximum error decreased from approximately 0.12 m to under 0.03 m.

Table 6.5: Data components that generate the most accurate sea ice thickness inversion results for the slush-covered sea ice segment on transect Q-11 (15 to 35 m). Numbers in brackets are the lowest calculated RMSE values, reported in meters.

Inversion data input	4 m coil spacing	2 m coil spacing	1 m coil spacing
1 component	QDzx (0.03), IPzz (0.03)	QDzz (0.03), IPzz (0.03)	QDzz(0.05),IPzz (0.05)
2 components	IPzxQDzx (0.02)	IPzxQzz (0.02), IPzzQDzz (0.02)	IPzzQDzz (0.03)
3 components	QDzzQDzxIPzx (0.02) IPzzQDzzIPzx (0.02)	IPzzQDzzIPzx (0.02)	IPzzQDzzQDzx (0.07)
4 components	IPzzQDzzIPzxQDzx (0.02)	IPzzQDzzIPzxQDzx (0.04)	NA

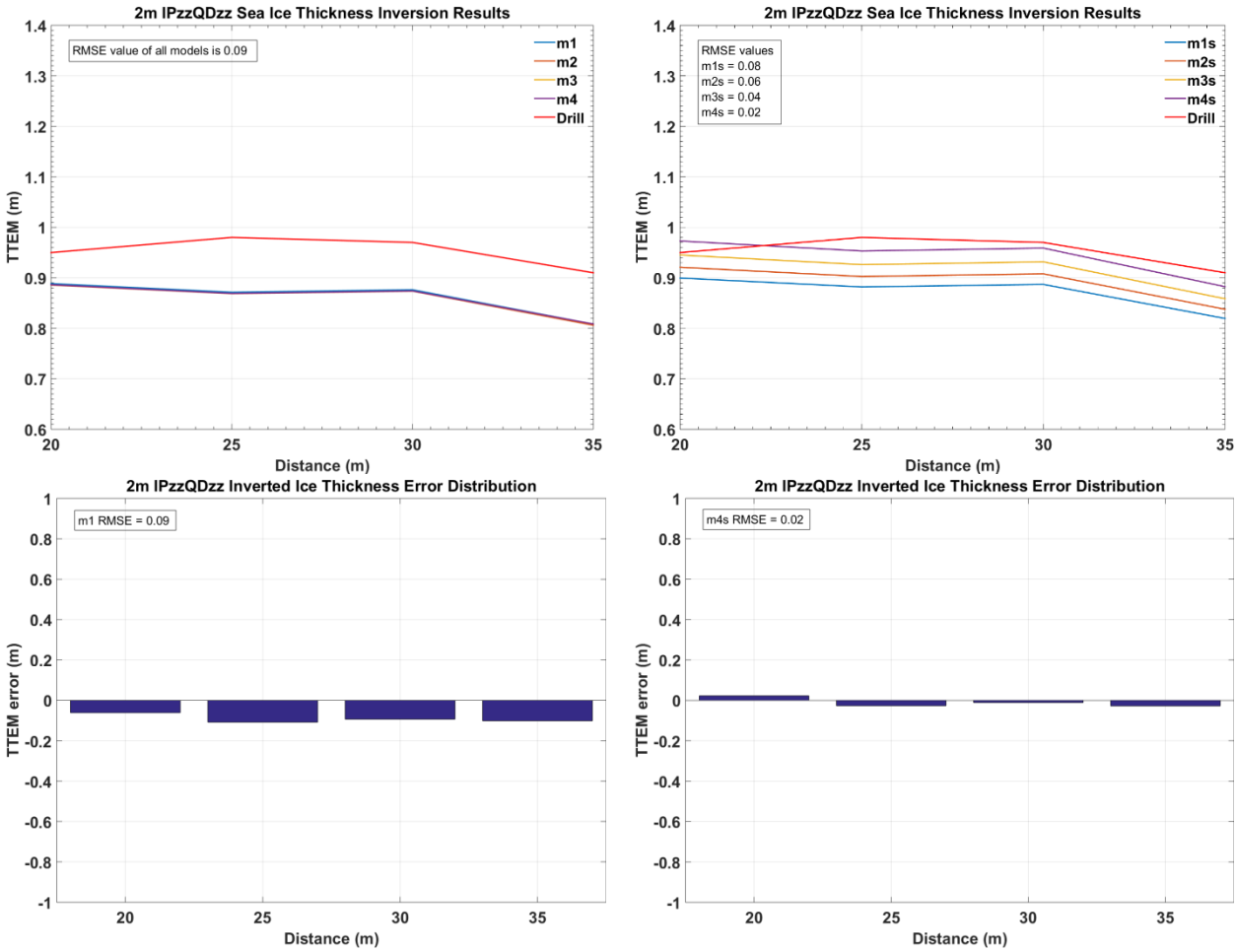

Fig. 6.10: Examples of sea ice thickness inversion results of the slush-covered segment (station 20 to 35) of transect Q-11. 2 m IPzzQDzz results are used to demonstrate the improvements made when two-layered starting models are adjusted to higher bulk sea ice conductivity values. The top left figure illustrates inversion results using the original 4 starting models. The top right plot illustrates the inversion results using the 4 adjusted starting models. The plots below show their corresponding error distribution for models that show the lowest RMSE values.

A four-layered earth model was also employed in the inversion of the slush-covered sea ice EM data (Fig. 6.11). The objective was to investigate if utilization of a multi-layered earth model in the inversions can provide accurate thickness estimates of the layers defined in Fig. 6.11.

The inversion results showed that using four-layered earth models provide accurate thickness estimates of individual layers. The results are tabulated in Table 6.12. Most overall accurate estimates were generated by 4 m IPzzQDzxIPzx input data, Fig. 6.12. However, many other configurations also generated very good results.

σ_1= 0.001 - 0 .015 S/m T_1= 0.3 - 0 .5 m	Snow and Ice
σ_2= 0. 1 – 1 S/m T_2= 0.03 - 0 .12 m	Slush
σ_3= 0.001 - 0.015 S/m T_3= 0.45 - 0 .55 m	Sea Ice
σ_4=2.55 S/m T_4= ∞	Sea Water

Fig. 6.11: Schematic diagram of four-layered earth model employed for inversion of slush EM data of transect Q-11.

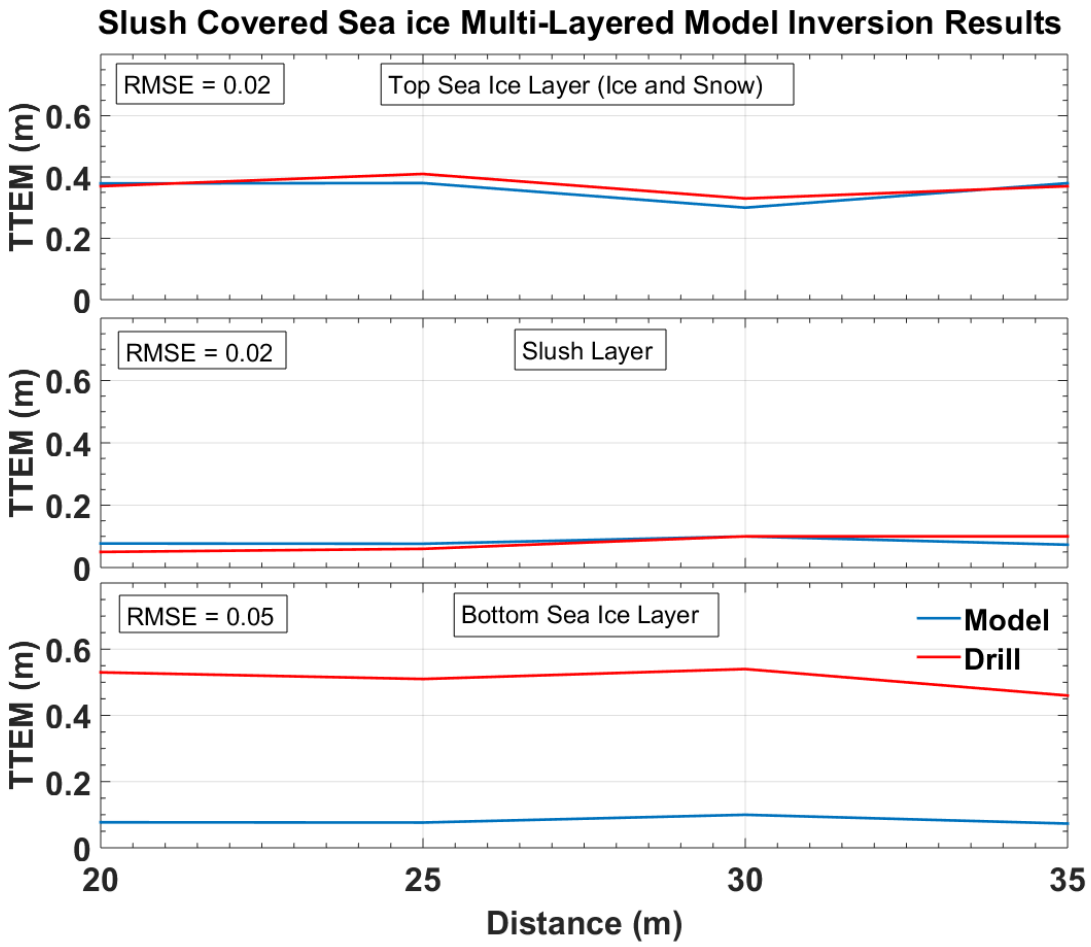

Fig. 6.12: Transect Q-11, Inverted sea ice thicknesses from a multi-layered inversion model using 4 m IPzzQDzxIPzx multi-data component.

Transect Q-13

The thickness of slush observed on transect Q-13 was significantly larger than that observed on transect Q-11. The area surrounding Q-13 was flooded a day before the drill hole and SIS survey from a nearby hole that was opened in the ice for scuba-diving. Just prior to conducting the survey, the diving hole was re-opened, allowing a large amount of seawater to flood the sea ice surface again. The slush conditions (depth and wetness) were highly variable along the transect and intensified throughout the time period in which the drill and SIS surveys were carried out due to the constant flow of seawater from the diving hole. The drill measurements were taken at variable distance intervals along the transect with the intention of covering the variability in the slush conditions along the transect.

Surprisingly, graphical analyses of the inversion results reveal that the same sea ice thickness underestimation observed over slush segment of Q-11 does not occur for transect Q-13 (Fig. 6.10 cf. Fig. 6.13). In fact, the inversion results tend to overestimate sea ice thickness along Q-13. Nevertheless, the accuracy of inverted sea ice thicknesses was very good showing low RMSE values.

Regardless, similar to transect Q-11, new staring models (Table 6.4), with adjusted conductivities for the sea ice layer, were tested. The inversion results did not improve using the adjusted starting models; rather they became worse (Fig. 6.14).

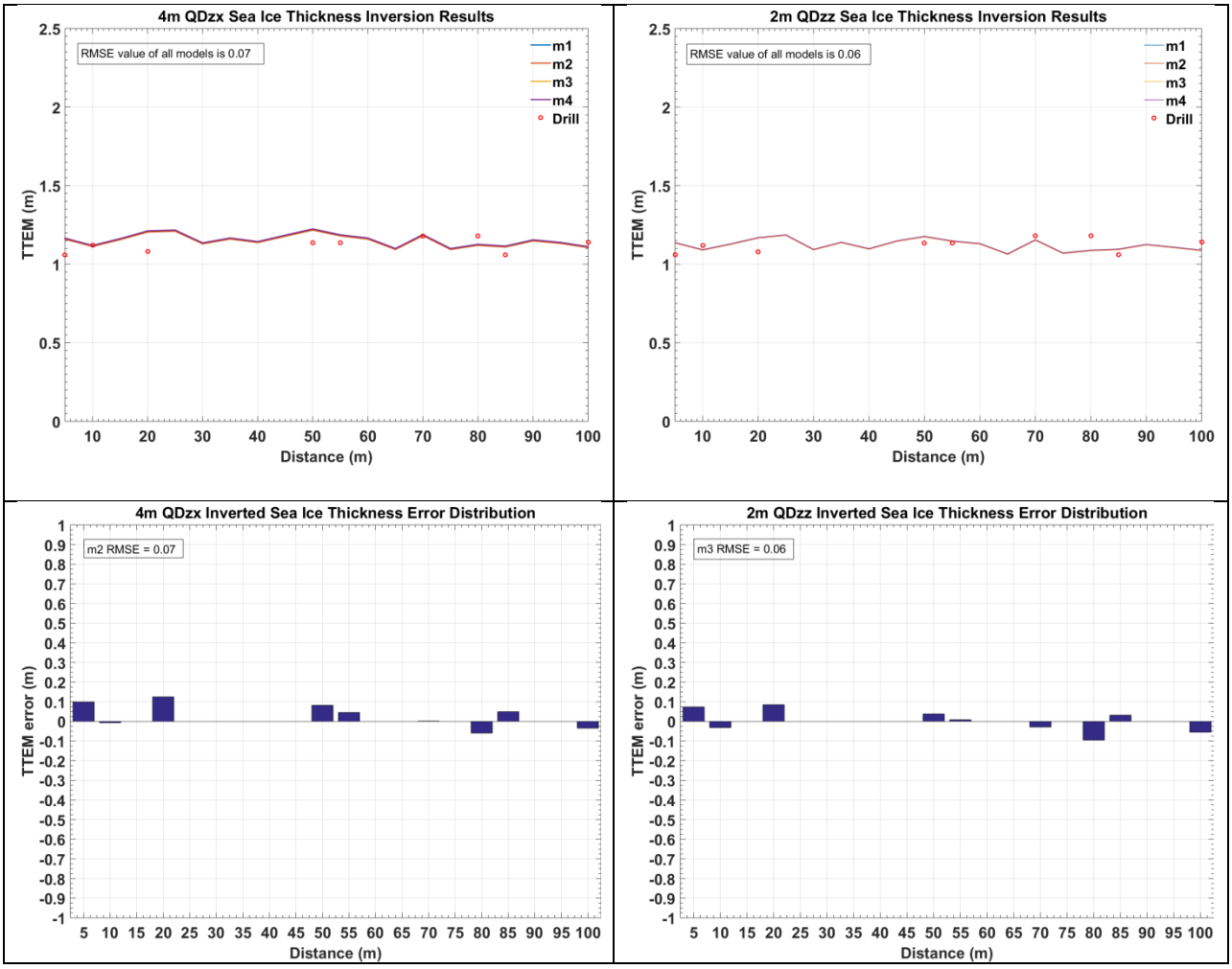

Fig. 6.13: Transect Q-13 example inversion results for 4 m (left plots) and 2 m (right plots) coil spacings using a single data component. Results show accurate sea ice thickness estimates. The drill measurements (red circles) were taken at variable intervals along the transect.

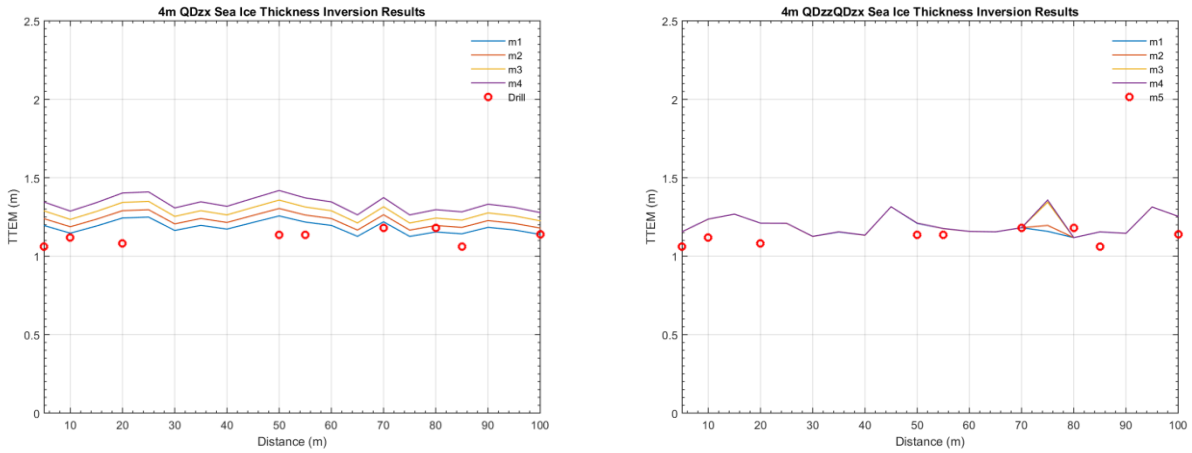

Fig. 6.14: Transect Q-13 example inversion results for 4 m coil spacing QDzx and QDzzQDzx data components using starting models adjusted for slush covered sea ice type (Table 6.4).

This difference in the inversion results between Q-11 and Q-13 is most likely caused by instrument height errors introduced into Q-13 inversions. The instrument height used in the inversions of both transects was equally 0.2 m. This height is based on the actual field observation made at the start of each survey. However, do to the extreme and dynamic slush conditions of Q-13, the sled runners SIS was positioned on, penetrated deeper into the snow during the survey. Therefore the actual instrument height was considerably smaller than the input height used in the inversions, leading to an overall overestimation of sea ice thicknesses of transect Q-13.

Evaluation of the inversion results using the original starting models (Table 6.1) reveals that the best ice thickness estimates are achieved by 4 m and 2 m coil spacings using single, paired and 3 data components, as indicated in Table 6.3

6.5 Conclusion

Two-layered and multi-layered inversion models were used to evaluate inversion results. The two-layered inversion models were solely used to estimate bulk sea ice thickness (sea ice – sea water interface depth). Results generated very good bulk sea ice thickness estimates for all sea ice types investigated in this research. The multi-layered models were only used for melt pond and slush-covered sea ice type.

The inversion results indicated that using 2 m coil spacing quadrature signal component (2 m QDzz) with two-layered earth inversion models is sufficient and most reliable for generating accurate bulk sea ice thickness estimates for most sea ice types.

Analysis of the sea ice thickness error distribution along the transects showed that errors are lowest and more or less uniformly distributed for level sea ice. Errors where highest for ridged sea ice transects; particularly over areas that show a sharp change in sea ice thickness within short distance intervals.

Two-layer inversion results for slush covered sea ice varied and is not conclusive to all slush sites. For transect Q-13, original starting models appeared to yield accurate results. Using the same original starting models lead to the underestimation of sea ice thickness for transect Q-11. However, upon adjusting the starting models to have higher bulk conductivity values for the sea ice layer, the results improved significantly for transect Q-11 (Fig. 6.10). For this particular sea ice type, the utilization of paired and three data component at 4 m and 2 m coil spacings provided the most accurate inversion results. The difference observed between the two slush sites (transect Q-11 and Q-13) may be explained by the instrument height error in Q-13 inversions. However, more field data is needed to validate this conclusion.

Utilization of multi-layered inversion models generated very good thickness estimates of melt pond and slush layers (Fig. 6.8 and Fig. 6.12). For the melt pond, 1 m coil spacing IPzzQDzzIPzx multi-data components yielded the most accurate results (Fig. 6.8). It appeared that 1 m coil spacing EM data performs better than longer coil spacings. For slush site however the 4 m coil spacing with IPzzQDzxIPzx multi-data components yielded best results (6.12).

7 Effect of coil orientation changes on inversion results

7.1 Introduction

A common assumption made in EM data interpretation is that the transmitter-receiver coils are level with respect to the ground surface without any tilt or rotation. However, during EM survey operations (both airborne and in situ surface-based EM surveys), platforms containing EM instruments are continuously subject to oscillations that cause constant variable orientation (rotation and tilt) of transmitter-receiver coils. Re-orientation of transmitter-receiver coils changes the EM coupling response between the coils and the conductive subsurface, such as the sea ice-sea water interface.

Traditional surface-based EM instruments, such as Geonics's EM-31, do not measure or record sensor orientation parameters (pitch or roll) and assume that variability of the sensor orientation is minimized by the operator and that the impact of pitch and roll changes on the measured electromagnetic signal are negligible. Therefore, the potential effect of sensor pitch and roll has not been considered for surface-based EM measurements of the sea ice. The SIS simultaneously measures and records changes in the sensor's orientation (pitch and roll). The recorded pitch and roll data are used by SISinvert to model the EM response more accurately than if zero pitch and roll were assumed. This minimizes errors caused by instrument pitch and roll changes in the inversion results.

In this chapter, the effect of SIS rotational changes on the measured EM response is analyzed. The objective of this chapter is to determine whether or not SISinvert is capable of effectively estimating accurate sea ice thicknesses when sensor pitch and roll angles are variable.

7.2 Background & historical studies

EM responses are affected by the geometry of the transmitter-receiver coils (rotation, separation, and heights) relative to sea ice- sea water interface. Variable orientation of EM instruments changes the geometric relationship between the transmitter-receiver coils and the sea ice-sea water interface, thereby altering the measured EM coupling response from sea ice-sea water interface (Fitterman and Yin 2004). In this chapter, only pitch and roll changes are considered (Figure 7.1).

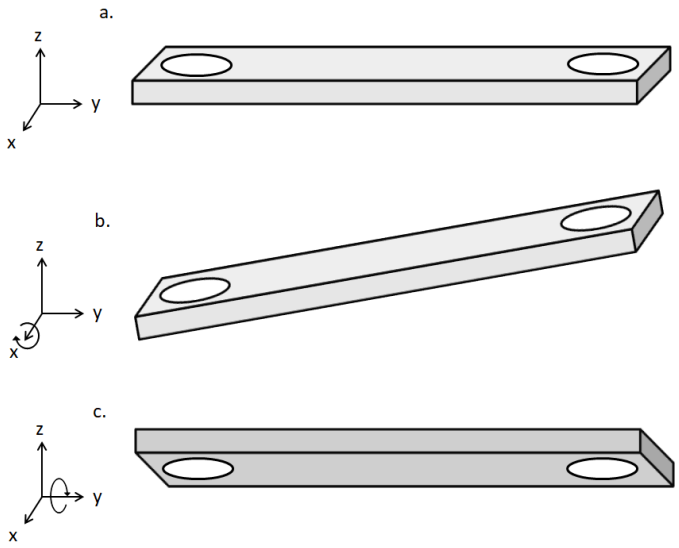

Fig. 7. 1: Illustration of pitch and roll coil rotations. (a) EM instrument leveled with no rotation along any axis. Pitch and roll angles are 0°. (b) EM instrument rotated around the x-axis (pitch). (c) EM instrument rotated along the y-axis (roll). Clockwise rotation yields positive values.

Previous studies on the effect of transmitter-receiver rotational changes on the measured EM response are mainly concentrated on airborne EM surveys (Yin and Fraser 1997, 2004; Holladay et al. 1997). Theoretical estimation of the transmitter-receiver coil orientation effect on the measured EM response is discussed in detail by Fitterman and Yin (2004). Effects are commonly considered to be negligible for coil orientation changes that are normally observed in the field. Computer models have shown that pitch or roll angles of 10° produce a maximum error of 1.5% in the measured EM response for a HCOP coil configuration (Holladay et al. 1997). When both pitch and roll angles are 10º the measured EM response yielded a 2.9% error for a HCOP coil

configuration (Holladay et al. 1997). Holladay et al. (1997) demonstrated that including sensor pitch and roll as parameters in EM data inversion significantly improved the accuracy of airborne sea ice thicknesses estimates derived by inversion by reducing errors to less than 4%.

7.3 Field observations

Analyzing pitch and roll recordings of field data indicated that there is a continuous change in the pitch and roll angles of the transmitter-receiver coils. Pitch and roll changes are significantly higher for SIS transects acquired during the Polarstern campaign compared to the Qikiqtarjuaq campaign. This is expected as the Polarstern transects contained ridged sea ice (rough sea ice), while the sea ice surface was generally leveled for all Qikiqtarjuaq transects. Figure 7.2 illustrates the pitch and roll variation of selected transects that are representative of the Polarstern and Qikiqtarjuaq data (P-05, P-11, and Q-10). Pitch and roll statistical information derived from all surveyed transects are summarized in Tables 7.1 and 7.2.

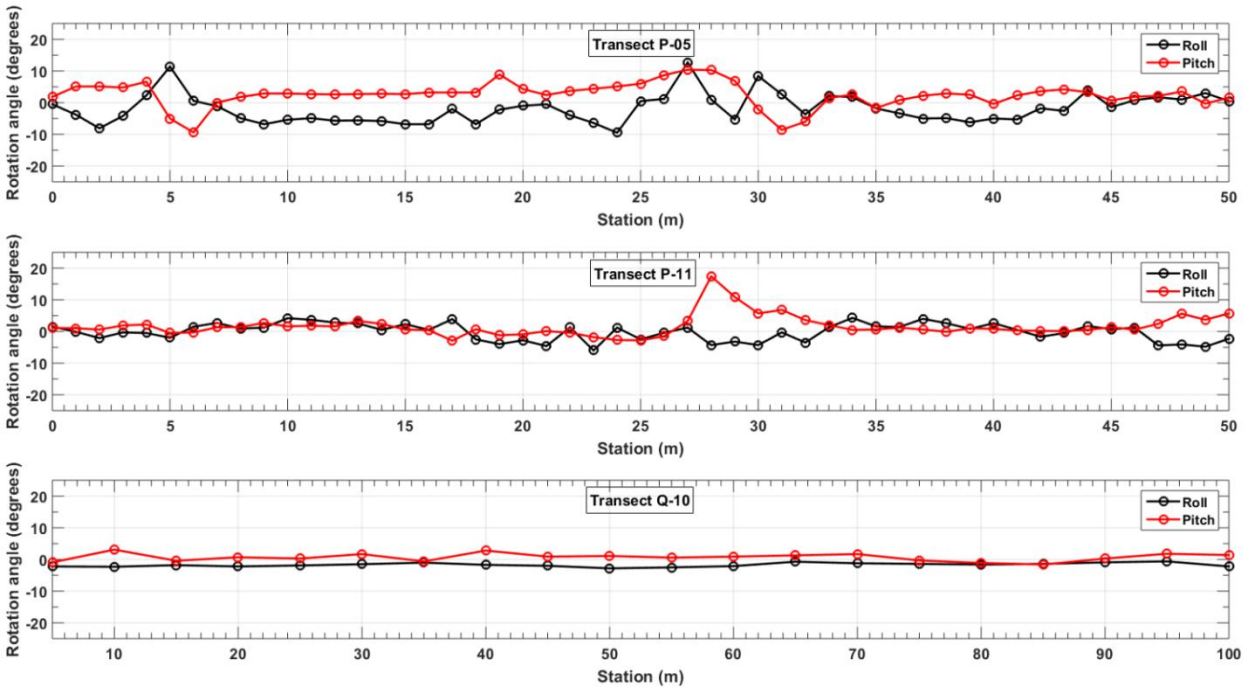

Fig. 7. 2: Pitch (red) and roll (black) variation recorded by SIS for transect P-05, P-011, and Q-11. Selected transects represent the typical pitch and roll variations observed in each study region (Polarstern and Qikiqtarjuaq). The Polarstern transects possess the highest variation in pitch and roll.

Table 7. 1: Statistical summary of pitch and roll data acquired during the Polarstern survey transects.

	P-05		P-11	
Parameter	Pitch	Roll	Pitch	Roll
Min	-9.4	-9.5	-2.9	-6
Max	10.4	12.7	17.4	4.3
Mean	2.5	-1.8	1.6	-0.1
SD	3.9	4.6	3.3	2.7

Table 7. 2: Statistical summary of pitch and roll data acquired during the Qikiqtarjuaq survey transects. Transect Q-14 has the highest pitch and roll variation among all the Qikiqtarjuaq transects.

	Q-10		Q-11		Q-12		Q-13		Q-14	
	Pitch	Roll	Pitch	Roll	Pitch	Roll	Pitch	Roll	Pitch	Roll
Min	-1.6	-2.8	-3.1	-5.1	-0.8	-0.9	-2.3	-1.7	-1.5	2.6
Max	3.1	-0.6	4.2	6	0.8	4.9	2.1	4.5	2.1	8.4
Mean	0.6	-1.7	-0.1	1.4	-0.1	2.3	-0.3	1.1	0.1	5.3
SD	1.3	0.6	1.5	2.0	0.5	1.7	1.2	1.8	0.9	1.5

7.4 Pitch and roll evaluation procedure

Evaluation of pitch and roll effects on the inversion results was conducted in two separate experiments. In the first experiment, a random test site was selected over a level sea ice surface in the Qikiqtarjuaq study area. SIS was placed on the snow surface and EM measurements were acquired while pitch and roll angles were systematically changed. Two different cases were tested:

1. Pitch was kept at 0º while roll angles were systematically changed.

2. Roll was kept at 0º while pitch angles were systematically changed.

Sea ice thickness drill measurements of the site were taken at the end of the experiment for accuracy analysis. Unfortunately, the data file acquired for the pitch experiment (case 1) was discovered to be corrupt only after returning from the field location, and therefore could not be used for this research.

In the second experiment, data collected along transect P-05 with a 2 m coil spacing were inverted to derive sea ice thickness estimates using four different cases:

1. Pitch and roll angles set to 0^o

2. Pitch set to 0^o. Roll set to the actual field observations

3. Roll set to 0^o. Pitch set to the actual field observations

4. Actual pitch and roll used

Transect P-05 was chosen to be the most suitable transect for this experiment as the standard deviations of both pitch and roll measurements were highest along this transect. Data collected with a 2 m coil spacing were selected for this experiment because according to previous analysis it yielded the most accurate sea ice thicknesses for transect P-05 (Table 6.6/ Appendix A).

7.5 Experiment 1 – Field test result over level sea ice

Figures 7.3 shows the quadrature and in-phase field measurements as a function of roll angle for both HCOP and PRP coil orientations and for all three transmitter-receiver offsets. Analyzing these plots, it is evident that roll influences the measured EM response in all coil configurations. In general, an increasing roll angle leads to progressively smaller EM responses, which implies a thicker sea ice cover. 4 m Qzz, 2 m IPzx and 1 m IPzx coil configurations appear to yield anomalous data. The maximum and minimum roll angle SIS can measure is 28.5º and -27.5º. SIS flags measurements where the actual instrument pitch or roll were greater than 28.5 or less than -27.5 and these measurements are not processed by SISinvert. No field data acquired along the Polarstern or Qikiqtarjuaq transects exceeded these limits, and all data collected in the pitch and roll experiments were acquired within the allowable pitch and roll range.

EM response errors relative to 0º pitch and roll EM response are presented in Tables 7.3. According to this experiment, with the exception of the aforementioned anomalous coil configurations, the maximum response error is about 1.7% for roll angles less than 10 degrees. The response changes are very little for roll angles less than 5º, slight for roll angles less than 10º and increases exponentially for roll angles above 10º.

Table 7. 3: Percentage difference between measured EM responses using different roll angles and measured response using normal coil orientation (roll and pitch angles set at $0^{o)}$. Errors increase with increasing roll angles.

	1 m coil spacing				2 m coil spacing				4 m coil spacing			
Roll angle	**IPzz**	**QDzz**	**IPzx**	**QDzx**	**IPzz**	**QDzz**	**IPzx**	**QDzx**	**IPzz**	**QDzz**	**IPzx**	**QDzx**
28.2	11.67	10.89	4.5	12.39	11.03	9.46	11.66	12.76	8.28	-0.06	12.31	12.78
25	9	8.66	2.7	9.46	8.79	7.46	8.36	9.84	6.48	-0.12	9.24	9.93
15	3.67	3	-0.9	2.93	3.14	2.53	1.65	3.2	2.12	-0.33	2.26	3.44
10	1.67	1.36	1.8	1.03	1.33	1.06	0.82	1.24	0.85	-0.3	0.7	1.46
4.1	0.67	0.23	-0.9	0.22	0.29	0.17	-0.59	0.08	0.08	-0.12	-0.38	0.21
2.1	0.33	-0.11	0	-0.22	0	0.07	-0.24	-0.04	-0.03	-0.09	-0.37	0.04
-2.1	0.33	-0.26	0.9	-0.6	-0.1	-0.05	1.77	-0.4	-0.02	-0.09	-0.59	-0.06
-4.1	1	0.09	6.31	-0.38	0.05	0.17	3.3	-0.24	0.19	0.06	-0.35	0.11
-10.1	2.33	1.45	8.11	0.82	1.28	1.16	4.24	1.12	1.28	0.21	1.05	1.42
-15	4.33	3.45	12.61	2.45	3.14	2.82	7.07	2.96	2.73	0.5	3.31	3.39
-24.9	10	9.19	19.82	9.24	8.75	7.67	13.9	9.4	7.24	1.07	10.57	9.88
-27.5	11.67	11.3	29.73	11.58	10.79	9.36	17.9	11.84	8.79	1.27	13.15	12.25

To investigate the effect of roll on inverted sea ice thickness, the inversion results for different roll angles were compared to the inverted sea ice thickness at 0º roll. The results are presented in Figure 7.3. The percentage error of the inversion results relative to the actual sea ice thickness (1.45 m from the in situ drill measurement) is also provided in Table 7.5 in Appendix B.

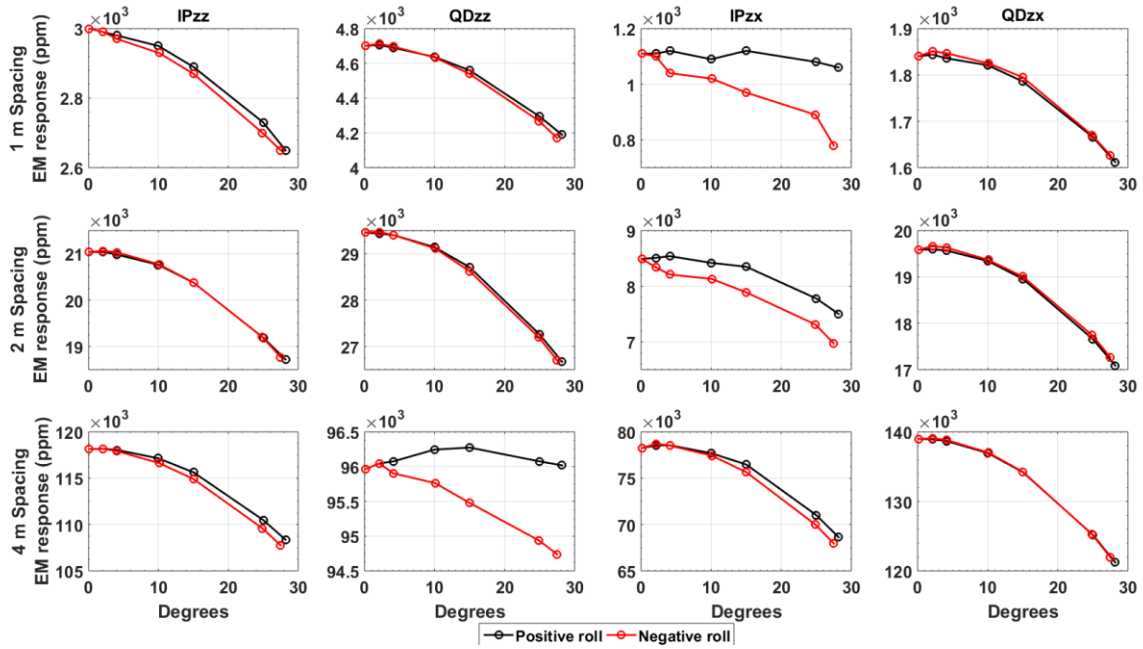

Fig. 7.3: EM response versus positive (black) and negative (red) roll angle for all coil configurations. EM responses 1 m and 2 m IPzx and 4 m QDzz coil configuration are anomalous. All other configurations show very strong agreement between positive and negative roll EM responses.

According to Figure 7.4, the inversion results for each coil configuration have a unique response to roll. In general, the inversion results indicate that an increase in roll angle increases the inversion error; however, the magnitude and rate at which this occurs varies between the coil configurations. For HCOP coil configurations (i.e. IPzz and QDzz), the errors increase significantly, with a 4 m coil spacing displaying the highest errors. This can be explained by the fact that the footprint size of the transmitter and receiver loops both shrink as the roll changes. PRP coil configurations (i.e. IPzx and QDzx) show a greatly reduced sensitivity to variations in the roll. This reduced sensitivity can be explained by the fact that in PRP coil orientation, it is only the transmitter coil that is changing position relative to the ice surface but the receiver coil position relative to the ice surface stays the same during a roll change. QDzx shows insignificant errors (less than 1%) for all coil spacings. IPzx display errors less than 2% for a 4 m coil spacing for all roll angle, although errors at 1 and 2 m coil spacings exceed this value for roll angles greater than 10º.

Overall with the exception of anomalous coil configurations, positive and negative roll tests show strong agreement for any given coil configuration. This indicates good repeatability of the results.

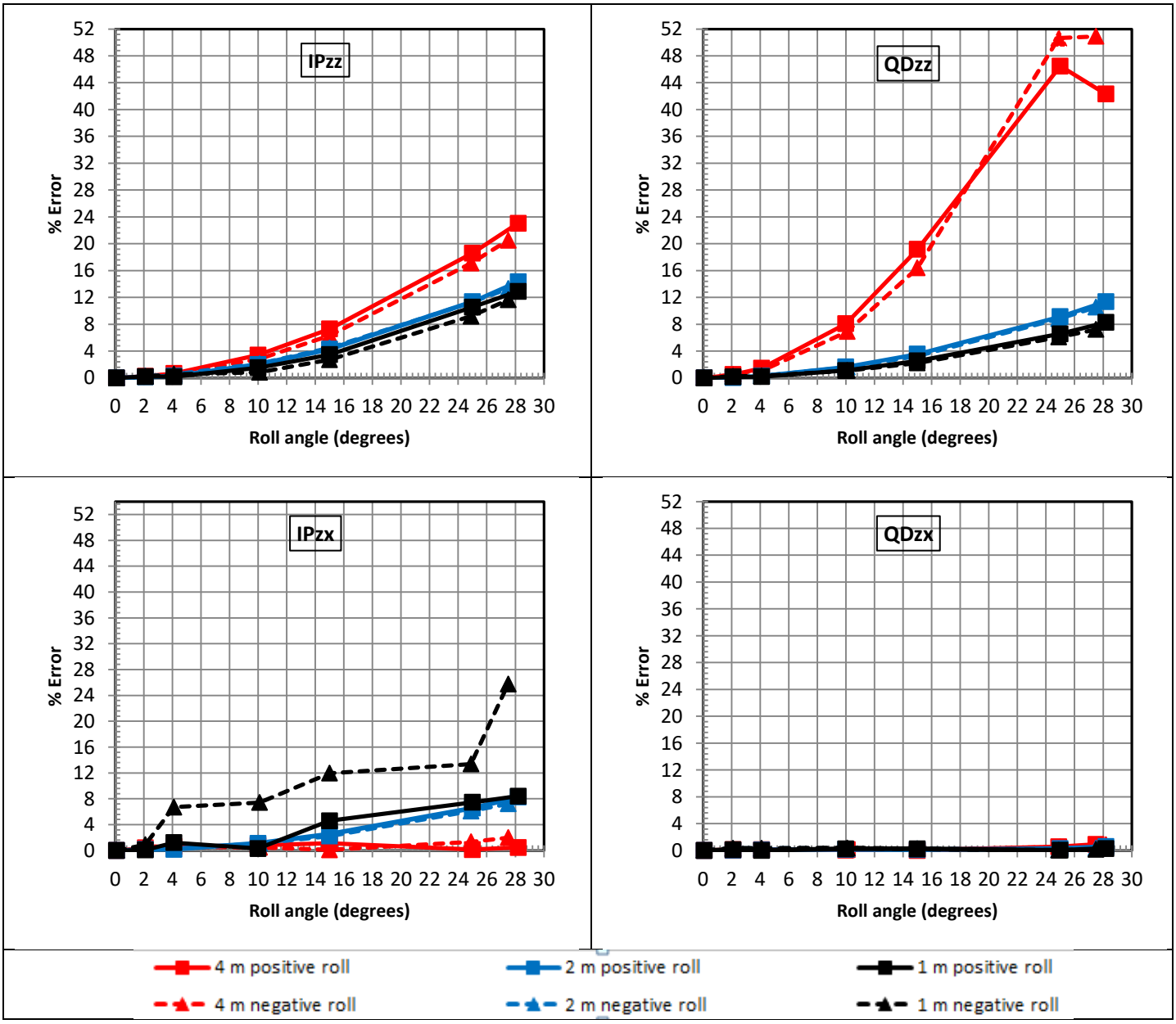

Fig. 7.4: Inverted sea ice thickness results for various roll angles displayed as percentage error relative to inverted sea ice thickness when SIS is oriented normally (0º roll and 0º pitch) over a level sea ice surface that is 1.45 m thick.

7.5 Experiment 2 – Re-inversion of Transect P-05 (ridged sea ice)

Transect P-05 EM data (2 m coil spacing) was re-inverted using four different pitch and roll scenarios mentioned in Section 7.3. Root mean square error (RMSE) was used to evaluate the accuracy of the inverted sea ice thickness estimates relative to the sea ice thicknesses as measured in situ at drill-holes. The error distribution of the inverted sea ice thicknesses for the four pitch and roll scenarios was also investigated to check for consistency of errors along transect P-05 and to evaluate any correlations in error fluctuations between coil configurations.

Analysis of calculated RMSE values indicated that using true pitch and roll measurements yield the most accurate sea ice thickness estimates (Table 7.5). Although the difference in RMSE values within each coil configuration is very small, setting pitch and roll to 0^o yielded the highest error in all coil configurations.

Table 7. 4: Calculated RMSE values (in meters) of inverted sea ice thickness estimates using different pitch and roll scenarios. RMSE units are in meters.

Coil orientation input	IPzz	QDzz	IPzx	QDzx
0 pitch and 0 roll	0.240	0.133	0.169	0.247
0 pitch & true roll	0.229	0.130	0.168	0.246
0 roll & true pitch	0.229	0.128	0.165	0.237
true pitch and roll	0.219	0.126	0.165	0.236

Drill-hole sea ice thicknesses were taken as a reference to calculate error distributions of the four inversion scenarios. The error distributions of all four scenarios are illustrated in Figures 7.5 and 7.6.

The differences between the maximum and minimum inversion errors for the majority of the drill hole stations are very small (< 2%). The maximum difference in errors occurs at station 27 (~4.4% for QDzz), which is the tip of the sea ice ridge, and at station 5 (9.6% for IPzz), which is just before a melt pond.

Analysis of the error distributions indicated that case 1 (0^o pitch and 0^o roll assumed) and case 4 (measured pitch and roll utilized) generally generate either the highest or lowest errors

along the transect. However, for the majority of the stations, case 4 yielded the lowest errors. On average, the difference between case 1 (generally maximum errors) and case 4 (generally minimum errors) inversion results along a transect was about 1.4% (IPzz), 0.35% (QDDzz), 0.005% (IPzx) and 0.15% (QDzx). Case 2 and case 3 errors generally fall in between case 1 and case 4 errors.

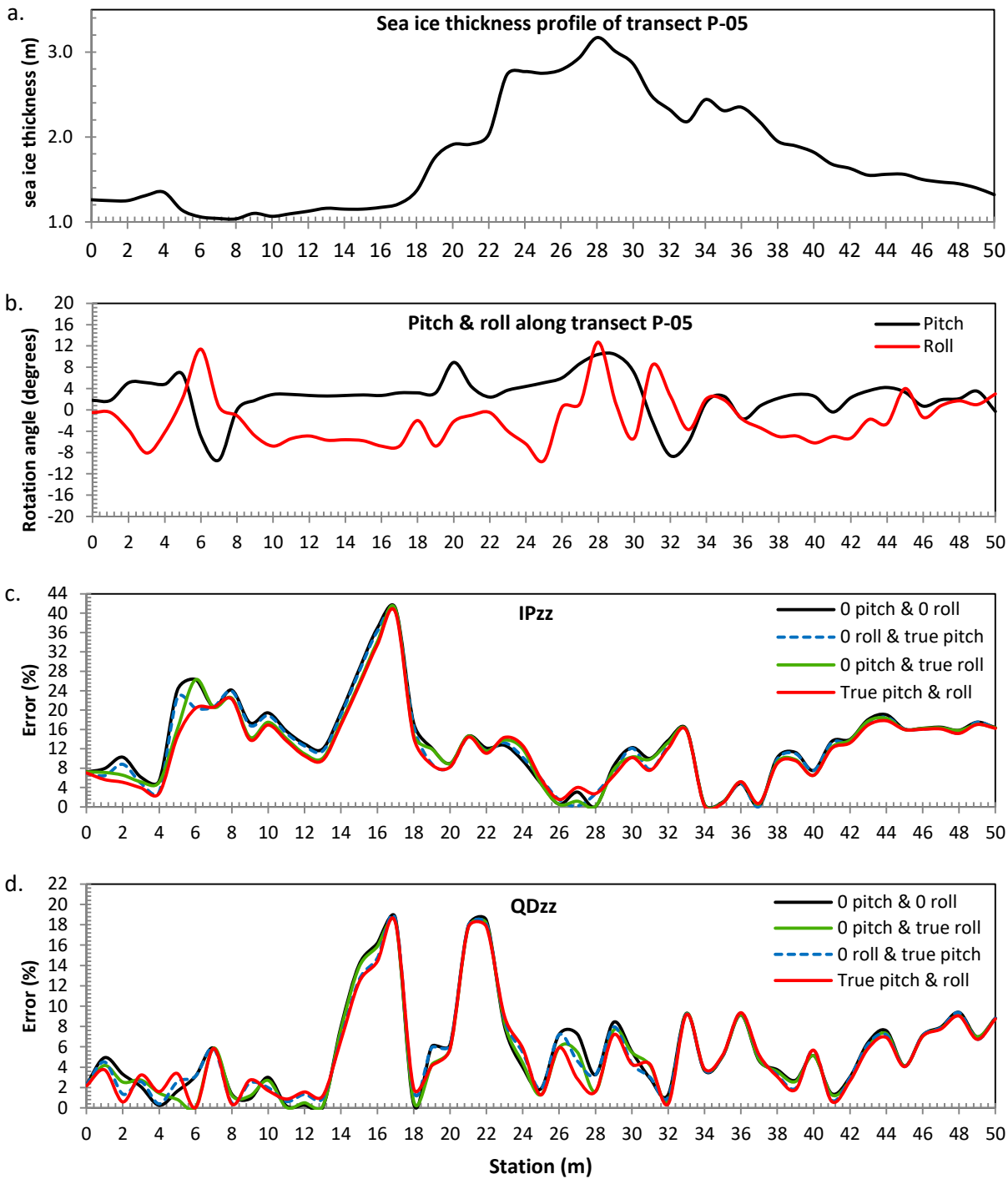

Fig. 7.5: (a) Sea ice thickness profile generated from drill-hole sea ice survey (b) SIS pitch and roll values along transect P-05.(b & c) Error distributions for IPzz, QDzz relative to true sea ice thickness. The errors are absolute.

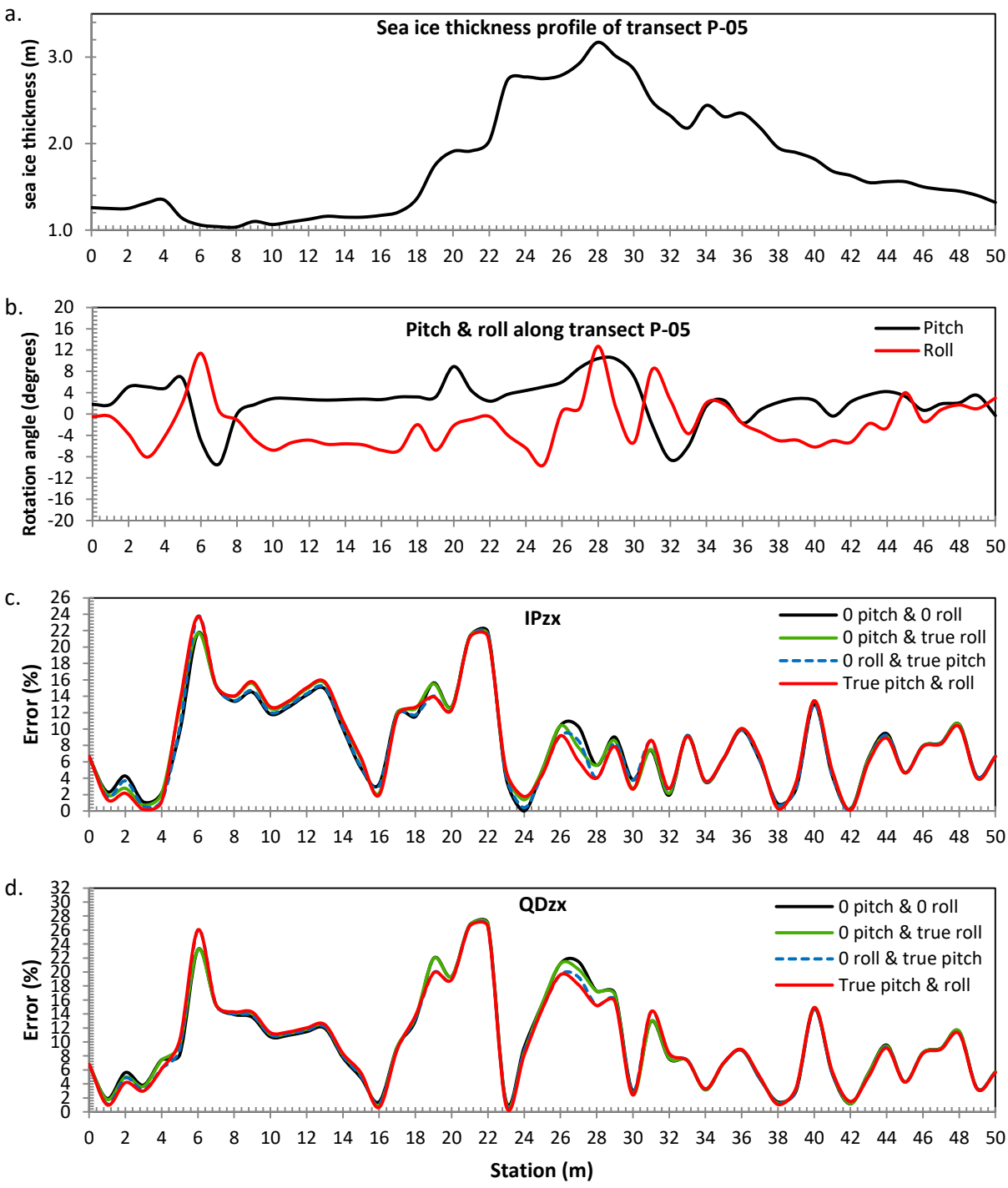

Fig. 7.6: (a) Sea ice thickness profile generated from drill-hole sea ice survey (b) SIS pitch and roll values along transect P-05.(b & c) Error distributions for IPzx, QDzx relative to true sea ice thickness. The errors are absolute.

7.6 Conclusion

Results from two experiments suggest that instrument pitch and roll introduce changes in the measured EM response, which leads to errors in the inversion results, for all coil configurations. Additionally, the effects of pitch and roll on inversion results vary between different coil configurations.

Field experiment 1, carried out over level first-year sea ice, indicated that HCOP coil configurations were more sensitive to roll. For this coil orientation, a 4 m coil spacings showed the highest sensitivity to roll, followed by 2 and 1 m coil spacings. PRP coil configurations were significantly less sensitive to roll, particularly the QDzx coil configuration, which yielded errors under 1%.

Field experiment 2, carried out over ridged multi-year sea ice, indicated that, overall, the utilization of instrument pitch and roll measurements generated the most accurate sea ice thicknesses for the pitch and roll variations observed in the field (up to ± 12º). This was particularly true for the section of the transect around the maximum ridge thickness, where results show a maximum error improvement of 4.4% (QDzz). However, the differences between inversion results that used the measured pitch and roll and those that did not use pitch and roll were generally very small (less than 2% for most stations). In some stations, results that did not use pitch and roll outperformed the inversion results that did use the measured pitch and roll values.

Overall, the accuracy of the inversion results improved with the utilization of instrument pitch and roll measurements. Accurate quantification of this improvement requires repeating experiments similar to experiment 1 over a variety of sites as well as over a variety of sea ice types.

8 Conclusion and outlook

8.1 Conclusion

The objective of this research thesis was to evaluate SIS capability to determine accurate sea ice thicknesses over a variety of sea ice types observed in field surveys. SIS performance over ridged sea ice type and slush covered sea ice type was particularly important because existing EM instrument has shown inaccurate results.

To achieve the research objective, SIS EM and drill-hole data were collected over a variety of sea ice types and the following investigations were performed:

Chapter 4 and 5 investigated theoretical and experimental signal sensitivity of SIS coil configurations with the intention of determining coil configurations that record the best quality reliable EM data over different sea ice types. Sensitivity analysis of SIS coil configurations showed that an increase in coil spacing size displays stronger EM responses from sea ice – sea water interface due to the larger skin depth of the larger coil spacings. In general, for 4m coil spacing configurations, the quadrature signal component in PRP coil orientation (4 m QDzz) displayed the best quality EM data. For 2 m and 1 m coil spacing configurations, the quadrature signal component of HCOP orientation (2 m QDzz and 1 QDzz) displayed the highest quality data. 1 m coil spacing configurations yielded the least reliable EM responses.

The variability observed in EM responses of all coil configurations was closely in line with the variation in actual sea ice thicknesses measured during drill-hole surveys. 2 m PRP and 1 m HCOP coil configurations were the most sensitive coil configurations to thin slush-covered sea ice. All coil configurations were influenced (stronger EM responses) by melt pond with the quadrature signal component showing the most significant influence of all.

In chapter 6, the capability of SIS's own inversion software (SISinvert) was investigated and the coil configuration(s) (data component(s)) that yield most accurate sea ice thickness estimates were determined. The accuracy of inverted sea ice thicknesses was primarily evaluated based on measuring the difference between inverted sea ice thicknesses and the in situ sea ice thickness measurements (RMSE).

Applying two-layered earth models and using proper starting model parameters in the inversions indicated that utilization of single coil spacing and a single data component is sufficient to acquire accurate bulk sea ice thickness estimates for all sea ice types surveyed in this research. For the rang of sea ice thicknesses observed (1 to 4.6 m), 2 m QDzz data component generally yielded accurate results for all sea ice types. However for melt pond and slush-covered sea ice where one is specifically interested in knowing the depth of the melt pond or slush, the two-layered earth model is no longer appropriate. Utilization of four-layered earth model and multi-data component generated accurate and reliable thickness estimates of not only the melt pond and slush layers but also the sea ice layers above and below it.

In chapter 7, the effect of pitch and roll changes on EM responses and inversion results were investigated. The main objective was to determine if the utilization of pitch and roll measurements in SISinvert correction procedure improves inversion results.

The results indicated that changes in pitch and roll changed measured EM responses. HCOP coil orientation was most sensitive to roll. Sensitivity increased with increasing coil spacing. PRP coil configuration was considerably less sensitive to change in roll. The least sensitive was QDzx with errors under 1%. Utilization of pitch and roll measurements in the inversions effectively improved the accuracy of sea ice thickness estimates within the pitch and roll changes observed in the field (up to $\pm 12^{o}$).

Overall SIS showed very accurate sea ice thickness estimates over a variety of sea ice types. Over ridged sea ice where most instruments overestimate ice thicknesses by as much as 50%, SIS showed that it can significantly increase accuracy (Fig.6.4). Utilization of SIS multi-configuration mode combined with multi-layered earth models can generate very accurate estimates of slush (RMSE of 0.03) and melt pond (RMSE of 0.06) depths. Within the limited range of sea ice thicknesses observed, employment of 4 m coil spacing is operationally unnecessary.

The findings presented so far in this research indicate that SIS is a reliable sea ice instrument that is potentially superior to its counterparts in profiling a wide range of sea ice types. Its multi-configurational capabilities plus pitch and roll measurement capability makes it more favorable over its counterparts.

8.2 Outlook

This research work was based on a limited number of case studies and within 1 to 4.6 m sea ice thickness range. Further work needs to be done over a wider range of sea ice thicknesses and a wider range of sea ice types to make better assessments of this research finding.

There as very limited slush and melt pond data available to firmly confirm present findings on these sea ice types. More SIS EM data and drill-hole measurements over slush and melt pond covered sea ice should be collected to further support results.

More pitch and roll experiments similar to experiment 1 (chapter 7.5) should be conducted over a variety of sea ice types to accurately quantify the effect of pitch and roll on the inverted sea ice thickness results.

An investigation should be made comparing SIS performance to other common sea ice surface-based EM instruments (e.g. EM31, EMP and GEM) by running all instruments simultaneously on exact same survey transects.

Bibliography

Anderson, Walter L. (1979): Numerical integration of related Hankel transforms of orders 0 and 1 by adaptive digital filtering. In *GEOPHYSICS* 44 (7), pp. 1287–1305. DOI: 10.1190/1.1441007.

Constable, Steven C.; Parker, Robert L.; Constable, Catherine G. (1987): Occam's inversion. A practical algorithm for generating smooth models from electromagnetic sounding data. In *GEOPHYSICS* 52 (3), pp. 289–300.

Eicken, Hajo (2009): Field techniques for sea ice research. Fairbanks, Alaska: University of Alaska Press; Bristol : University Presses Marketing [distributor].

Fitterman, David V.; Yin, Changchun (2004): Effect of bird maneuver on frequency-domain helicopter EM response. In *GEOPHYSICS* 69 (5), pp. 1203–1215. DOI: 10.1190/1.1801937.

Golub, G. H.; Reinsch, C. (1970): Singular value decomposition and least squares solutions. In *Numer. Math.* 14 (5), pp. 403–420. DOI: 10.1007/bf02163027.

Haas, Christian (1998): Evaluation of ship-based electromagnetic-inductive thickness measurements of summer sea-ice in the Bellingshausen and Amundsen Seas, Antarctica. In *Cold Regions Science and Technology* 27 (1), pp. 1–16. DOI: 10.1016/S0165-232X(97)00019-0.

Haas, Christian (2010): Sea ice. Dynamics versus Thermodynamics: The Sea Ice Thickness Distribution. With assistance of David N. Thomas, Gerhard Dieckmann. 2nd ed. Oxford: Wiley-Blackwell.

Haas, Christian; Gerland, Sebastian; Eicken, Hajo; Miller, Heinz (1997): Comparison of sea-ice thickness measurements under summer and winter conditions in the Arctic using a small electromagnetic induction device. In *GEOPHYSICS* 62 (3), pp. 749–757. DOI: 10.1190/1.1444184.

Haas, Christian; Lobach, John; Hendricks, Stefan; Rabenstein, Lasse; Pfaffling, Andreas (2009): Helicopter-borne measurements of sea ice thickness, using a small and lightweight, digital EM system. In *Journal of Applied Geophysics* 67 (3), pp. 234–241. DOI: 10.1016/j.jappgeo.2008.05.005.

Haykin, Simon S. (1994): Remote sensing of sea ice and icebergs. New York, Chichester: Wiley (A Wiley-Interscience publication).

Holladay, J. S.; Lo, B.; Prinsenberg, S. K. (1997): Bird orientation effects in quantitative airborne electromagnetic interpretation of pack ice thickness sounding. In : Oceans '97. MTS/IEEE Conference Proceedings. Oceans '97. MTS/IEEE Conference Proceedings. Halifax, NS, Canada, 6-9 Oct. 1997: IEEE, pp. 1114–1119.

Holladay, J.Scott (1980): Interpretation of electromagetic sounding data for stratifies earth by means of non-linearr regression. Masters thesis. University of Toronto.

HUANG, H.; Palacky, G. J. (1991): Damped least-squares inversion of time-domain airborne EM data based on singular value decomposition. In *Geophys Prospect* 39 (6), pp. 827–844. DOI: 10.1111/j.1365-2478.1991.tb00346.x.

Keller, George Vernon; Frischknecht, Frank C. (1966): Electrical methods in geophysical prospecting. 1st. ed. Oxford, New York: Pergamon Press (International series of monographs in electromagnetic waves, 10).

Kottmeier, Christoph; Olf, Jens; Frieden, Wolfgang; Roth, Rainer (1992): Wind forcing and ice motion in the Weddell Sea region. In *J. Geophys. Res.* 97 (D18), p. 20373. DOI: 10.1029/92jd02171.

Kovacs, A.; Holladay, J. S. (1990): Sea-ice thickness measurement using a small airborne electromagnetic sounding system. In *GEOPHYSICS* 55 (10), pp. 1327–1337. DOI: 10.1190/1.1442780.

Kovacs, Austin; Morey, Rexford M. (1986): Electromagnetic measurements of multi-year sea ice using impulse radar. In *Cold Regions Science and Technology* 12 (1), pp. 67–93. DOI: 10.1016/0165-232X(86)90021-2.

Kovacs, Austin; Morey, Rexford M. (1991): Sounding sea ice thickness using a portable electromagnetic induction instrument. In *GEOPHYSICS* 56 (12), pp. 1992–1998. DOI: 10.1190/1.1443011.

Kovacs, Austin; Valleau, N.C; Holladay, J.Scott (1987): Airborne electromagnetic sounding of sea ice thickness and sub-ice bathymetry. In *Cold Regions Science and Technology* 14 (3), pp. 289–311. DOI: 10.1016/0165-232X(87)90021-8.

Kwok, Ronald; Untersteiner, Norbert (2011): The thinning of Arctic sea ice. In *Physics Today* 64 (4), pp. 36–41. DOI: 10.1063/1.3580491.

Larsson, Jonas (2007): Electromagnetics from a quasistatic perspective. In *American Journal of Physics* 75 (3), pp. 230–239. DOI: 10.1119/1.2397095.

Levenberg, Kenneth (1944): A method for the solution of certain non-linear problems in least squares. In *Quart. Appl. Math.* 2 (2), pp. 164–168. DOI: 10.1090/qam/10666.

Liu, Guimin; Becker, Alex (1990): Two-dimensional mapping of sea-ice keels with airborne electromagnetics. In *GEOPHYSICS* 55 (2), pp. 239–248.

Marquardt, Donald W. (1963): An Algorithm for Least-Squares Estimation of Nonlinear Parameters. In *Journal of the Society for Industrial and Applied Mathematics* 11 (2), pp. 431–441. DOI: 10.1137/0111030.

Morey, Rexford M.; Kovacs, Austin; Cox, G.F.N (1984): Electromagnetic properties of sea ice. In *Cold Regions Science and Technology* 9 (1), pp. 53–75. DOI: 10.1016/0165-232X(84)90048-X.

Nabighian, Misac N. (Ed.) (1991): Electromagnetic Methods in Applied Geophysics: Society of Exploration Geophysicists.

Pfaffling, Andreas (2006): Helicopter electromagnetic sea ice thickness estimation. An induction method in the centimetre scale. Thesis (doctoral). University of Bremen, Bremerhaven.

Rossiter, James R.; Holladay, J. Scott (1994): Remote Sensing of Sea Ice and Icebergs. Ice-Thickness Measurment. New York, Chichester: Wiley (A Wiley-Interscience publication).

Rossiter, James R.; Langhorne, Pat J.; Ridings, T.; Allan, A. J. (Eds.) (1977): Study of sea ice using impulse radar. With assistance of POAC Conference 77. Proceedings of the 4th International Conference on Port and Ocean Engineering under Arctic Conditions (POAC 77), Newfoundland Memorial University, Canada, September 26-30.

Rothrock, D. A.; Yu, Y.; Maykut, G. A. (1999): Thinning of the Arctic sea-ice cover. In *Geophys. Res. Lett.* 26 (23), pp. 3469–3472. DOI: 10.1029/1999GL010863.

Sinha, A. K. (1976): A Field Study For Sea - Ice Thickness Determination By Electromagnetic Means.

Strass, Volker H. (1998): Measuring sea ice draft and coverage with moored upward looking sonars. In *Deep Sea Research Part I: Oceanographic Research Papers* 45 (4-5), pp. 795–818. DOI: 10.1016/S0967-0637(97)00065-4.

Telford, W. M.; Geldart, L. P.; Sheriff, R. E. (1990): Applied geophysics. 2nd ed.

Thorndike, A. S.; Rothrock, D. A.; Maykut, G. A.; Colony, R. (1975): The thickness distribution of sea ice. In *J. Geophys. Res.* 80 (33), pp. 4501–4513. DOI: 10.1029/jc080i033p04501.

Wadhams, P. (2000): Ice in the ocean. Australia: Gordon and Breach.

Yin, Changchun; Fraser, Douglas C. (2004): Attitude corrections of helicopter EM data using a superposed dipole model. In *GEOPHYSICS* 69 (2), pp. 431–439. DOI: 10.1190/1.1707063.

Appendix A:

Table 6.6: Transect P-05 calculated RMSE values derived from inverted sea ice thicknesses and drill measurements for 4 different starting models. Empty cell indicates unreliable data readings. Units are in meters.

4 m coil configurations

Models	IPzz	QDzz	Ipzx	QDzx	IPzzQDzz	IPzzQzx	IPzxQzz	IPzxQzx	QDzzQDzx	IPzzQDzxIPzx	IPzzQDzzIPzx	IPzzQDzzQDzx	QDzzQDzxIPzx	IPzzQDzzIPzxQDzx	MinErr.
m1	0.22	0.35	0.43	0.16	0.26	0.20	0.30	0.22	0.15	0.30	0.19	0.16	0.19	0.19	0.15
m2	0.22	0.34	0.42	0.14	0.25	0.20	0.30	0.20	0.14	0.27	0.18	0.14	0.18	0.18	0.14
m3	0.22	0.35	0.43	0.16	0.26	0.17	0.35	0.29	0.15	0.42	0.22	0.16	0.25	0.22	0.15
m4	0.22	0.35	0.43	0.14	0.26	0.17	0.46	0.45	0.16	0.50	0.23	0.17	0.27	0.23	0.16
Min Err.	0.21	0.34	0.42	0.14	0.25	0.17	0.30	0.20	0.14	0.27	0.18	0.14	0.18	0.18	

2 m coil configurations

Models	IPzz	QDzz	Ipzx	QDzx	IPzzQDzz	IPzzQzx	IPzxQzz	IPzxQzx	QDzzQDzx	IPzzQDzxIPzx	IPzzQDzzIPzx	IPzzQDzzQDzx	QDzzQDzxIPzx	IPzzQDzzIPzxQDzx	MinErr.
m1	0.22	0.14	0.19	0.30	0.15	0.80	0.16	0.30	0.20	1.09	0.17	0.19	0.21	0.20	0.14
m2	0.22	0.13	0.16	0.24	0.14	0.75	0.15	0.25	0.17	1.01	0.15	0.16	0.18	0.17	0.13
m3	0.23	0.14	0.19	0.30	0.16	0.75	0.25	0.31	0.17	1.55	0.22	0.17	0.20	0.18	0.14
m4	0.23	0.14	0.19	0.30	0.19	0.75	0.38	0.33	0.18	1.64	0.24	0.17	0.19	0.18	0.14
Min Err.	0.22	0.13	0.16	0.24	0.14	0.75	0.15	0.25	0.17	1.01	0.15	0.16	0.18	0.17	

1 m coil configurations

Models	IPzz	QDzz	Ipzx	QDzx	IPzzQDzz	IPzzQzx	IPzxQzz	IPzxQzx	QDzzQDzx	IPzzQDzxIPzx	IPzzQDzzIPzx	IPzzQDzzQDzx	QDzzQDzxIPzx	IPzzQDzzIPzxQDzx	MinErr.
m1	0.18	0.19		0.45	0.16	1.16			0.26			0.23			0.16
m2	0.18	0.16		0.37	0.15	1.01			0.23			0.22			0.15
m3	0.18	0.19		0.43	0.15	1.01			0.22			0.19			0.15
m4	0.18	0.19		0.43	0.15	1.01			0.26			0.19			0.15
Min Err.	0.18	0.16		0.37	0.15	1.01			0.22			0.19			

Table 6.7: Transect P-011 calculated RMSE values derived from inverted sea ice thicknesses and drill measurements for 4 different starting models. Measured field data were on reliable for 1 m coil spacing. Units are in meters.

4 m coil configurations

Models	IPzz	QDzz	Ipzx	QDzx	IPzzQDzz	IPzzQzx	IPzxQzz	IPzxQzx	QDzzQDzx	IPzzQDzxIPzx	IPzzQDzzIPzx	IPzzQDzzQDzx	QDzzQDzxIPzx	IPzzQDzzIPzxQDzx	MinErr.
m1	0.56	0.46	0.75	0.38	0.50	0.43	0.50	0.46	0.38	0.59	0.43	0.41	0.42	0.43	0.38
m2	0.55	0.46	0.74	0.36	0.50	0.42	0.49	0.43	0.37	0.56	0.42	0.40	0.40	0.42	0.36
m3	0.56	0.46	0.75	0.38	0.50	0.43	0.65	0.62	0.39	0.73	0.46	0.42	0.49	0.46	0.38
m4	0.55	0.46	0.74	0.36	0.50	0.51	1.10	0.81	0.46	0.91	0.56	0.42	0.58	0.56	0.38
Min Err.	0.55	0.46	0.74	0.36	0.50	0.42	0.49	0.43	0.37	0.56	0.42	0.40	0.40	0.42	

2 m coil configurations

Models	IPzz	QDzz	Ipzx	QDzx	IPzzQDzz	IPzzQzx	IPzxQzz	IPzxQzx	QDzzQDzx	IPzzQDzxIPzx	IPzzQDzzIPzx	IPzzQDzzQDzx	QDzzQDzxIPzx	IPzzQDzzIPzxQDzx	MinErr.
m1	0.51	0.38	3.23	1.59	0.40	1.15	0.39	0.58	0.42	1.30	0.40	0.41	0.43	0.41	0.38
m2	0.50	0.38	3.23	0.49	0.40	1.03	0.38	0.47	0.38	1.14	0.40	0.38	0.40	0.39	0.38
m3	0.51	0.38	3.11	0.87	0.42	1.03	0.46	0.52	0.39	1.78	0.41	0.40	0.41	0.40	0.38
m4	0.51	0.38	3.19	0.87	0.54	1.03	0.55	0.51	0.41	1.86	0.41	0.44	0.41	0.41	0.38
Min Err.	0.50	0.38	3.11	0.49	0.40	1.03	0.38	0.47	0.38	1.14	0.40	0.38	0.40	0.39	

Table 6.8: Transect Q-10 calculated RMSE values derived from inverted sea ice thicknesses and drill measurements for 4 different starting models. Empty cell indicates unreliable field data readings. Units are in meters.

4 m coil configurations

Models	IPzz	QDzz	Ipzx	QDzx	IPzzQDzz	IPzzQzx	IPzxQzz	IPzxQzx	QDzzQDzx	IPzzQDzxIPzx	IPzzQDzzIPzx	IPzzQDzzQDzx	QDzzQDzxIPzx	IPzzQDzzIPzxQDzx	MinErr.
m1	0.05	0.20	0.10	0.05	0.06	0.29	0.08	0.06	0.05	0.05	0.05	0.05	0.06	0.05	0.05
m2	0.05	0.19	0.09	0.05	0.06	0.30	0.08	0.06	0.05	0.05	0.05	0.05	0.05	0.05	0.05
m3	0.05	0.20	0.10	0.05	0.06	0.16	0.08	0.06	0.05	0.05	0.06	0.04	0.06	0.06	0.04
m4	0.05	0.20	0.10	0.05	0.06	0.16	0.08	0.06	0.05	0.05	0.06	0.04	0.06	0.06	0.04
Min Err.	0.05	0.19	0.09	0.05	0.06	0.16	0.08	0.06	0.05	0.05	0.05	0.04	0.05	0.05	

2 m coil configurations

Models	IPzz	QDzz	Ipzx	QDzx	IPzzQDzz	IPzzQzx	IPzxQzz	IPzxQzx	QDzzQDzx	IPzzQDzxIPzx	IPzzQDzzIPzx	IPzzQDzzQDzx	QDzzQDzxIPzx	IPzzQDzzIPzxQDzx	MinErr.
m1	0.06	0.05	0.07	0.07	0.05	0.28	0.06	0.07	0.06	0.82	0.06	0.06	0.06	0.06	0.05
m2	0.06	0.05	0.06	0.06	0.05	0.28	0.05	0.07	0.06	0.82	0.05	0.06	0.06	0.06	0.05
m3	0.06	0.05	0.07	0.07	0.05	0.31	0.15	0.09	0.06	0.82	0.14	0.06	0.08	0.08	0.05
m4	0.06	0.05	0.07	0.07	0.05	0.31	0.15	0.09	0.06	0.82	0.14	0.06	0.06	0.08	0.05
Min Err.	0.06	0.05	0.06	0.06	0.05	0.28	0.05	0.07	0.06	0.82	0.05	0.06	0.06	0.06	

1 m coil configurations

Models	IPzz	QDzz	Ipzx	QDzx	IPzzQDzz	IPzzQzx	IPzxQzz	IPzxQzx	QDzzQDzx	IPzzQDzxIPzx	IPzzQDzzIPzx	IPzzQDzzQDzx	QDzzQDzxIPzx	IPzzQDzzIPzxQDzx	MinErr.
m1	0.09	0.07		0.09	0.07	0.80			0.08			0.08			0.07
m2	0.08	0.06		0.08	0.07	0.77			0.07			0.07			0.06
m3	0.09	0.07		0.09	0.07	0.79			0.07			0.07			0.07
m4	0.09	0.07		0.09	0.07	0.79			0.07			0.07			0.07
Min Err.	0.08	0.06		0.08	0.07	0.77			0.07			0.07			

Table 6.9: Transect Q-11 calculated RMSE values derived from inverted sea ice thicknesses and drill measurements for 4 different starting models. Empty cell indicates unreliable field data readings. Units are in meters.

4 m coil configurations

Models	IPzz	QDzz	Ipzx	QDzx	IPzzQDzz	IPzzQzx	IPzxQzz	IPzxQzx	QDzzQDzx	IPzzQDzxIPzx	IPzzQDzzIPzx	IPzzQDzzQDzx	QDzzQDzxIPzx	IPzzQDzzIPzxQDzx	MinErr.
m1	0.09	0.30	0.17	0.09	0.10	0.31	0.18	0.09	0.09	0.09	0.09	0.09	0.09	0.09	0.09
m2	0.09	0.31	0.17	0.09	0.10	0.31	0.17	0.09	0.09	0.09	0.09	0.09	0.09	0.09	0.09
m3	0.09	0.30	0.17	0.09	0.10	0.08	0.18	0.10	0.09	0.09	0.10	0.09	0.10	0.10	0.08
m4	0.09	0.30	0.17	0.09	0.10	0.08	0.20	0.10	0.08	0.09	0.10	0.08	0.10	0.10	0.08
Min Err.	0.09	0.30	0.17	0.09	0.10	0.08	0.17	0.09	0.08	0.09	0.09	0.08	0.09	0.09	

2 m coil configurations

Models	IPzz	QDzz	Ipzx	QDzx	IPzzQDzz	IPzzQzx	IPzxQzz	IPzxQzx	QDzzQDzx	IPzzQDzxIPzx	IPzzQDzzIPzx	IPzzQDzzQDzx	QDzzQDzxIPzx	IPzzQDzzIPzxQDzx	MinErr.
m1	0.08	0.08	0.12	0.11	0.08	0.14	0.08	0.09	0.10	1.09	0.08	0.10	0.10	0.10	0.08
m2	0.08	0.09	0.12	0.11	0.08	0.13	0.08	0.09	0.11	1.09	0.08	0.10	0.10	0.10	0.08
m3	0.08	0.08	0.12	0.11	0.08	0.13	0.07	0.09	0.10	1.09	0.08	0.10	0.10	0.09	0.07
m4	0.08	0.08	0.12	0.11	0.08	0.13	0.07	0.09	0.07	1.09	0.08	0.10	0.10	0.09	0.07
Min Err.	0.08	0.08	0.12	0.11	0.08	0.13	0.07	0.09	0.07	1.09	0.08	0.10	0.10	0.09	

1 m coil configurations

Models	IPzz	QDzz	Ipzx	QDzx	IPzzQDzz	IPzzQzx	IPzxQzz	IPzxQzx	QDzzQDzx	IPzzQDzxIPzx	IPzzQDzzIPzx	IPzzQDzzQDzx	QDzzQDzxIPzx	IPzzQDzzIPzxQDzx	MinErr.
m1	0.08	0.12	0.68	0.14	0.11	0.45			0.13			0.13			0.08
m2	0.08	0.12	0.68	0.15	0.11	0.43			0.14			0.13			0.08
m3	0.08	0.12	0.68	0.14	0.11	0.45			0.13			0.13			0.08
m4	0.08	0.12	0.68	0.14	0.11	0.45			0.09			0.13			0.08
Min Err.	0.08	0.12	0.67	0.14	0.11	0.43			0.09			0.13			

Table 6.10: Transect Q-12 calculated RMSE values derived from inverted sea ice thicknesses and drill measurements for 4 different starting models. Empty cell indicates unreliable field data readings. Units are in meters.

4 m coil configurations

Models	IPzz	QDzz	Ipzx	QDzx	IPzzQDzz	IPzzQzx	IPzxQzz	IPzxQzx	QDzzQDzx	IPzzQDzxIPzx	IPzzQDzzIPzx	IPzzQDzzQDzx	QDzzQDzxIPzx	IPzzQDzzIPzxQDzx	MinErr.
m1	0.21	0.20	0.47	0.19	0.20	0.12	0.37	0.24	0.18	0.35	0.23	0.19	0.23	0.23	0.12
m2	0.20	0.20	0.46	0.18	0.20	0.12	0.36	0.23	0.17	0.32	0.22	0.18	0.22	0.22	0.12
m3	0.21	0.20	0.47	0.19	0.20	0.14	0.39	0.27	0.18	0.36	0.26	0.18	0.27	0.26	0.14
m4	0.21	0.20	0.47	0.19	0.20	0.14	0.39	0.27	0.18	0.36	0.26	0.18	0.27	0.26	0.14
Min Err.	0.20	0.20	0.46	0.18	0.20	0.12	0.36	0.23	0.17	0.32	0.22	0.18	0.22	0.22	

2 m Coil Configurations

Models	IPzz	QDzz	Ipzx	QDzx	IPzzQDzz	IPzzQzx	IPzxQzz	IPzxQzx	QDzzQDzx	IPzzQDzxIPzx	IPzzQDzzIPzx	IPzzQDzzQDzx	QDzzQDzxIPzx	IPzzQDzzIPzxQDzx	MinErr.
m1	0.18	0.15	0.15	0.18	0.16	0.62	0.38	0.34	0.16	0.98	0.34	0.17	0.25	0.24	0.15
m2	0.18	0.14	0.13	0.16	0.15	0.60	0.36	0.34	0.15	0.94	0.34	0.15	0.24	0.23	0.13
m3	0.18	0.15	0.15	0.18	0.16	0.59	0.36	0.35	0.16	2.18	0.36	0.17	0.26	0.24	0.15
m4	0.18	0.15	0.15	0.18	0.16	0.59	0.36	0.35	0.17	2.26	0.36	0.17	0.26	0.24	0.15
Min Err.	0.18	0.14	0.13	0.16	0.15	0.59	6	0.34	0.15	0.94	0.34	0.15	0.24	0.23	

1 m Coil Configurations

Models	IPzz	QDzz	Ipzx	QDzx	IPzzQDzz	IPzzQzx	IPzxQzz	IPzxQzx	QDzzQDzx	IPzzQDzxIPzx	IPzzQDzzIPzx	IPzzQDzzQDzx	QDzzQDzxIPzx	IPzzQDzzIPzxQDzx	MinErr.
m1	0.14	0.15		0.31	0.15	1.33			0.24			0.21			0.14
m2	0.13	0.13		0.25	0.13	1.25			0.18			0.18			0.13
m3	0.14	0.15		0.31	0.14	1.24			0.22			0.18			0.14
m4	0.14	0.15		0.31	0.14	1.24			0.22			0.18			0.14
Min Err.	0.13	0.13		0.25	0.13	1.24			0.18			0.18			

Table 6.11: Transect Q-13 calculated RMSE values derived from inverted sea ice thicknesses and drill measurements for 4 different starting models. Empty cell indicates unreliable field data readings. Units are in meters.

4 m coil configurations

Models	IPzz	QDzz	Ipzx	QDzx	IPzzQDzz	IPzzQzx	IPzxQzz	IPzxQzx	QDzzQDzx	IPzzQDzxIPzx	IPzzQDzzIPzx	IPzzQDzzQDzx	QDzzQDzxIPzx	IPzzQDzzIPzxQDzx	MinErr.
m1	0.10	0.10	0.29	0.07	0.09	0.30	0.26	0.10	0.07	0.09	0.10	0.07	0.10	0.10	0.07
m2	0.09	0.10	0.29	0.07	0.09	0.30	0.25	0.10	0.07	0.08	0.10	0.07	0.10	0.10	0.07
m3	0.10	0.10	0.29	0.07	0.09	0.09	0.26	0.18	0.07	0.09	0.12	0.07	0.14	0.12	0.07
m4	0.10	0.10	0.29	0.07	0.09	0.09	0.26	0.18	0.07	0.09	0.12	0.07	0.14	0.12	0.07
Min Err.	0.09	0.10	0.29	0.07	0.09	0.09	0.25	0.10	0.07	0.08	0.10	0.07	0.10	0.10	

2 m coil configurations

Models	IPzz	QDzz	Ipzx	QDzx	IPzzQDzz	IPzzQzx	IPzxQzz	IPzxQzx	QDzzQDzx	IPzzQDzxIPzx	IPzzQDzzIPzx	IPzzQDzzQDzx	QDzzQDzxIPzx	IPzzQDzzIPzxQDzx	MinErr.
m1	0.08	0.06	0.09	0.09	0.06	0.23	0.07	0.09	0.08	0.88	0.07	0.07	0.08	0.08	0.06
m2	0.08	0.06	0.09	0.09	0.06	0.23	0.07	0.09	0.08	0.88	0.07	0.07	0.08	0.07	0.06
m3	0.08	0.06	0.09	0.09	0.06	0.26	0.19	0.09	0.07	0.88	0.18	0.07	0.08	0.08	0.06
m4	0.08	0.06	0.09	0.09	0.06	0.26	0.19	0.09	0.06	0.88	0.18	0.07	0.08	0.08	0.06
Min Err.	0.08	0.06	0.09	0.09	0.06	0.23	0.07	0.09	0.06	0.88	0.07	0.07	0.08	0.07	

1 m coil configurations

Models	IPzz	QDzz	Ipzx	QDzx	IPzzQDzz	IPzzQzx	IPzxQzz	IPzxQzx	QDzzQDzx	IPzzQDzxIPzx	IPzzQDzzIPzx	IPzzQDzzQDzx	QDzzQDzxIPzx	IPzzQDzzIPzxQDzx	MinErr.
m1	0.12	0.09		0.14	0.09	0.69			0.12			0.11			0.09
m2	0.12	0.09		0.14	0.09	0.67			0.12			0.12			0.09
m3	0.12	0.09		0.14	0.07	0.65			0.11			0.10			0.07
m4	0.12	0.09		0.14	0.07	0.65			0.07			0.10			0.07
Min Err.	0.11	0.09		0.14	0.07	0.65			0.07			0.10			

Table 6.12: Transect Q-13 calculated RMSE values derived from inverted sea ice thicknesses and drill measurements using adjusted starting models. Units are in meters.

4m Coil configurations

Models	IPzz	QDzz	Ipzx	QDzx	IPzzQDzz	IPzzQzx	IPzxQzz	IPzxQzx	QDzzQDzx	IPzzQDzxIPzx	IPzzQDzzIPzx	IPzzQDzzQDzx	QDzzQDzxIPzx	IPzzQDzzIPzxQDzx	MinErr.
m1s	0.04	0.29	0.10	0.07	0.11	0.04	0.12	0.02	0.05	0.08	0.02	0.05	0.02	0.02	0.02
m2s	0.03	0.28	0.12	0.05	0.08	0.03	0.14	0.03	0.05	0.09	0.03	0.07	0.04	0.03	0.03
m3s	0.03	0.26	0.15	0.03	0.08	0.03	0.14	0.06	0.05	0.09	0.06	0.06	0.06	0.06	0.03
m4s	0.05	0.26	0.17	0.04	0.08	0.04	0.14	0.09	0.05	0.09	0.09	0.06	0.10	0.09	0.04
Min Err.	0.03	0.26	0.10	0.03	0.08	0.03	0.12	0.02	0.05	0.08	0.02	0.05	0.02	0.02	0.02

2m Coil Configurations

Models	IPzz	QDzz	Ipzx	QDzx	IPzzQDzz	IPzzQzx	IPzxQzz	IPzxQzx	QDzzQDzx	IPzzQDzxIPzx	IPzzQDzzIPzx	IPzzQDzzQDzx	QDzzQDzxIPzx	IPzzQDzzIPzxQDzx	MinErr.
m1s	0.06	0.09	0.13	0.12	0.08	0.06	0.05	0.04	0.06	1.05	0.05	0.11	0.10	0.10	0.04
m2s	0.04	0.07	0.09	0.08	0.06	0.06	0.03	0.06	0.06	1.05	0.03	0.05	0.07	0.07	0.03
m3s	0.03	0.05	0.05	0.05	0.04	0.04	0.02	0.15	0.06	1.05	0.02	0.04	0.04	0.04	0.02
m4s	0.03	0.03	0.07	0.08	0.02	0.04	0.03	0.14	0.06	1.05	0.03	0.03	0.05	0.05	0.02
Min Err.	0.03	0.03	0.05	0.05	0.02	0.04	0.02	0.04	0.06	1.05	0.02	0.03	0.04	0.04	

1m Coil Configurations

Models	IPzz	QDzz	Ipzx	QDzx	IPzzQDzz	IPzzQzx	IPzxQzz	IPzxQzx	QDzzQDzx	IPzzQDzxIPzx	IPzzQDzzIPzx	IPzzQDzzQDzx	QDzzQDzxIPzx	IPzzQDzzIPzxQDzx	MinErr.
m1s	0.50	0.13		0.14	0.12	0.27			0.11			0.09			0.09
m2s	0.52	0.09		0.08	0.08	0.27	NA	NA	0.11	NA	NA	0.08	NA	NA	0.08
m3s	0.55	0.05		0.23	0.05	0.26			0.11			0.07			0.05
m4s	0.57	0.07		0.44	0.03	0.26			0.11			0.07			0.03
Min Err.	0.50	0.05		0.08	0.03	0.26			0.11			0.07			

Table 6.12: Transect Q-11, Slush section multi-layered models inversion results RMSE values. Units are in meters.

	4 m coil spacing			2 m coil spacing			1 m coil spacing		
Data component	1st layer	2nd layer	3rd layer	1st layer	2nd layer	3rd layer	1st layer	2nd layer	3rd layer
QDzz	0.10	0.05	0.03	0.08	0.03	0.04	0.08	0.03	0.06
QDzx	0.07	0.03	0.04	0.08	0.03	0.05	0.07	0.04	0.05
IPzz	0.07	0.03	0.02	0.07	0.03	0.03	0.07	0.03	0.03
IPzx	0.05	0.04	0.05	0.08	0.03	0.06			
IPzzQDzz	0.07	0.04	0.02	0.08	0.03	0.04	0.08	0.03	0.05
IPzzQDzx	0.07	0.04	0.07	0.05	0.03	0.05			
IPzxQDzz	0.09	0.04	0.03	0.09	0.04	0.05			
IPzxQDzx	0.08	0.05	0.04	0.08	0.04	0.03			
QDzzQDzx	0.07	0.04	0.03	0.07	0.03	0.06	0.07	0.03	0.06
IPzzQDzzIPzx	0.07	0.05	0.03	0.08	0.04	0.05			
IPzzQDzzQDzx	0.07	0.04	0.02	0.07	0.03	0.06	0.07	0.03	0.06
QDzzQDzxIPzx	0.06	0.05	0.05	0.07	0.04	0.05			
IPzzQDzxIPzx	0.02	0.02	0.05	0.10	0.05	0.05			